SECTION I

RESEARCH IN PROGRESS

NUCLEAR REACTIONS--EXPERIMENTAL

OBSERVATION OF ENHANCED TRANSPARENCY IN NUCLEUS-NUCLEUS TOTAL REACTION CROSS SECTIONS

R. A. Loveman,[a] J. G. Cramer,[a] D. D. Leach,[a] A. J. Lazzarini,[a] W. G. Lynch, M. B. Tsang, and J. van der Plicht

At low energies the total reaction cross section for nucleus-nucleus scattering is determined primarily by average collective nuclear behavior, and σ_r is essentially geometrical. As the collision energy is increased and characteristic wavelengths become shorter the average nuclear behavior becomes less important and the individual collisions of nucleons in the target with those in the projectile assume more and more prominence. At the same time the total cross section for nucleon-nucleon scattering decreases dramatically with energy as the repulsive hard-core effects of the nucleon-nucleon interaction become dominant.

Using the approximation that the reaction cross section arises exclusively from the scattering of a single nucleon in the target on a single nucleon in the projectile (the optical limit of Glauber theory[2]), DeVries and Peng[1] predicted that σ_r should decrease for nucleon-nucleus and nucleus-nucleus interactions, as the bombarding energy increases from 10 MeV/A to 100 MeV/A. These calculations agree remarkably well, for bombarding energies in excess of 20 MeV/A, with both the nucleon-nucleus data[3] and with the rather small amount of available nucleus-nucleus data.[4-10] The success of this model suggests that the decrease with energy of the nucleon-nucleon interaction is the dominant factor influencing the energy dependence of the nucleus-nucleus total reaction cross section. Here we report total reaction cross section measurements for $^{12}C+^{12}C$ and $^{12}C+^{90}Zr$ which provide for the first time a test of these predictions for heavier systems. In contrast to observations with light systems, the decrease with energy in reactions cross sections for the $^{12}C+^{90}Zr$ system exceeds considerably that imposed upon Glauber calculations by the energy dependence of the nucleon-nucleon interaction.

The total reaction cross sections were extracted from forward angle elastic scattering measurements using a ^{12}C beam at energies of 15 MeV/A, 25 MeV/A, and 35 MeV/A and the S-320 spectrometer of the National Superconducting Cyclotron Laboratory of Michigan State University. Targets of isotopically enriched ^{12}C and ^{90}Zr with thicknesses of about 1 mg/cm^2 were used, along with a ^{197}Au target which was used for determination of the absolute scattering angle as described below. The energy resolution was a maximum of 860 keV FWHM for ^{12}C at 35 MeV/A , permitting separation of elastic from inelastic scattering for all energies, angles, and targets. The charge resolution of 4.2% FWHM for the entire detection system was more than adequate to resolve scattered carbon particles from other reaction products.

The angular acceptance used for the spectrometer were dictated by count rate limitations and was defined by an aperture located 198 cm downstream from the target. Two apertures with acceptances of 0.069^0 and 0.138^0 in the horizontal plane were used. The accuracy in determining the absolute scattering angles was better than 0.02^0 and was limited principally by the measurement of 0^0 (the beam axis). This zero setting was measured by two independent methods: (1) focusing the beam on the target and then rotating the spectrometer until the beam was centered on a scintillator at the focal-plane, and (2) measuring the scattering cross section on gold at 2^0 and computing the angular offset from differences between equivalent measurements on opposite sides of the beam. The first and second methods determined zero degrees with an accuracy estimated to be 0.04^0 and 0.02^0, respectively. The angular stability of the beam was monitored by four plastic scintillators mounted symmetrically in the upper right, lower right,

upper left, and lower left quadrants at an angle of 7.1^0 from the beam. Known beam movements of 0.03^0 due to accelerator tuning were easily detected. Beam intensity was also monitored with these detectors. Corrections to the data due to the finite extent of the beam spot (1 mm horizontal and 3 mm vertical) were negligible.

The experimental elastic scattering differential cross sections are shown in Fig. 1.

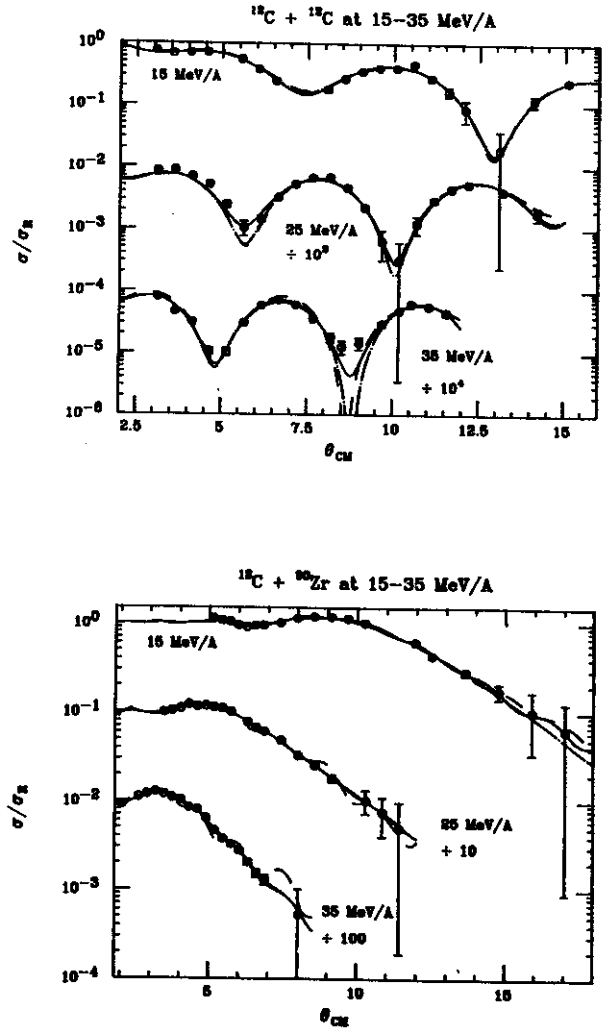

Fig. 1 Typical elastic scattering data from $^{12}C+^{12}C$ and $^{12}C+^{90}Zr$ used in the determination of total reaction cross sections. Curves are predictions of the various models mentioned in the text: Solid=McIntyre, Dashed-dotted=WS-Optical, Dashed=Folded-Optical.

At each energy the elastic differential cross section data were fitted using three different models: (1) the S-matrix parameterization of McIntyre et. al.[12], (2) the optical model using independent Woods-Saxon geometries for the real and imaginary parts of the optical potential, and (3) the optical model using a microscopic folding model real potential[13] and a Woods-Saxon geometry for the imaginary potential. Fits with models 1,2,3 are indicated by the solid, dashed, and dotted curves respectively. The S-matrix of each model at each energy was used to calculate a total reaction cross section. The overall total reaction cross section for each system at each energy was taken to be a average of these S-matrix fits. The values are listed in Table I.

The errors in σ_r due to uncertainties in the differential cross-section measurements, e.g., uncertainties in absolute scattering angle, target thickness, etc. , were determined numerically in a manner similar to that employed by Cole, et. al[5]. The net variance produced by these errors was found to be between 0.5% and 1.5%.

One type of uncertainty which is not easily accounted for is the dependence of σ_r on which model is used to fit the data. One can examine this uncertainty experimentally by comparing σ_r from beam attenuation measurements, which are essentially model independent, with elastic measurements of σ_r which require model-dependent analysis. For the $^{12}C+^{12}C$ system, beam attenuation measurements[8,9] agree with elastic scattering measurements[4,5,10] at similar energies to within their uncertainties, typically 4% in this energy range. Our model dependent uncertainties were minimized by fitting the data with three different models at each energy and averaging the values of σ_r obtained. In these averages, the models were given equal weight for lack of an objective criterion quantifying the relative validity of these models. The model dependent uncertainties were estimated from the variance of the three calculated reaction cross sections to be between 2.5% and 6.8%. This was the dominant

contribution to the total uncertainty.

These experimental total reaction cross sections for two systems at three energies were compared with the predictions of the Glauber model. The total reaction cross sections for the $^{12}C+^{12}C$ system were found to be in excellent

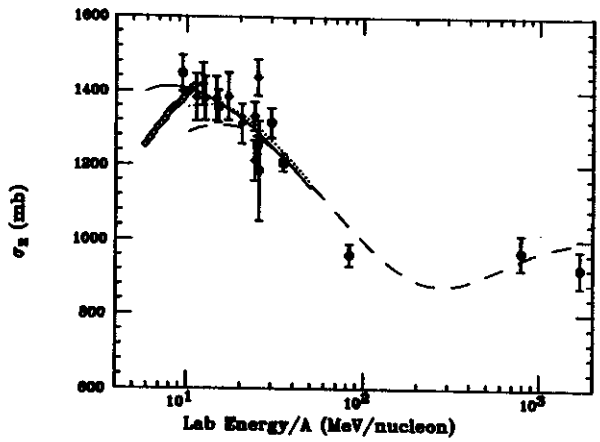

Fig. 2 Summary of total reaction cross section (σ_r) experimental data and calculations for the system $^{12}C+^{12}C$. The full curve is the prediction of a simple Galuber model calculation[1] performed by the authors. The dotted and dashed curves are the predictions of the more detailed microscopic Glauber model calculations of DiGiacomo and DeVries[14] using a deep and a shallow nuclear potential, respectively. The solid circles indicate present measurements, the open diamonds indicate other scattering measurements[4,5,7,8], the open squares indicate transmission measurements[9,10], and the single cross indicates a sum of measured reaction cross sections[11]. Error bars for present work reflect both statistical and model-dependent systematic errors.

agreement with both previous data for the same system and with Glauber model calculations. This is shown in Fig. 2. The transparency[15], defined as the deviation of the measured σ_r from the Coulomb-corrected geometric cross section divided by the geometric cross section itself, was found to increase with energy as the Glauber model predicts[12].

In contrast, the measured σ_r values for the $^{12}C+^{90}Zr$ system, which are shown in Fig. 3, are

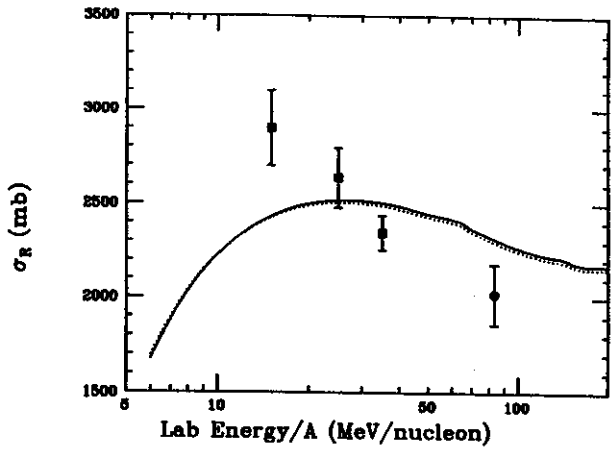

Fig. 3 Summary of total reaction cross section (σ_r) data and predictions for ^{12}C on mass 89 and 90 targets. The full curve is the the prediction of a simple Galuber model calculation[1] performed by the authors for the $^{12}C+^{90}Zr$ system. The dotted curve below it is a similar prediction for the $^{12}C+^{89}Y$ system. The solid triagles indicate the results of the present work on $^{12}C+^{90}Zr$. The open square shows a datum from a transmission measurement[10] for $^{12}C+^{89}Y$. Error bars for present work reflect both statistical and model-dependent systematic errors.

in clear disagreement with Glauber model predictions. The experimental total reaction cross section data are significantly larger than the predictions at 15 MeV/A and significantly smaller than the prediction at 35 MeV/A. More significant is the energy dependence of σ_r, which is considerably stronger than the Glauber model predictions. The increase in transparency[15] with energy for this system is twice that of the $^{12}C+^{12}C$ system, while the Glauber model predicts the same transparency increase for both systems. This is the first systematic study of a nucleus-nucleus reaction cross section to show this new and unanticipated behavior. Two previous measurements of σ_r at one energy have been found to be in significant disaggreement with Glauber calculations. One of these, a σ_r measurement of the $^{12}C+^{89}Y$ system[10], is included in Fig. 2 and is consistent with the energy trend of the present work.

The simple microscopic Glauber calculations performed by the authors, shown in Figs. 2 and 3 (solid lines) and described in Ref. 1, do not

include three important effects: (1) Fermi motion which alters the velocities of colliding nucleons, (2) Pauli blocking which prevents n-n scatterings to occupied momentum states, and (3) the strong nuclear force which deflects nuclear trajectories toward smaller collision distances. The more detailed Glauber calculations of DiGiacomo and DeVries[14] for the $^{12}C+^{12}C$ system, which include all of these effects and are shown in Fig. 2 (dotted and dashed lines), give reaction cross sections for this system which are only sightly different (<5%) from the simpler Glauber calculations of Ref. 1. This is apparently the result of a near cancellation between effects (1) and (2), which tend to decrease σ_r, and effect (3) which tends to increase σ_r.

Detailed calculations for this heavier system are clearly needed to investigate whether nuclear potential effects remain in balance with the effects of Fermi motion and Pauli blocking. In any case, we can identify no reasonable mechanism which might lead to near cancelation of these effects in the $^{12}C+^{12}C$ system but not in the $^{12}C+^{90}Zr$ system. As demonstrated in Ref. 3 and Ref. 14 where the inclusion of these effects had negligible influence above 25 MeV/A, effects (1)-(3) are expected to decrease markedly with bombarding energy. While a single high experimental value of σ_r at 15 MeV/A might plausibly be accomodated within the Glauber model, the overall energy dependence of σ_r for $^{12}C+^{90}Zr$ would seem to require a significant departure from existing Glauber descriptions.

---

a NPL,University of Washington, Seattle, WA

References

1. R. M. DeVries and J. C. Peng, Phys. Rev. C22,1055 (1980).
2. W. Czyz and L. C. Maximon, Ann. of Phys. 52,59(1969).
3. N. J. DiGiacomo, R. M. DeVries, and J. C. Peng, Phys. Rev. Lett. 45,527(1980).
4. M. Buenerd et. al., Phys. Lett. 102B,242 (1981); M. Buenerd et. al., Phys. Rev. C26, 1299(1982).
5. A. J. Cole et. al., Phys. Rev. Lett. 47, 1705(1981).
6. R. M. DeVries et. al., Phys. Rev. C26,301 (1982).
7. H. G. Bohlen et. al., Z. Phys. A308,121 (1982). .IO
8. C. Perrin et. al., Phys. Rev. Lett 49,1905(1982).
9. S. Kox et. al., Nucl. Phys. A420,162(1984).
10. M. Buenerd et. al., Nucl. Phys. A424,313 (1984).
11. S.H. Simon, et. al., Nucl. Phys. A340,249(1984).
12. J. A. McIntyre, K. H. Wang, and L. C. Becker, Phys. Rev 117,1337(1960).
13. G. R. Satchler and W. G. Love, Phys. Rep. 55,183(1979).
14. N. J. DiGiacomo and R. M. DeVries, Comments Nucl. Part. Phys. 12,111(1984).
15. P. U. Renberg et. al., Nucl. Phys. A183,81 (1972).

A STUDY OF EVAPORATION RESIDUES PRODUCED IN THE REACTION $^{14}N + ^{154}Sm$ AT 35 MeV/A.M.U.

G. Nebbia[a], D. Fabris[a], K. Hagel[a], Z. Majka[a], G. Mouchaty[a], J.B. Natowitz[a], R.P. Schmitt[a], M.N. Namboodiri[b], H. Ho[c], P. Gonthier[d], B. Wilkins[e]

Measurements of Linear Momentun Transfer (LMT) and Angular Momentum Transfer (AMT) in heavy ion collisions in the intermediate energy range (10-100 MeV/U) can provide some information on the partial wave dependence of the reaction mechanisms involved.

Comparisons with statistical model calculations can give some indications as to whether these processes still lead to statistically equilibrated systems or not.

A standard experimental technique to estimate the LMT consists in measuring the evaporation residue (ER) velocity distributions (1) or (if the system is heavy enough) the fission fragment correlation angle (2).

We have attempted to establish a trend in the LMT distribution by comparing experimental results obtained in the reaction 490 MeV ^{14}N + ^{154}Sm with the predictions of the code LILITA (statistical model) (6).

The experiment was performed in the 60" scattering chamber at NSCL bombarding a 250 microgram/cm2 ^{154}Sm target with the 35 MeV/U ^{14}N beam.

In order to get the ER mass and velocity distributions we used a microchannel-plate-SBD time of flight arm which was our master trigger; we also measured gamma-ray multiplicities in coincidence with the ER by means of four 3" by 3" NaI detectors.

The experimental setup is shown in Fig. 1.

The data were recorded on an event-by-event basis and analyzed later at the Texas A & M University.

The measured ER velocity distribution is shown in Fig. 2.

In order to get an estimate of the LMT we transformed the raw velocity distribution into the $\frac{1}{v^2}\frac{\partial^2\sigma}{\partial v \partial \Omega}$ double differential cross section

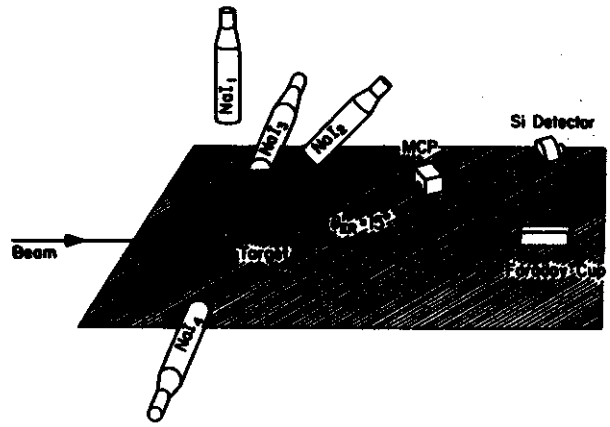

Fig. 1 Experimental setup

and we relate the fraction of LMT to the velocity using the approximate relation (3):

$$\frac{P_{11}}{P_{in}} = \frac{M\ target}{M\ proj.} = \frac{v_{er}}{v_{Proj.} - v_{er}}$$

The LMT distribution of Fig. 3 peaks at a value lower than total momentum transfer

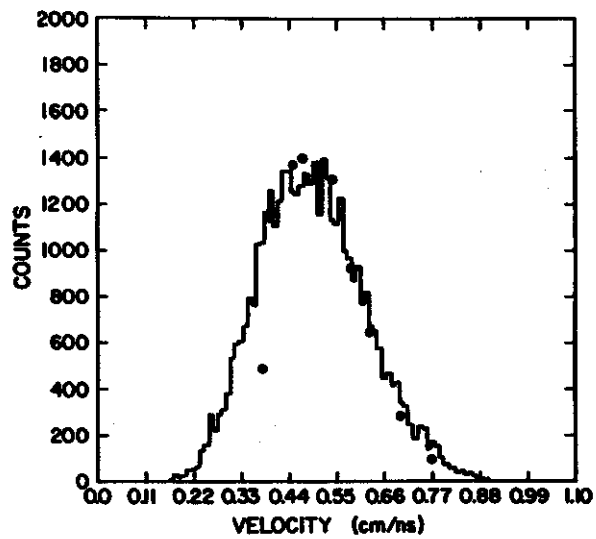

Fig. 2 Residue velocity distribution (symbols) compared to the weighted convolution of the calculated velocity spectra (histogram)

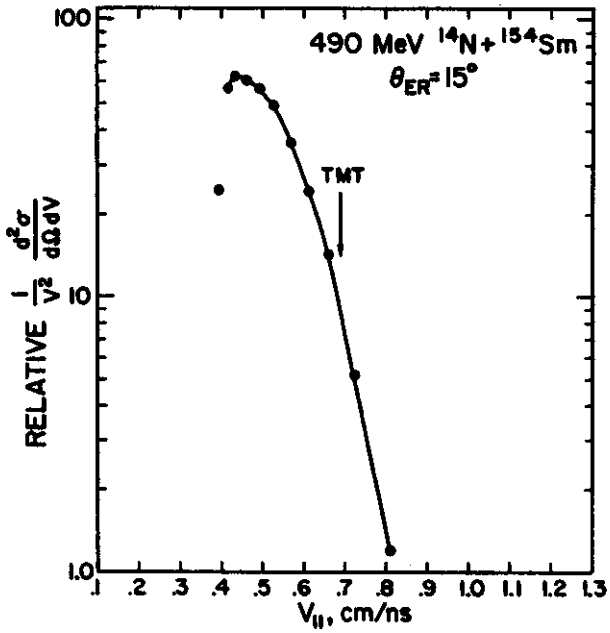

Fig. 3 Residue velocity distribution transformed. Velocity corresponding to full momentum transfer is indicated.

consistent with earlier systematic observations. The sharp cut occurring at V=.4 cm/ns represents our experimental threshold due to the instrumental difficulty in detecting heavy residues of mass around 130-150 a.m.u. with energies of a few MeV.

We present in Fig. 4 the experimental ER

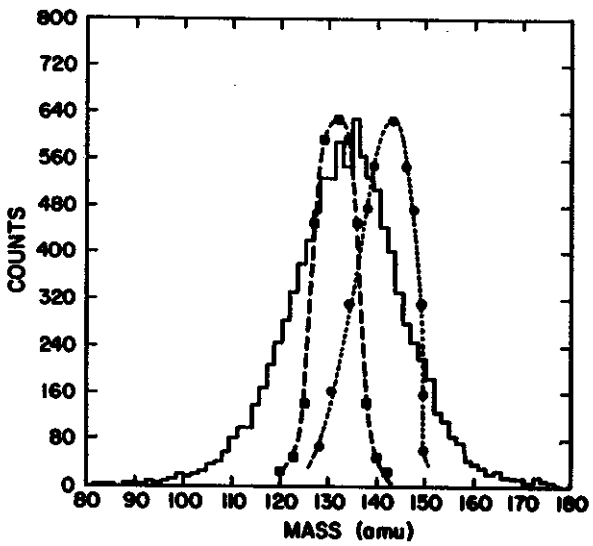

Fig. 4 Residue mass distribution (histogram), calculated mass distribution (dashed line), mass distribution for the reaction 420 MeV ^{12}C + ^{154}Sm of Ref. 5 (dotted line).

mass distribution. We have employed the scheme of Kaufman et al. (4) to correct the observed energies for the pulse height defect. As a test of our method we compare the radiochemically determined mass distribution for the similar reaction 420 MeV ^{12}C + ^{154}Sm (5).

The broader distribution in our case probably reflects the difficulty in accurately ascertaining the pulse height defects which represent a significant part of the total energy for such low velocity recoils.

Recognizing that there are some uncertainties in the process, one can, neverless compare the mass distributions for different regions of ER velocity to observe trends in those distributions. In Fig. 5 mass distributions derived for three different regions of LMT are presented.

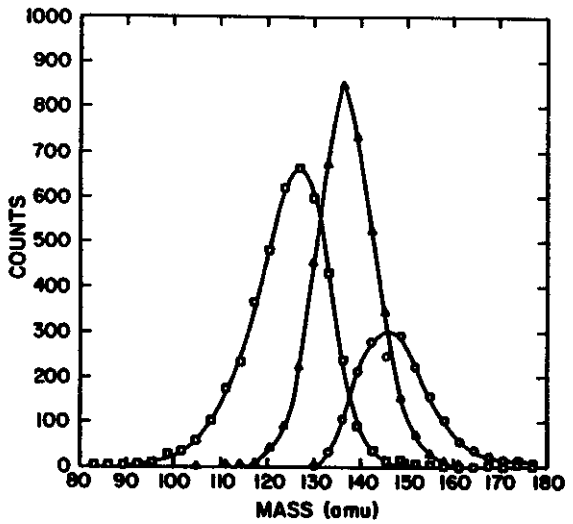

Fig. 5 Residue mass distribution for three different windows of fractional momentum transfer: <LMT>=.925 (squares); <LMT>=.775 (triangles); <LMT>=.625 (circles).

As the LMT, and therefore the exitation energy, increases we notice a shift toward lower masses. It seems therefore reasonable to consider the full process as a convolution of different entrance channels, each leading to a thermally equilibrated system that evaporates particles in a statistical way.

In order to test such an assumption we have attempted to reproduce the experimental velocity

distribution convoluting, with appropriate weights, the calculated velocity spectra corresponding to different values of LMT.

The result is represented by the histogram in Fig. 2.

We used the same weighting factors to sum the corresponding calculated mass spectra; a comparison with the experimental mass distribution is shown in Fig. 4.

The measured gamma-ray multiplicities give an average angular momentum transfer <L> = 21 ħ throughout the velocity distribution.

Calculations are currently underway in order to compare this result with recent models.

---

a Cyclotron Institute Texas A&M University, College Station, Texas

b Nuclear Chemistry Division Lawrence Livermore Laboratory, Livermore CA

c Institut für Kernphysik Heidelberg, Federal Republic of Germany

d Physics Department Hope College, Holland, MI

e Chemistry Division Argonne National Laboratory, Argonne, IL

1. H. Morgenstern et al., Z Physik A313,39(1983)
2. G. Nebbia et al., Z. Physik A311,247(1983)
3. B. Borderie et al., Z. Physik A316,243(1984)
4. S.B. Kaufman et al., Nucl. Inst. and Meth. 115,47(1974)
5. K. Aleklett et al., (preprint)
6. J. Gomez del Campo and R.G. Stokstad, ORNL Report ORNL TM 7295(1981)

The failure of the sum rule model at the higher bombarding energies can be understood in terms of the fact that the same range of entrance channel partial waves leads to complete fusion, α transfer, etc., regardless of the incident projectile energy. Thus, a configuration in which the nuclei are barely touching will lead to complete fusion at 8.5 and 35 MeV/nucleon projectile energy. This is simply unrealistic given the difference in projectile trajectories at low and intermediate energies.

---

1. J. Wilczynski, K. Siwek-Wilczynska, J. van Driel, S. Gonggrijp, D.C.J.M. Hagemann, R.V.F. Janssens, J. Lukasiak, and R.H. Siemssen, Phys. Rev. Lett. 45,606(1980).
2. C. Toepffer, Z. Physik, 253,78(1972).
3. P.L. McGaughey, LBL-15325, November 1982.
4. A.M. Zebelman and J.M. Miller, Phys. Rev. Lett. 30,27(1973).

OBSERVATION OF HIGH ENERGY GAMMA RAYS IN INTERMEDIATE ENERGY NUCLEUS-NUCLEUS COLLISIONS

K.B. Beard, W. Benenson, C. Bloch, E. Kashy, J. Stevenson, D.J. Morrissey, J. van der Plicht, B. Sherrill, and J.S. Winfield

Recent measurements of subthreshold pion production at very low energies[1,2,3] have yielded cross sections too large to be explained by incoherent processes. Other manifestations of coherent processes such as the production of gamma rays, electrons and nucleons with energies approaching the total energy available in the laboratory system have received little attention. High fluxes of leptons are often observed in detection systems but are usually attributed to uncharacterised background. During an experiment to measure charged pion production for ^{14}N + Cu collisions at E/A = 40 MeV using an Enge split-pole magnetic spectrograph[4], a much larger than expected background of high energy electrons and positrons was observed. By comparison of the target-in to target-out spectra, it was deduced that most of the leptons were produced by gamma rays from the Faraday cup which were converted to electron-positron pairs in the material of the entrance aperture of the spectrograph. The possibility that the production of these high energy γ-rays might have a large cross section and be an important probe of the collision convinced us to convert the experiment to a measurement of high energy γ production.

The method for the detection of the high energy gamma rays was to convert the photons to electron-positron pairs right at the target and measure the energy spectrum of the electrons and positrons with an Enge magnetic spectrograph. The beam was $^{14}N(5+)$ accelerated by the K500 cyclotron to an energy E/A = 40 MeV. The target was 0.77 g/cm^2 of Cu, which is sufficiently thick to stop the ^{14}N ions. The target was backed with a 3 g/cm^2 converter of either Be, Cu, or Pb. The three converter elements (including target) had very different conversion efficiencies (4%,13%,and 24% for 50 MeV gamma rays) which permitted the separation of the yield of electrons and positrons due to the pair conversion of gamma rays from that originating from other background sources.

The position-sensitive element of the detector telescope was placed on the focal plane of the Enge split pole spectrograph and consisted of a multiwire proportional counter designed for efficient detection of fast singly-charged particles at 45° incidence[5]. It was backed by a plastic scintillator and two plastic Cherenkov detectors, all 2.5 cm thick. During analysis, the requirement for a valid event was that both planes of the proportional counter, the scintillator and both Cherenkov counters fire. A variety of tests were conducted to check that the electrons and positrons had energies consistent with those calculated from the field setting of the spectrograph. Absorbers were placed between elements, and the detector responded as one would expect for electrons. The detector was calibrated using electrons from the beta decay of ^8Li (13.1 MeV endpoint). The ^8Li were made by bombarding a Be target with the same ^{14}N beam.

The positron energy spectra taken at a laboratory angle of 17° are shown in figure 1 for the three different converters. In order to obtain a γ-ray yield, a Planck distribution of the form

$$\frac{dN}{dE} = \frac{K E^2}{e^{E/T} - 1}$$

and a exponential form ($Ke^{-E/T}$) for the gamma ray distribution were assumed. In these equations, K is the overall normalization. For the Planck form, T is a temperature, and in the exponetial form, T is the slope parameter. Fitting was done by simulating the converter plus spectrograph system in a Monte Carlo program which included multiple scattering and

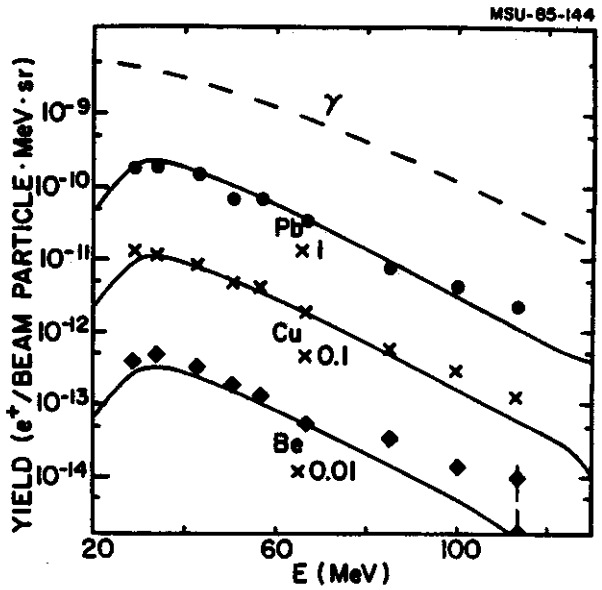

Figure 1. The data points give the e^+ yield as a function of energy for ^{14}N + Cu at E/A = 40 MeV for three different converters at θ_{Lab} = 17°. The dashed curve shows an assumed γ-ray yield based upon a thermal source and the solid curves show results of the Monte Carlo calculation described in the text for the conversion positrons.

the momentum sharing by the electron positron pair[8]. The electron or positron was assumed to be emitted at zero degrees with respect to the gamma ray, which is a good approximation for pair production at these energies. The best fit thermal photon spectrum and resultant positron spectra are shown in figure 1. The temperature parameters for a Planck distribution at 0°, 17°, and 40° are 12.1 ± 2, 12.2 ± .8, and 10.7 ± 1.4 MeV, respectively and the slope parameters are 16.9 ± 3, 17.5 ± 2, and 15.0 ± 2.5 for the exponential form. Since a stopping target was used, only the thick target cross section was measured. It is most probable, however, that the cross section increases rapidly with increasing beam energy, and that the present measurement is equivalent to a thin target measurement at a beam energy not far below 40 MeV/A. Clearly, any quantitative comparison with theoretical predictions would require an assumption concerning the beam energy dependence of the cross section.

One way to compare theoretical models to the results of the present experiment is to assume a Planck form for the gamma ray distribution and to use a beam energy dependence in which the temperature of the source is proportional to the beam energy. The yield can then be calculated by integrating over the beam energy. Corrections can also be made for the Doppler shift of the gamma rays using a source velocity taken from the fireball model[7] (β= 0.117). With this energy dependence and assuming isotropy, we obtain a total cross section of .65 mb. at E/A = 40 MeV for production of photons of energy above 25 MeV.

The positron energy spectra at 0°, 17°, and 40° show little difference, as can be seen in fig. 2. Multiple Coulomb scattering in the converter would smooth the angular dependence. This is expected for low energy positrons (θ_{rms}=27° for 20 MeV gamma rays in the Pb converter), but the high energy positrons (E(e^+) >70 MeV) should closely follow the angular distribution of the gamma rays (θ_{rms}=8° at 70 MeV).

Vasak et. al[9] have suggested that nucleus-

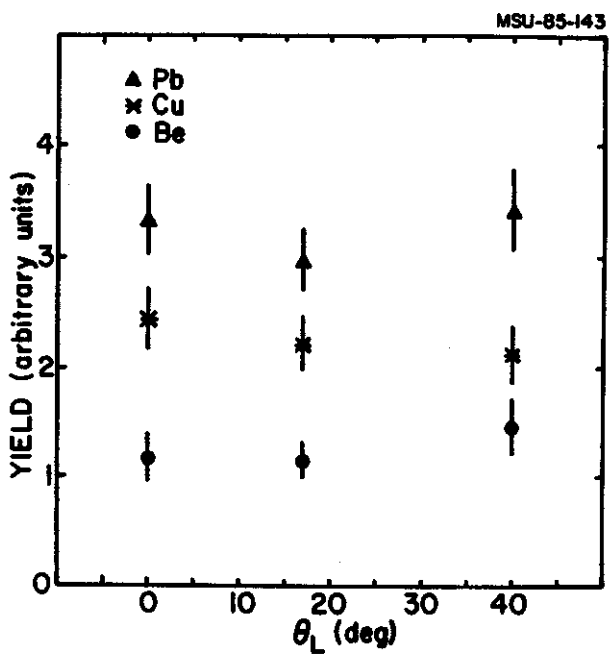

Figure 2. The angular distribution of high energy (70-105 MeV) e^+ for the Pb, Cu, and Be converters.

nucleus bremsstrahlung may be the mechanism of pion production at these intermediate energies and that high energy gamma rays should also be produced. The bremsstrahlung model we have used to compare to our data is based on the earlier work of Budiansky et al.[10,11]. The model treats the projectile and target as uniform density spheres which interpenetrate and come to rest without changing shape. The velocities of the nuclei in the center of mass are assumed to exponentially decay with a characteristic stopping time τ_s. All motion is assumed to take place parallel to the beam axis. This last condition, while simplifying the problem, results in a quadrupole angular distribution with zeroes at θ=0°, 180° and another minimum at 90°. There is no hint of this structure in the data which is more suggestive of thermal production. Nevertheless, in figure 3 the angle-averaged calculated bremsstrahlung energy spectrum is compared with the data. Note the strong dependence of the bremsstrahlung yield on the stopping time τ_s. A stopping time τ_s=15 fm/c gives the best fit to the gamma ray yield and roughly reproduces the slope of the energy spectrum. This stopping time is considerably longer than the value of 6 fm/c obtained by Vasak et al. in analyzing the π^0 data from 35 MeV/A ^{14}N+Ni of ref. 9.

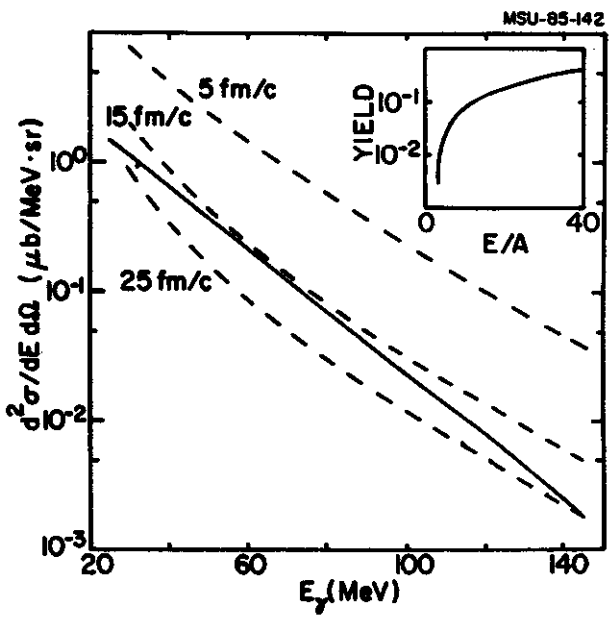

Figure 3. Calculated bremsstrahlung production with stopping time τ_s = 5, 15, and 25 fm/c (dashed curves). The insert shows the beam energy dependence of 50 MeV photons in this process assuming τ_s = 15 fm/c. The solid line is the gamma yield at 40 MeV/A estimated from the data assuming the bremsstrahlung model's beam energy dependence.

Ko et al.[12] have recently calculated gamma ray bremsstrahlung in a cascade framework. Although this model is not applicable to beam energies as low as in the present work, a conclusion of their calculation is that incoherent bremsstrahlung due to neutron-proton scattering dominates the bremsstrahlung yield for all but the heaviest systems. This incoherent bremsstrahlung is nearly isotropic much like our data. Their calculation predicts a 1/E gamma ray energy dependence, which is less steep than the data.

The source of these high energy gamma rays is an interesting question which will require further work, both experimental and theoretical. An improved experiment designed to convert the photons to a electron-positron pairs at the front of a stack of Cherenkov counters has already been approved. If the source is thermal, comparisons between the π^0 and γ yields may give new insights into the hot region. If the source is nucleus-nucleus bremsstrahlung, high energy gamma rays may prove to be a powerful new probe of the dynamics of nucleus-nucleus collisions and may serve as a signature for central collisions.

1. H. Heckwolf, E. Grosse, H. Dabrowski, O. Klepper, C. Michel, W.F.J. Müller, H. Noll, C. Brendel, W. Rösch, J. Julien, G.S. Pappalardo, G. Bizard, J.L. Laville, A.C. Mueller, and J. Peter, Z.Physik A315,243(1984).
2. H. Noll, E. Grosse, P. Braun-Munzinger, H. Dabrowski, H. Heckwolf, O. Klepper, C. Michel, W.F.J. Müller, H. Stelzer, C. Brendel, and W. Rösch, Phys. Rev. Lett.52,1284(1984).
3. P.Braun-Munzinger, P. Paul, L. Ricken, J. Stachel, P.H. Zhang, G.R. Young, F.E. Obenshain, and E. Grosse, Phys. Rev. Lett.52,255(1984).
4. J.E. Spencer and H.A. Enge, Nucl.Instrum. Methods 49,181(1967).
5. K. Beard, W. Benenson, E. Kashy, B. Sherrill, J. van der Plicht, J. Yurkon, Michigan State

University Annual Report 1982-83,p.102(1984).
6. J. Gosset, H.H. Gutbrod, W.G. Meyer, A.M. Poskanzer, A. Sandoval, R. Stock, and G.D. Westfall, Phys.Rev.C16,629(1977).
7. H.A. Bethe and L.C. Maximon, Phy.Rev.93 768(1984).
8. T. deReus and W. Greiner, private communication.
9. D. Vasak, W. Greiner, B. Mueller, Th. Stahl, M. Uhlig, Nucl. Phys. A428,291c(1984).
10. M.P. Budiansky, Ph.D. thesis, University of California, Berkeley, 1981(unpublished).
11. M.P. Budiansky, S.P. Ahlen, G. Tarle, and P.B. Price, Phys. Rev. Lett. 49,361(1982).
12. C.M. Ko, G. Bertsch, and J. Aichelin, private communication.

EXCITED STATES OF LIGHT FRAGMENTS AND NUCLEAR TEMPERATURES

D. J. Morrissey, W. Benenson, E. Kashy C. Bloch, M. Lowe, R. A. Blue, R. M. Ronningen, B. Sherrill, and H. Utsunomiya

We have recently proposed and made an independent test of the existence of a thermalized zone in heavy-ion reactions in a recent measurement of the distribution of complex fragments among their excited states.[1] The principle of equal partition of energy among the degrees of freedom of a system dictates that the temperature of such a thermalized system will be reflected in the excited state populations as well as in kinetic energy of motion. The initial measurements of the population of the excited states of lithium and beryllium nuclei observed near 90° from the reaction of 490 MeV ^{14}N with silver showed much lower populations than those expected for temperatures determined from their velocity distributions.[1] Simple estimates of the temperatures by the two methods were different by more than an order of magnitude. Such a discrepancy would have important consequences for thermal models of heavy-ion reactions and therefore needed to be verified. Here we report a new measurement of the production of excited states of lithium and beryllium nuclei from the reaction of 490 MeV ^{14}N with Ag. The experimental technique used in our previous measurement was improved so that accurate values of the small fractions of nuclei in excited states could be obtained.

The ^{7}Li and ^{7}Be nuclei are particularly good probes of statistical equilibrium for three reasons: (a) they have virtually only one excited state that decays by γ-ray emission[2], and this state can not be appreciably fed from above, (b) the gamma emitting states of both A=7 nuclei are spin $^{1}/_{2}^{-}$, and therefore the states decay by isotropic γ-ray emission, and (c) the two nuclei have slightly different feeding from unbound higher mass nuclei, which provides an internal check on the importance of any feeding. However, the energy level spacings of ^{7}Li and ^{7}Be are only 478 and 429 keV, respectively, and this limits the sensitivity of their population distributions to temperatures of a few MeV or less. Two other lithium nuclei, ^{6}Li and ^{8}Li, are also good probes of temperature over a broader range. The excitation energy of the levels are 981 and 3562 keV with spins of 1+ and 0+ for the ^{8}Li and ^{6}Li nuclei, respectively. These latter nuclei also have only one excited state that decays by γ-ray emission,[2] but the ^{6}Li γ-ray is difficult to measure, and the ^{8}Li γ-ray is anisotropic.

In the simplest picture with no particle decay, the ratio, R, of the populations of two states is:

$$R = \frac{(2 j_{EX} + 1)\ e^{-\Delta E/kT}}{(2 j_{GS}+1)} \qquad (1)$$

where j_{GS} and j_{EX} are the spins of the ground and excited states, respectively, and ΔE is the energy difference between the states. This ratio is not directly measurable as the lifetimes of the γ-ray emitting states under consideration are short compared to the flight time of the nuclei from the target to the particle detectors. Thus, γ-ray detectors can measure the excited state populations via their decay while particle detectors can measure the production of both the excited and ground states. The ratio of the two measurements is the fraction, f, in the excited state and is related to the population ratio by the equation: $f = R / (1 + R)$. Under the assumption of thermal equilibrium the dependence of the fraction, f, with temperature is the simple expression plotted in fig. 1 for the lithium and beryllium nuclei suitable for these studies.

A beam of 490 MeV $^{14}N^{5+}$ ions was provided by the K500 cyclotron. The target was a self supporting foil of natural silver, 2.0 mg/cm^2

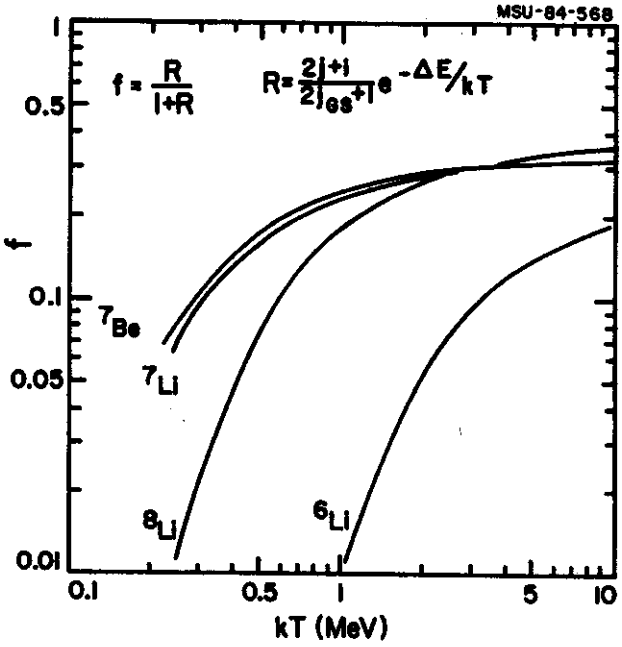

Fig. 1. The fraction of nuclei in their excited states as a function of temperature for a system in thermal equilibrium, see text.

thick, with its plane at 45° with respect to the beam. The beam intensity was generally between 0.1 and 0.3 particle nA. Such a low beam intensity was used to maintain the count rates in the γ-ray detectors below 20 thousand per second, and thereby avoid gain shifts.

The light ion products were detected in a set of two-element Si surface barrier telescopes located at +50°, ±70°, and -90° with respect to the beam (positive angles clockwise with respect to the beam). Placing the particle telescopes at these large angles reduces the possibility of detecting projectile fragments or direct reaction products (the classical grazing angle is only 5°). The first element of each particle telescope was either a 100 μm (+50°, -90°) or a 50 μm (±70°) ΔE detector, and the second element of each particle telescope was a 1000 μm E detector. A set of eight NaI(Tl) scintillation detectors, 7.6 cm x 7.6 cm right cylinders, were used to detect γ-rays in coincidence with the particles. The center lines of the detectors were placed above the scattering plane on the surface of a right cylindrical cone, centered on the target. The good resolution (≤6.5% at 662 keV) of the NaI(Tl) scintillators (as compared to 14% for the BGO's in the previous work) was necessary for the present study to determine accurately the small value of the population of the excited states (approximately 0.1) in the presence of approximately 10 continuum γ-rays from the target residue. The overall efficiency of the coincidence electronics was measured with a ^{249}Cf source. This source emits an α-particle in coincidence with a 388 keV γ-ray which allowed us to measure the coincidence efficiency of the entire setup including the effect of γ-ray absorbers, the electronics, and data acquisition computer.

The inclusive energy and angular distributions of the fragments were obtained for comparison to our previous study and as input for the moving-source model fits. The laboratory energy spectra of all the lithium and beryllium isotopes range between 20 and 120 MeV and exhibit an exponential slope. A chi-squared minimization procedure was used to obtain the best values of the parameters of a Maxwell-Boltzmann function. The source parameters for the various isotopes fluctuated about the averages, $\langle T \rangle = 12. \pm 2.$ MeV and $\langle v \rangle = 2.2 \pm 0.3$ cm/ns. The slope parameters or temperatures extracted from this data are very close to that expected from previous systematics. If we accept the average temperature of 12 MeV at face value, we would expect from the Boltzmann factor to find f = 0.32, 0.35 and 0.33 for ^{7}Li, ^{8}Li and ^{7}Be, respectively.

Figure 2 shows the summed γ-ray spectra in the fragment rest frame (fragments emitted at 70° in the laboratory) for the beryllium and three lithium nuclei. The γ-ray corresponding to the decay of the excited state is clearly visible for ^{7}Li, ^{8}Li and ^{7}Be as is some hint of the random coincidence source, ^{137}Cs, now broadened by the variation in the various Doppler shifts. We note that the ^{7}Li γ-ray is broader than expected and that a small "bump" is visible in the ^{6}Li spectrum, fig. 2B, near 500 keV, probably due to a target γ-ray or annihilation radiation. None the less, only a

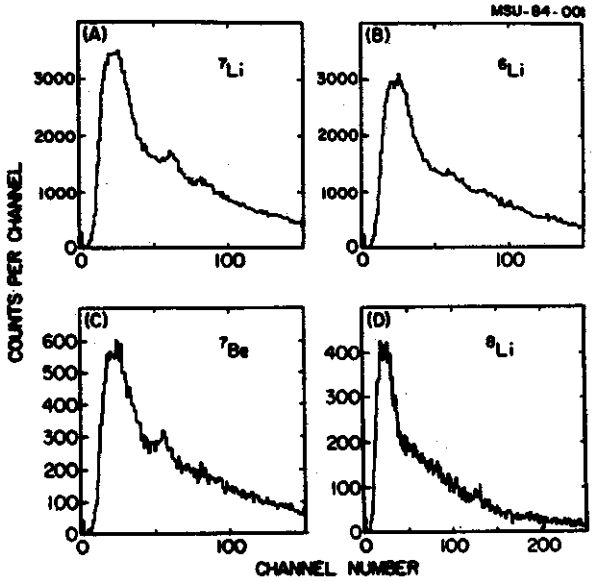

Fig. 2. Random-corrected coincident γ-ray spectra in the rest frame of ^{7}Li, (A); ^{6}Li, (B); ^{7}Be, (C); and ^{8}Li, (D). Note the compressed energy scale for ^{8}Li.

small fraction of the γ-rays expected from a Boltzmann distribution were observed.

The fraction of nuclei in the excited state was obtained from the number of counts in the full energy γ-ray peak of each isotope at each angle, N_γ, with the expression:

$$f = \frac{N_\gamma}{\varepsilon_\gamma} \frac{1}{N_I} \frac{1}{\mu C} \qquad (2)$$

where ε_γ is the total photopeak efficiency of the eight γ-ray detectors, N_I is the number of inclusive fragments per microCoulomb of beam current and μC is the number of microCoulombs during the coincidence run. The statistical errors and systematic errors in evaluating in N_γ dominated the other sources of error. The number of γ-rays and the corresponding fractions are given in Table I and are compared to the previous measurement in fig. 3. The present results indicate that the fraction does not

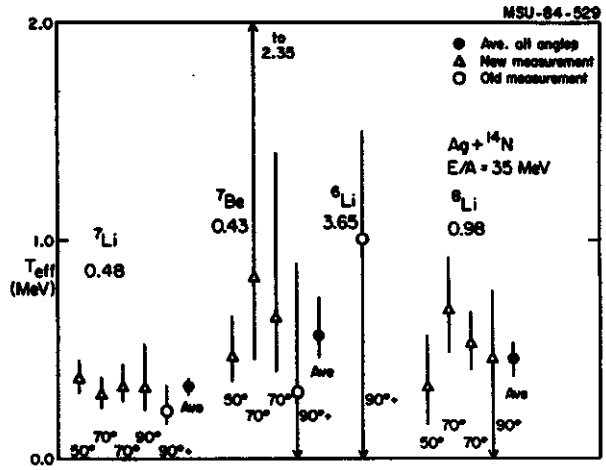

Fig. 3. The calculated fraction of the nuclei in their excited states from this and the previous measurements [1].

TABLE I. Summary of Numerical Results

Isotope	E_γ(MeV)	f(ke*)	Angle	Counts	f(obs)	kT† (MeV)	
^{7}Li	0.478	0.32	50°	1546 ± 252	.119 ± .025	.370	+.08 /-.07
			70°	477 ± 152	.091 ± .034	.295	+.09 /-.07
			-70°	620 ± 164	.106 ± .033	.330	+.10 /-.07
			-90°	117 ± 68	.102 ± .064	.325	+.20 /-.10
^{8}Li	0.981	0.35	50°	51 ± 38	.027 ± .022	.330	+.08 /-.15
			70°	76 ± 29	.123 ± .052	.680	+.24 /-.20
			-70°	59 ± 24	.081 ± .037	.520	+.14 /-.13
			-90°	9 ± 12	.061 ± .081	.455	+.31 /-.46
^{7}Be	0.428	0.33	50°	422 ± 81	.168 ± .040	.480	+.18 /-.12
			70°	194 ± 47	.229 ± .066	.830	+1.5 /-.37
			-70°	200 ± 49	.209 ± .062	.650	+.75 /-.25
			-90°	0 ± 15	.0 ± .135	.0	+.38 /-.0

notes: * From fitting kinetic energy spectra, see text.

† Simple result representative of the population distributions. The errors are asymmetric due to the logarithmic function.

depend on angle over the 40° degree angular range studied, and that small differences are observed among the three average values of the fraction. However, all three fractions give a temperature which is more than an order of magnititude lower than those expected from the kinetic energy spectra.

The main purpose of the present experiment was to verify the very low excited state production observed in a previous experiment[1] which was quite limited by statistics. The present results have much better precision, and additional nuclei were studied. However the conclusion is the same, namely that the fraction of nuclei in excited states is substantially smaller than expected from models of the reaction which assume equilibrium. More refined models of the reaction mechanism in the future will need to predict this new measurable quantity, the excited state production, as well as the energy spectra and angular distributions produced in the reaction.

---

1. D.J. Morrissey, W. Benenson, E. Kashy, B. Sherrill, A.D. Panagiotou, R.A. Blue, R.M. Ronningen, J. van der Plicht and H. Utsunomiya, Phys. Lett. 148B, 423 (1984).
2. F. Ajzenberg-Selove, Nucl. Phys. A413, (1984) 1; only one state has been observed to γ-decay for both ^{7}Li and ^{7}Be; ^{8}Li and ^{8}Li each have only one state with a significant γ-ray branch.

PRODUCTION OF EXCITED STATES IN THE REACTION OF ^{14}N WITH ^{12}C

D. J. Morrissey, W. Benenson, E. Kashy, C. Bloch, M. Lowe, R. A. Blue, R. M. Ronningen, B. Sherrill, and H. Utsunomiya

We have recently proposed and made an independent test of the existence of a thermalized zone in heavy-ion reactions in a recent measurement of the distribution of complex fragments among their excited states.[1] The initial and the follow-up measurements of the population of the excited states of lithium and beryllium nuclei observed near 90° from the reaction of 490 MeV ^{14}N with silver showed much lower populations than those expected for temperatures determined from their velocity distributions. This leads to the conclusion that either the nuclear system is not in thermal equilibrium or that the population ratio has been altered by nuclear structure effects (e.g., sequential decay). In order to determine the validity of the technique we have recently measured the production of light fragments in their ground and excited states in a compound nuclear system that has been shown by previous workers to be in full thermal equilibrium[2].

Beams of 8, 12, 15, 20 and 25 MeV/A ^{14}N ions from the K500 cyclotron were used to irradiate a self supporting foil of natural carbon, 0.5 mg/cm^2 thick, with its plane at 45° with respect to the beam. The light ion products were detected in four ΔE/E Si surface barrier telescopes located at +30°, +50°, -40° and -60° with respect to the beam (positive angles clockwise with respect to the beam). After approximately 12 hours of data acquisiton the particle telescopes were shifted to larger angles by 5°, and data acqusition continued for approximately 12 hours more. Thus we obtained a rather large set of data over a broad angular range. The γ-rays in coincidence with the light charged particles were detected in a set of eight NaI(Tl) scintillation detectors, 7.6 cm x 7.6 cm right cylinders. The overall efficiency of the coincidence electronics was measured with a ^{249}Cf source was discussed before[1].

The inclusive energy and angular distributions of the fragments were obtained for comparison to previous studies and as input for the moving-source model fits. We fully expect that the the fragments would be emitted from the compound nucleus, and so the velocity and temperature of the so-called moving-source should be those of the compound nucleus. The results of a preliminary fit to some of the isotopes from the reaction of 112 MeV ^{14}N with carbon are shown in figure 1. The fitted source parameters for the various isotopes are more or less consistent with the expected values.

Fig. 2 shows the γ-ray spectra (summed for all the NaI(Tl) detectors) in the fragment rest frame (fragments emitted at 35° in the laboratory). The γ-ray corresponding to the decay of the excited state is clearly visible in contrast to the previous studies because the number of γ-rays emitted by the reaction partner is small. However, in contrast to earlier studies, a large amount of annhilation radiation is present in the vacinity of the peaks of interest. Note that the spectrum in coincidence with ^6Li represents the background for the other isotopes.

The main purpose of the present experiment was to verify the production of nuclear excited states in a well known system. The recent experiment has been only partially analyzed. The preliminary results show that the moving source parameters are consistent with the expected results. The fraction of the ^7Be fragments in their excited state was 0.3 ± 10%, in agreement with thermal equilibrium at 112MeV. However, the fraction of ^7Li nuclei in their excited is lower, 0.04 ± 10%. This indicates a

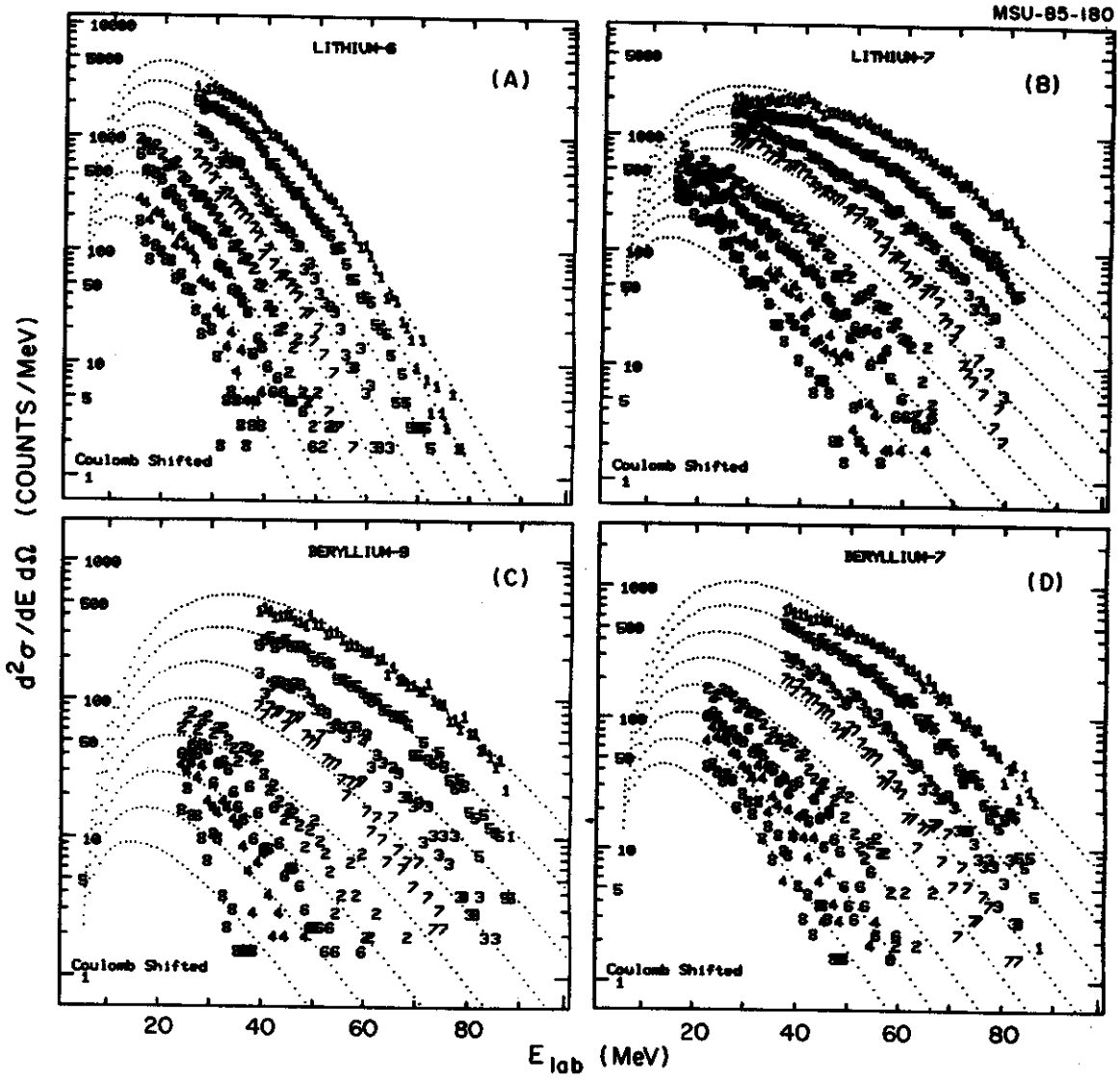

1. The laboratory kinetic energy spectra for fragments from the reaction of 112 MeV ^{14}N with C and the results of moving sources fits, see text.

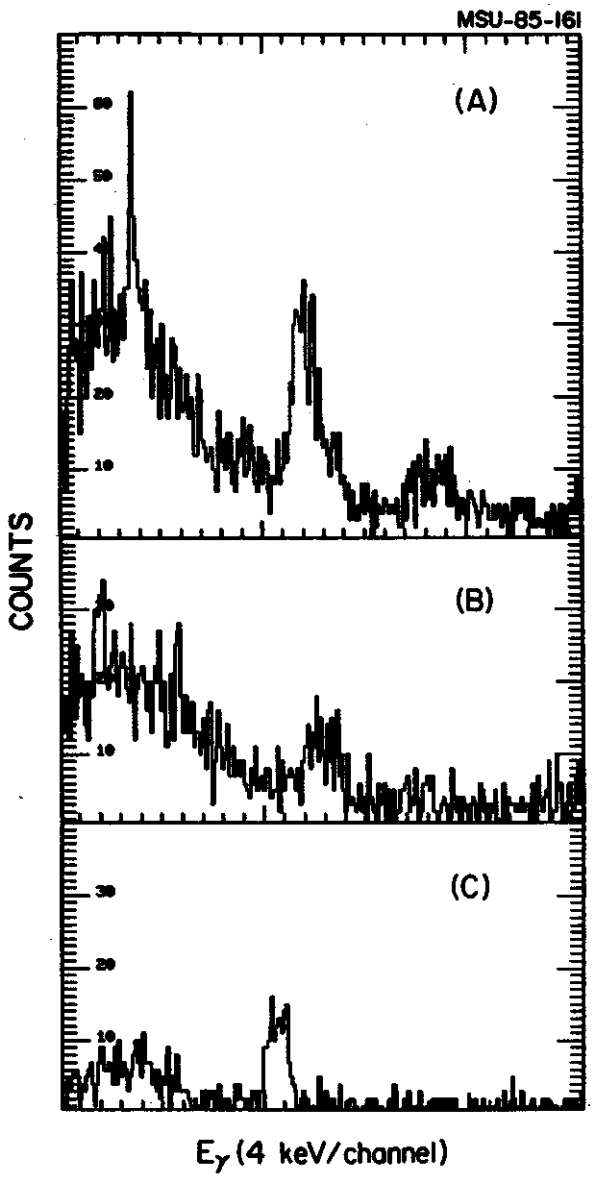

2. Random-corrected coincident γ-ray spectra in the rest frame of ^{7}Li, (A); ^{8}Li, (B); ^{7}Be, (C).

additional contribution to the production of the latter nuclei. Further analysis of this data is continuing which should yield a large amount of information and demonstrate the visibility of our new technique.

1. D.J. Morrissey, W. Benenson, E. Kashy, B. Sherrill, A.D. Panagiotou, R.A. Blue, R.M. Ronningen, J. van der Plicht and H. Utsunomiya, Phys. Lett. 148B, 423 (1984).
2. J. Gomez del Campo, et al., Phys. Rev. C29 1722,(1984), and references therein.

INCLUSIVE FRAGMENT SPECTRA FROM COLLISIONS OF 35 MeV/NUCLEON ^{14}N WITH ^{165}Ho.

G. Caskey, B. Remington, A. Galonsky, M.B. Tsang, C.K. Gelbke, A. Kiss[a], F. Deak[b], Z. Seres[c], J.J. Kolata[d], J. Hinnefeld[d], and J. Kasagi[e]

This report will focus on a few aspects of inclusive fragment spectra obtained in an experiment designed to measure neutron-fragment coincidences. We shall focus on the momentum widths and optimum Q-values of the quasi-elastic, or fragmentation, peak. Momentum widths observed in our quasi-elastic peaks are not well described by the fragmentation model of Goldhaber[1]. In particular, the widths do not follow the trend suggested by the parabolic rule (Eq. 1 of Ref. 1), but this is also observed in other studies of projectile fragmentation at intermediate energies. Peak energies vary from isotope to isotope in a manner which is close to a simple estimate based on Coulomb energy considerations and on a "minimum-body" breakup of the projectile into one piece which is detected as a QE fragment and another which is unobserved, but is not directly transferred to the target.

Experimental details are given elsewhere[2]; the salient points are reported here. Fragment detectors were placed at 10° and 30° (lab angles). These detectors were either double or triple element ΔE-E particle identification telescopes. The front one or two elements were surface barrier detectors, and the rear element was a 5 mm thick Si(Li) device in both cases. The detector solid angles were approximately 10 msr, and the angles were known to within about 0.5°. An electronics failure in a prescaling unit excluded singles events in the 10° detector, but these were recovered in the accidental coincidences with neutrons by using singles measurements at 30°. The accidental coincidence rate A_θ for neutrons in one of the neutron detectors and fragments in the fragment detector at angle θ depends on the product of the singles rate of neutrons, N_n, and the singles rates of fragments at angle θ, F_θ. The relationship is given by $A_\theta = 2\tau N_n F_\theta$, where τ is the coincidence resolving time. If the fragment singles rate is known at, say, 30°, and the accidental coincidence rates are known at both 30° and 10°, then the 10° singles rate is just $F_{10°} = F_{30°}(A_{10°}/A_{30°})$. In practice, the rates are integrated over time and yields are used.

We acheived good mass separation by peak fitting of mass distributions gated on various fragment energies. The statistical accuracy of the data is generally on the order of a few to 10 percent. Reproduction of cross sections, in various fits of the mass distributions gated on a given fragment energy bin, was about ±20% for the smallest cross sections and better than ±5% for the largest.

Figure 1 shows the 10° inclusive momentum distribution for the ^{10}B isotope. Momentum

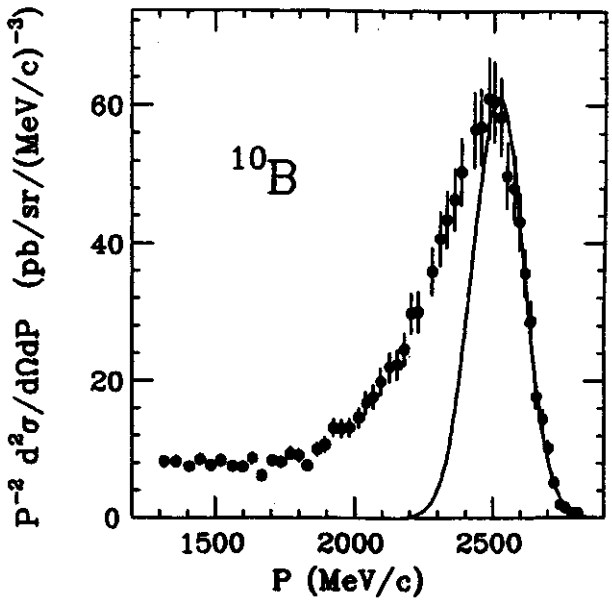

Fig. 1 Momentum distribution of ^{10}B fragments at 10° determined experimentally (points) and as fitted with a guassian momentum distribution (solid line).

widths and peak locations for isotopes of Be, B, and C were empirically determined by fitting the quasi-elastic peak, which was obvious in all spectra, with the expression

$$p^{-2}\, d^2\sigma/d\Omega dp \propto e^{-(p + p_0)^2/2\sigma^2}. \quad \text{(Eq. 1)}$$

This transforms into the energy distribution

$$d^2\sigma/d\Omega dE = \sqrt{\varepsilon_F}\, e^{-A^2u(\varepsilon + \varepsilon_0 - 2\sqrt{\varepsilon\varepsilon_0}\cos\theta)/\sigma^2}, \quad \text{(Eq. 2)}$$

where A is the fragment mass number, u=931.5016 MeV, σ is the momentum width in MeV/c, ε is the fragment kinetic energy per nucleon, p_0 is the fitted momentum centroid to which ε_0 corresponds, and θ is the fragment emission angle.

Optimum Q-values or, equivalently, fragmentation peak energies were extracted from the fits to the data (a sample fit is shown in Fig. 1). This peak energy ε_p is the energy where Eq. 2 has its maximum, and it differs from the value of ε_0. The general trend is that

Table I Quasi-elastic peak cross section locations determined from the data and from a calculation using Q-values as described in the text. Uncertainties determined from the χ^2 error matrix. The observed peak energies ε_p were obtained by the relationship between P_0 and ε_0 and the peak in the energy distribution implied by them. In general, ε_0 is not the peak in the energy distribution, but it is close.

	Quasi-elastic Peak Location			
Isotope	Observed peak cross section momenta and energies		Calculated peak cross section energies and Q-values	
	P_0 (MeV/c)	ε_p (MeV/nucleon)	ε_p (MeV/nucleon)	Q (MeV)
^{7}Be	1763 ± 65	33.24 ± 2.45	31.75	-27.82
^{9}Be	2223 ± 32	31.83 ± 0.92	32.19	-20.16
^{10}Be	2320 ± 6.4	28.29 ± 0.16	30.01[1]	-39.68[1]
^{10}B	2516 ± 46	33.05 ± 1.21	33.84	-11.61
^{11}B	2715 ± 19	31.79 ± 0.45	32.65	-20.74
^{12}B	2884 ± 120	30.19 ± 2.51	32.06	-25.09
^{13}B	-	-	29.97[2]	-20.20[2]
^{10}C	2611 ± 96	33.65 ± 2.47	32.51[3]	-35.08[3]
^{11}C	2839 ± 1.3	34.72 ± 0.03	33.40	-22.74
^{12}C	3064 ± 22	33.96 ± 0.49	34.14	-10.27
^{13}C	3259 ± 20	32.74 ± 0.40	34.03	-7.55
^{14}C			32.18[4]	+0.63[4]

1) Q determined from 3-proton + 1-neutron separation.

2) Q determined from stationary neutron pickup and 2-proton separation.

3) Q determined from ^{3}H+p+^{10}C final state.

4) Q determined from 1-proton separation and pickup of a stationary neutron.

these peak energies lie near the beam energy per nucleon with variations observed from isotope to isotope. These differences in peak locations are reasonably well understood as arising from differences in Coulomb energies between the entrance and exit channels, plus a two body Q-value for breakup of the projectile. Here we assume that the projectile dissociates into a detected projectile-like fragment (PLF) and another piece which we term the projectile residue (PR). A reasonable estimate of the expected peak location can be computed with the expression

$$E_f = E_i - Z_1Z_2e^2/R - m(E_i - Z_1Z_2e^2/R)/A + Q + Z_3Z_4e^2/R \qquad \text{(Eq. 3)}$$

where E_f, E_i are the fragment and projectile kinetic energies, respectively. The projectile, target, PLF, and residual target-like fragment (TLF) charge numbers are Z_1, Z_2, Z_3, and Z_4, respectively, A is the projectile mass number, and Q is a Q-value for break-up of the projectile. In Eq. 3, recoil of the TLF is neglected, and we selected Q-values which lead to two bound clusters which were originally constituents of the ^{14}N projectile. If the PR is unbound, then the Q-value for breakup into the least number of bound clusters was assumed. The distance of closest approach R was obtained from the touching condition of the projectile and target spheres with a radius parameter r_0 = 1.2 fm. The value of m is the number of nucleons originally residing in the projectile which do not survive in the PLF, and all m of them are assumed to carry away a kinetic energy equal to the incident kinetic energy per nucleon minus the Coulomb energy lost in the approach to the distance of closest approach. These estimates are given in Table I together with the empirical findings. In most cases, the calculated peak energy agrees with the observed energy to within 50%, though sometimes the agreement is worse. Figure 2 shows a comparison

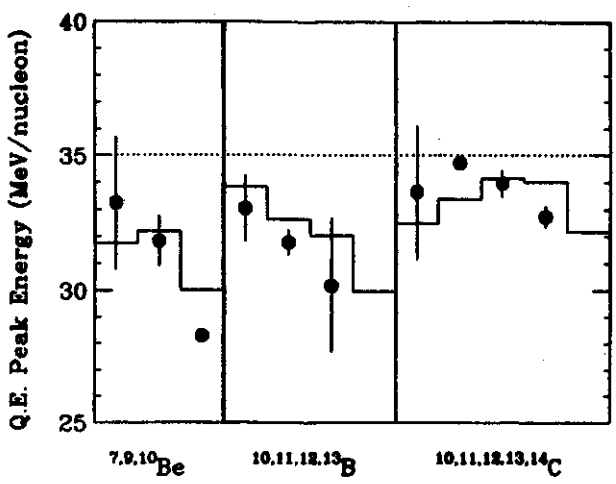

Figure 2. Quasi-elastic peak energies for various isotopes grouped by element. The experimentally determined values are plotted as solid circles, and the computed values (see text) are shown as a histogram. Beam velocity projectile fragments would have peak energies at the dotted line (35 MeV/nucleon).

of the computed versus observed peak energies. Thile the calculations are systematically higher than the data, they are below the 35 MeV/nucleon (dotted line in Fig. 2) corresponding to beam velocity. This relatively good agreement between the observed and computed peak locations, which is not acheived by the beam velocity PLF in the Goldhaber model[1], gives some confidence that we have included the major effects in this calculation.

The momentum widths determined from fitting of the data should follow the parabolic law (Eq. 1 of Ref. 1) using a single σ_0 (referred to as a "reduced momentum width"). The parameter σ_0 in the parabolic law is related to the fermi momentum P_f by the expression $\sigma_0 = P_f/\sqrt{5}$, and can be determined by, for example, electron scattering. Our widths are compared to the parabolic law in Fig. 3. No single σ_0 describes our findings very well. Also, from considerations of the fermi momentum, one expects momentum widths on the order of 110 MeV/c or so, not the ~60 MeV/c which we observe. Of course, this observation is not new. Presently, the best approach to explaining all

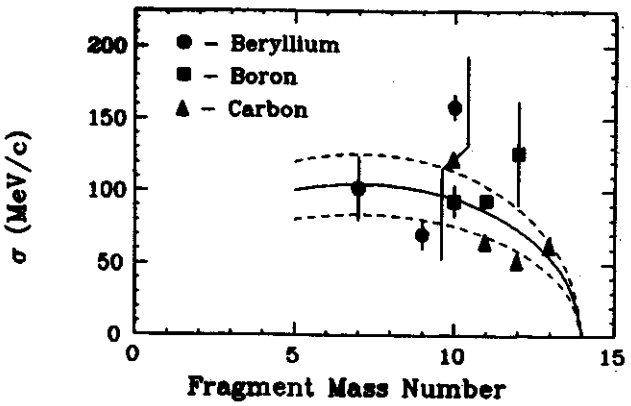

Fig. 3 Comparison of experimentally determined momentum widths for quasi-elastic peaks with predicted values (solid lines) using the parabolic rule. Curves for various values of the "reduced width" σ_0 are shown. The solid line is for σ_0 = 54 MeV/c and the dashed lines represent ±20% deviations from 54 MeV/c.

the data seems to be the peripheral model of Friedman[3], which incorporates nuclear structure (in particular, cluster structure) and the effects of the Coulomb force. Recent analysis[4] of fragmentation data from collisions of 20 MeV/nucleon ^{14}N with ^{165}Ho involved this model, but it was modified to insure conservation of energy and finite geometry effects. Using this extension, the model was then able to predict fragmentation peak shapes, and was successful in describing the experimentally determined shapes and positions of these peaks with no free parameters. We hope to apply such an analysis to our data in the near future to see of the agreement obtained at 20 MeV/nucleon can be extended to our higher energy.

Further work is underway to understand characteristics of the quasi-elastic peak using the peripheral model of Friedman. Also, new data for the ^{14}N + ^{165}Ho reaction at 35 MeV/nucleon recently became available at a larger number of angles forward of 30°. This data is presently being analyzed by our group and should bear more information on the peripheral component of the reactions at these energies.

a. Dept. of Atomic Physics, Eötvös University, Budapest, Hungary.
b. Central Research Institute for Physics (KFKI) Budapest, Hungary.
c. Physics Department, University of Notre Dame Notre Dame, Indiana.
d. Department of Physics, Tokyo Institute of Technology, Tokyo, Japan.

References

1. A.S. Goldhaber, Phys. Lett. 53B, 306(1974).
2. G. Caskey, A. Galonsky, B. Remington, M.B. Tsang, C.K. Gelbke, A. Kiss, F. Deak, Z. Seres, J.J. Kolata, J. Hinnefeld, and J. Kasagi, Phys. Rev. C (in press).
3. W.A. Friedman, Phys. Rev. C 27, 569(1983).
4. E. Deci, private communication.

NEUTRON-FRAGMENT COINCIDENCE MEASUREMENTS IN ^{14}N + Ho, Ni AND C REACTIONS AT 35 MeV/NUCLEON

B. Remington, G. Caskey, A. Galonsky, J. Heltsley, M.B. Tsang, C.K. Gelbke, A. Kiss[a], F.Deak[a], Z.Seres[a], J. Kasagi[b], J.J. Kolata[c] and J. Hinnefeld[c]

A recent experiment has been completed on the NSCL K500 cyclotron to study neutrons in coincidence with various fragments resulting from 35 MeV/nucleon ^{14}N bombarding targets of Ho, Ni, and C. Neutrons were detected in ten NE213 liquid scintillators placed at laboratory angles θ_n= ±10°, ±30°, ±70°, ±110° and ±160° relative to the beam axis. Projectile-like fragments (PLF) were detected in six triple-element silicon telescopes at angles θ_{PLF}= 7°, 10°, 15°, 18° and 23° in the horizontal plane and out-of-plane at 15° below the beam. Figure 1 shows a schematic of the experimental layout.

Fragments from lithium to oxygen were identified in ΔE-E identification spectra. Figure 2 shows a linearized version of such a spectrum, labeled with the corresponding fragment identifications, for the target nucleus carbon. Fragments were separated fairly well isotopically, but gates were set across entire element groups to improve the statistical accuracy of the corresponding neutron spectra. The reactions were divided into two categories, quasi-elastic (QE) and strongly-damped (SD), depending on the energy of the detected fragment. Figure 3 shows a typical PLF energy spectrum with gates distinguishing QE from SD reactions for carbon fragments detected at θ_{PLF}= 10° in coincidence with a neutron for the target nucleus Ho. The fragment energy spectrum at this angle is dominated by the QE peak. The physical interpretation of such a quasi-elastic reaction is that the carbon nucleus pre-exists

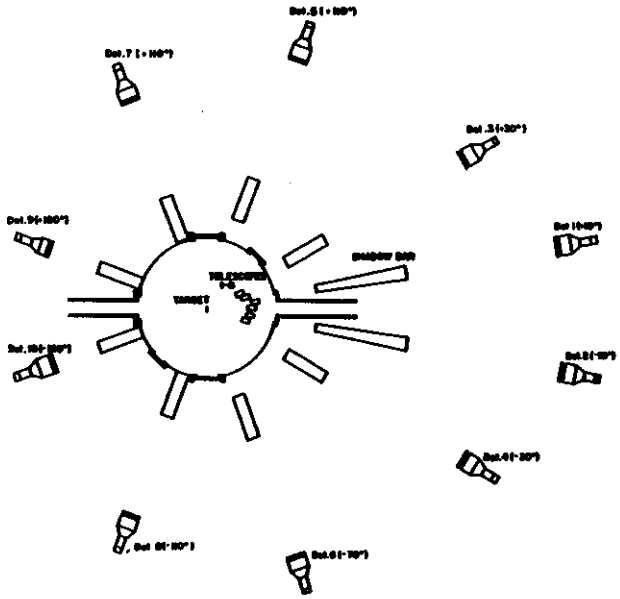

Fig. 1 Schematic of the experimental setup. Note: each of the ten neutron detectors has a 6 mm proton veto plastic scintillator in front of it. Also, the positions of the shadow bars are indicated. Periodically throughout the run, the shadow bars were put in place to measure the background (scattered) neutrons.

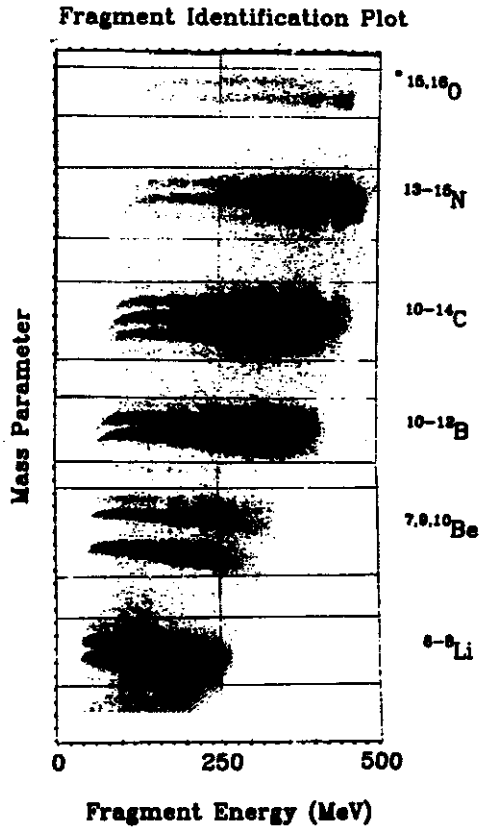

Fig. 2 A linearized fragment identification spectrum at θ_{PLF}= 10° for the target nucleus carbon. The various fragments are identified and labeled along the right vertical axis, and the gates separating element groups by Z are indicated.

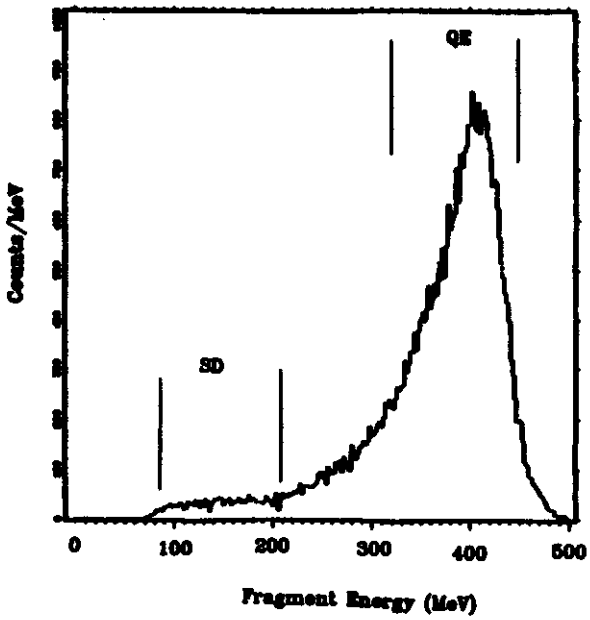

Fig. 3 A typical fragment energy spectrum showing the gates set for QE and SD reactions. The fragment was carbon at θ_{PLF}= 10° for the Ho target.

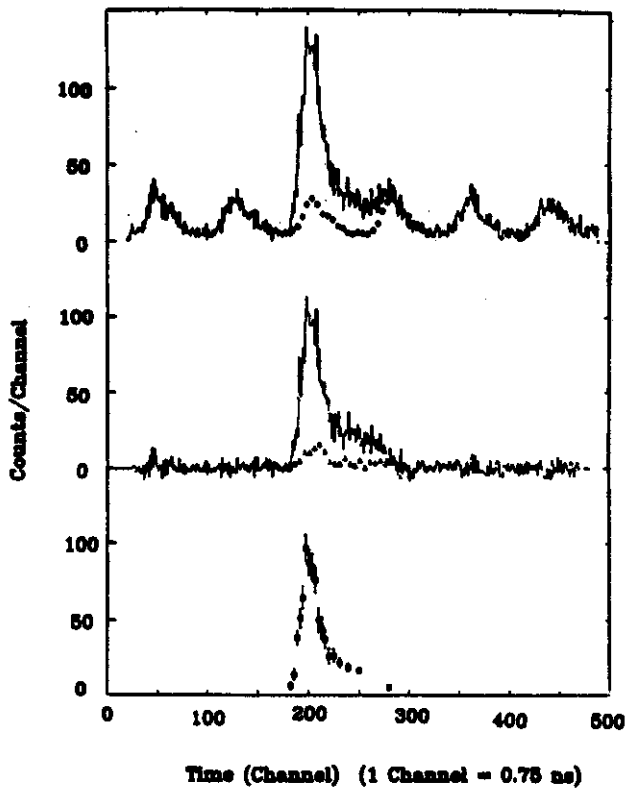

Fig. 4 A neutron TOF spectrum showing both the level of accidental coincidences (circles) and of prompt, background coincidences (triangles), as well as the final "true" TOF spectrum (squares). The coincident fragment was QE lithium at θ_{PLF}= 10° for the Ho target.

as a cluster at the moment of interaction of the ^{14}N projectile with the ^{165}Ho target. Those nucleons not part of this preformed carbon subset are sheared off the projectile, leaving the carbon to then scatter from the target nucleus. The width of the QE peak reflects the internal motion of the preformed cluster relative to the projectile rest frame.

A typical neutron TOF spectrum is shown in Fig. 4. It is for θ_n= 10° in coincidence with QE lithium fragments at θ_{PLF}= 10° on the opposite side of the beam. One notices in this TOF spectrum the level of accidental coincidences (circles), the level of prompt, background coincidences (triangles) after subtraction of accidentals, and the final "true" TOF spectrum (squares). The "true" TOF neutron spectra were transformed relativistically into energy spectra and compared with curves produced using a 3-moving-source parameterization. In this framework, one imagines 3 moving sources, each parameterized by a temperature, velocity and a source strength. Each source evaporates neutrons isotropically in its rest frame. These 3 contributions are then transformed into the lab frame and summed together, forming the theoretical spectra to which the data are compared. Figures 5 and 6 show the neutron energy and angular distribution for QE and SD reactions, resp., for coincidence with a boron fragment at θ_{PLF}= 10°.

To make sense of the role played by each of the three sources, it is useful to examine the results of the fit that correspond with Fig. 5. In Table 1 are listed the actual parameters of the fit and the energy-integrated strength of each source for each of the ten angles. One notices that the backward-angle neutron energy spectra are dominated by the isotropic, low energy evaporation contribution of source #2, a target-like fragment (TLF) source sitting at rest in the lab frame. At the forward angles, the fast-moving projectile-like fragment (PLF) source, source #1, contributes a comparable

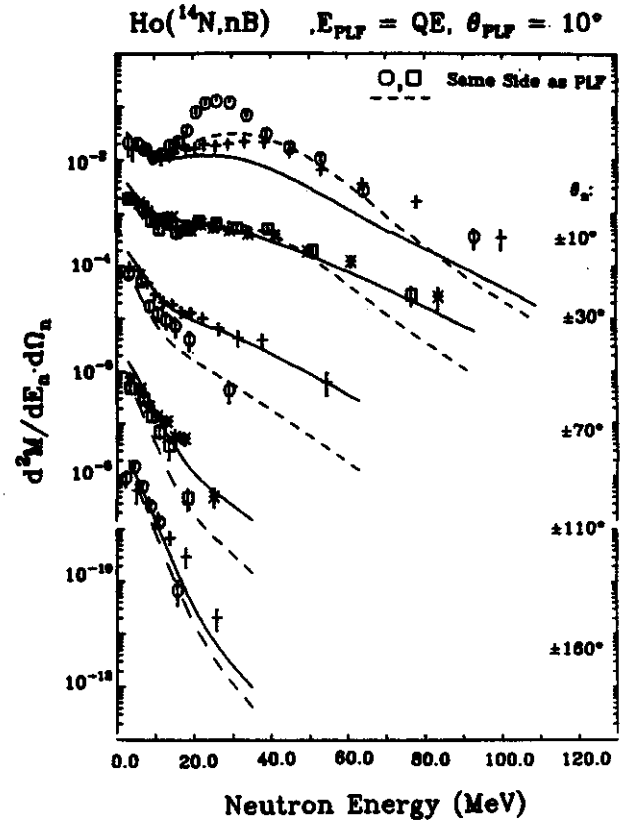

Fig. 5 Neutron energy and angular distribution for a coincident fragment of QE (quasi-elastic) boron at θ_{PLF} = 10° for the Ho target. The neutron spectra are plotted in symmetric angle pairs relative to the beam, each pair offset from the others. Starting from the top, the pairs are θ_n = ±10°, ±30°, ±70°, ±110° and ±160°. The curves are for three moving sources fitted to all but the ±10° data. Open symbols and the dashed lines correspond to neutrons on the same side of the beam the fragment was detected on.

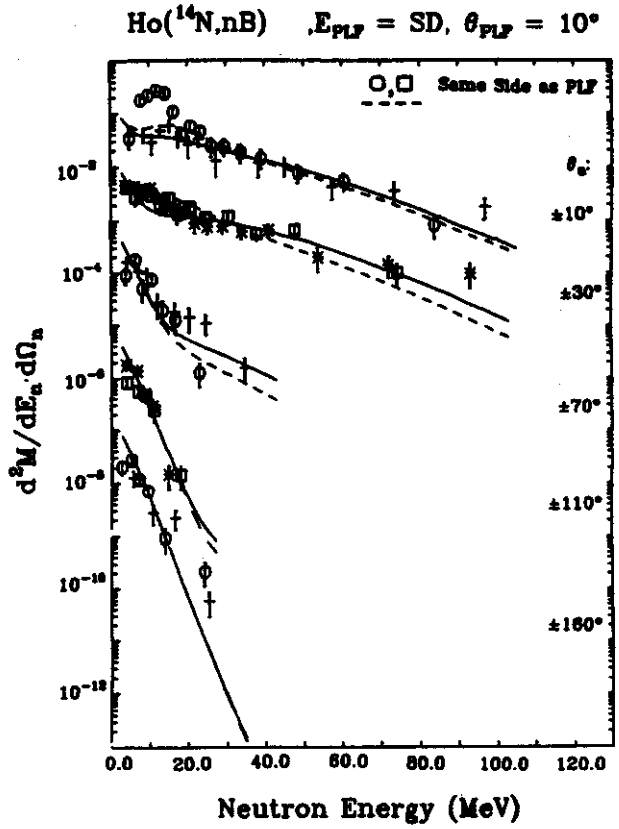

Fig. 6 Same as Fig. 5 except for SD (strongly-damped) reactions.

amount to the neutron energy spectra. Indeed, in the neutron detector at θ_n = +10° directly behind the fragment telescope, the PLF source provides the main contribution. But at the middle angles (70° and 110°) the spectra are significantly augmented by the contribution from source #3, a hot, intermediate-velocity source, often called the intermediate-rapidity source (IRS). This is especially true on the side of the beam opposite that where the fragment is detected, since the direction of the IRS is to 15° on the side opposite the PLF.

There are two unique features of the neutron spectra in coincidence with QE boron fragments at θ_{PLF} = 10°. First, in examining the neutron energy spectra at θ_n = +10° (i.e., from the neutron detector directly behind the fragment telescope), one notices in Figs. 5 and 6 a distinct peak centered about the energy/nucleon of the detected PLF. This effect has been seen before by us[4] and others[1,2] and can be understood as follows: Some excited fragments are in slightly unbound states just above the neutron separation energy so that neutrons are emitted with essentially zero velocity in the PLF rest frame. When the velocity of the PLF is then added to these neutrons, they are focused into the direction of the PLF, hence into the neutron detector directly behind the detector of the PLF.

One also notices in Fig. 5 that the neutron energy spectra at ±70° and ±110° are distinctly asymmetric relative to the beam axis, with more neutrons being detected on the side of the beam opposite to the detected fragment. Examination

of the corresponding energy spectra for the SD reaction (Fig. 6) shows that this asymmetry is much smaller or perhaps disappears all together. In a previous study by us of the same system[4], this asymmetry was observed at θ_n= ±60° and ±90°. The asymmetry of neutrons detected at middle angles (60° to 110°) seems to be associated with QE reactions, i.e., for reactions where the PLF is detected near the grazing angle (θ_{PLF}= 10° here and $\theta_{grazing}$= 8° in the lab system). The asymmetry decreases in magnitude as one moves away from the grazing angle, as verified by an examination of the data for θ_{PLF}= 7°, 10°, 15°, 18° and 30°, and disappears altogether for SD reactions.[3,4] On the other hand, it increases in magnitude with fragment Z, being strongest for Z=6 and essentially disappearing for Z=3.

In an examination (not presented in this report) of the neutron spectra taken for the Ni target, it is seen that there is a small asymmetry in the same sense as above for θ_{PLF}= 7°, but this asymmetry disappears at both θ_{PLF}= 10° and 18°. When note is taken that the grazing angle for 35 MeV/nucleon ^{14}N on Ni is $\theta_{grazing}$= 4° (in the lab system), then the above observation is consistent with the systematics for ^{14}N + Ho reactions in that the asymmetry appears to decrease as one moves away from the grazing angle.

On the other hand, when neutron spectra are examined for ^{14}N + C reactions (also not presented here), this asymmetry exists for the "QE" reactions for both θ_{PLF}= 10° and 18° (as compared to $\theta_{grazing}$= 1° in the lab), but not for SD reactions. It should be pointed out that for these reactions, $\theta_{PLF} >> \theta_{grazing}$, so that one cannot realistically label the peak region of the fragment energy spectrum as the QE region. Its energy/nucleon is considerably lower than the beam energy/nucleon. Nonetheless, the asymmetry of detected neutrons at θ_n= ±70° and ±110° exists for these "QE" reactions for both θ_{PLF}= 10° and 18° and disappears for SD reactions.

The above systematics of asymmetrically detected neutrons are not yet understood. In the framework of the moving source parameterization, it can be reproduced by allowing the third, hot source (IRS) to move off-axis on the side of the beam opposite the detected QE fragment (see Table 1). Requiring a coincidence with a PLF on one side of the beam may, of course, be selecting those events in which the IRS moves to the opposite side of the beam by simple conservation of momentum. The reality of moving sources is strengthened by the fact that the data require this selection.

It should also be pointed out that detecting a fragment on one side of the beam introduces a kinematic asymmetry for neutrons emitted from PLF-type sources, such as source #1 of Table 1. If one takes account of the recoil introduced to the PLF due to neutron emission, together with the strong angular dependence of QE fragments, an asymmetry in the same sense as seen in our data can be produced. This has been studied by one of us (G.C.), and found that it cannot explain both the energy-angle dependence

TABLE 1

FIT PARAMETERS

	SOURCE #1	SOURCE #2	SOURCE #3
Temp (MeV)	2.18	2.18	8.49
E/A (MeV/nucleon)	29.0	0.0	12.0
Angle (Degrees)	+10.0	-60.0	-15.1

SOURCE STRENGTHS

ANGLE	SOURCE #1	SOURCE #2	SOURCE #3
-10.0	6.08E-02	6.64E-02	1.79E-01
10.0	3.25E-01	6.64E-02	1.37E-01
-30.0	7.98E-04	6.64E-02	1.39E-01
30.0	6.08E-02	6.63E-02	6.68E-02
-70.0	4.90E-08	6.64E-02	2.54E-02
70.0	4.14E-06	6.63E-02	8.71E-03
-110.0	4.47E-10	6.64E-02	3.45E-03
110.0	2.59E-09	6.62E-02	1.59E-03
-160.0	8.39E-11	6.63E-02	7.78E-04
160.0	1.18E-10	6.62E-02	6.27E-04
TOTAL	7.393E-02	8.332E-01	2.893E-01

Fit parameters obtained by fitting the 3-moving-source parameterization to the neutron energy and angular distribution for a coincident fragment of QE boron detected at 10 degrees for the Ho target.

and the asymmetry of detected neutrons.[5] So recoil effects of the PLF at least are not the sole cause of the observed asymmetry; the IRS is responsible for most of it.

It should be noted that the full neutron energy and angular distribution cannot always be reasonably described by three moving sources if the ±10° neutron spectra are included in the fit. Presumeably this is indicative of a significant contribution from direct reactions or preequilibruim processes at the extreme forward angles. (Here, preequilibrium is taken to mean that component of the neutron spectra that cannot be described by three moving, thermal sources. Typically at slightly lower beam energies, say, 10-20 MeV/nucleon, this term has been taken to mean that component which connot be described by two thermal sources.[1,6])

In summary, neutron-fragment coincidence measurements are being studied in the framework of the moving-sources picture, focusing on QE and SD reactions. The moving-source parameterization works reasonably well provided a third, hot, intermediate-velocity source is introduced. Even with a third source, the entire neutron energy and angular distribution cannot be predicted in all cases if the extreme forward angle spectra are included in the fit. A strong asymmetry in the neutrons detected at middle angles occurs for QE reactions with a Ho target nucleus. It seems to increase in magnitude with fragment Z, but decreases as one moves away from the grazing angle and disappears altogether for SD reactions. The magnitude of this asymmetry is smaller when the target nucleus is Ni, but it is noted that the angle of the detected PLF (7°) is nearly twice as large as the grazing angle (4°) for this interaction. The asymmetry also exists for a C target nucleus for fragments detected at both 10° and 18°, whereas the corresponding grazing angle is 1°. This effect is currently not understood, and it is hoped that in determining the systematics of the asymmetry, we will help motivate corresponding theoretical studies to explain them.

---

a. Eötvös University and CRI Institute of Science, Budapest, Hungary

b. Tokyo Instityte of Technology, Tokyo, Japan

c. University of Notre Dame

1. A. Gavron et al., Phys. Rev. Lett. 46, 8(1981).
2. B. Chambon et al., Z. Phys. A312, 125(1983).
3. B. Remington, Doctoral Thesis, MSU Physics Dept., expected June 1985
4. G. Caskey et al., Phys. Rev. C (in press, scheduled for April 1985).
5. G. Caskey, elsewhere in this annual report.
6. D. Hilscher et al., Preprint HMI-P-84/3R from the Workshop on Coincidence Particle Emission from Continuum States at Bad Honnef, June 4-7, 1984.

EVAPORATION RECOIL EFFECTS: ASYMMETRIES IN NEUTRON-PROJECTILE-FRAGMENT COINCIDENCES FOR 35 MeV/NUCLEON ^{14}N + ^{165}Ho REACTIONS.

G. Caskey

A recent experiment[1] was conducted at the NSCL to observe neutrons emitted in coincidence with projectile-like fragments in ^{14}N + ^{165}Ho reactions at E(^{14}N) = 490 MeV. The neutron energy spectra were obtained at several angles between 10° and 110° in the laboratory system, and were in coincidence with either strongly damped or quasi-elastic projectile-like (A<14) fragments at θ = 10°. One feature of these spectra occured for quasi-elastic events: Neutrons detected at, say, 60° on the side of the beam axis opposite the detected fragment were more numerous than those observed at 60° on the same side of the beam axis as the fragment. Furthermore, this asymmetry was evident only for the higher energy neutrons (E_n>10 MeV) and could not be associated with evaporation from the target-like fragment. The purpose of this study is to determine whether the asymmetry observed in Ref. 1 could arise from recoil effects in projectile-fragment evaporation.

First consider the moving-source model, which does not include recoil effects. Excited projectile and target fragments emerge from a two-body rearrangement collisions. Both will have some velocity in the laboratory and can emit neutrons in flight. Neutrons are assumed to be emitted isotropically in the rest frame of the emitter. The motion of the emitters in the laboratory frame gives some initial velocity to which the neutron decay velocity, relative to the emitter, is added vectorially. Hence, the neutrons are "kinematically" focussed along the direction of motion of the fragments, and the degree of focussing depends directly on the fragment speed. In this model neutrons coming from the projectile-fragment would have a laboratory angular distribution which is peaked in the direction of the projectile-fragment, and likewise for neutrons from the target fragment. Indeed this is observed at lower bombarding energies.[2,3,4] However, the target-like fragment evaporation neutrons in Ref. 1 have a nearly isotropic angular distribution. This implies a nearly stationary target-like fragment. Hence, they do not contribute to the observed asymmetry. On the other hand, a traditional moving source for the projectile-like fragment would give more neutrons on the same side of the beam where the fragment is detected. So a two moving source model with projectile-like and target-like sources alone cannot describe the observed neutron-fragment angular correlations.

At beam energies above 35 MeV/nucleon the model used to fit inclusive nucleon emission spectra requires addition of a third source. Interpreting this source literally is questionable, but this might indicate that the moving source model is missing some relevant physics. This report focuses on one defect of the moving source model: namely, when neutrons are evaporated the emitter recoils.

To understand the significance of recoil effects, consider the quasi-elastic reaction ^{165}Ho(^{14}N,^{10}B n)X at E(^{14}N)=490 MeV (where X may represent more than one particle). We assume that the initial boron isotopes, which will decay by neutron emission(s) to $^{10}B_{gs}$, have an angular distribution characteristic of fragmentation reactions: viz.[5]

$$d^2\sigma/d\Omega dE \propto P_F(\varepsilon,\theta_F) =$$

$$\sqrt{\varepsilon}\, e^{-A^2u(\varepsilon + \varepsilon_0 - 2\sqrt{\varepsilon\cdot\varepsilon_0}\cos\theta)/\sigma^2}$$

(Eq. 1)

where ε_0 is the fragment energy per nucleon, corresponding to the gaussian momentum distribu-

tion centroid. The mass number of the fragment is A, ε is it's kinetic energy per nucleon, θ is the fragment direction of motion in the lab system, and u = 931.5016 MeV is the unified mass unit. A fragment detector placed at θ = 10°, as in Ref. 1, will, of course, detect those fragments initially heading toward 10° but which are not deflected out of the detector's acceptance by recoil upon emitting a neutron. However, there will also be contributions from fragments intitally headed to angles forward (backward) of 10°, which will recoil into the 10° detector acceptance if the neutron is emitted toward the opposite (same) side of the beam axis as the fragment. So a simple asymmetry as seen in the data of Ref. 1 is plausible due to this simple mechanism of evaporation recoil.

A simple technique was used to simulate recoil effects. Equation 1 served as the fragment angular and energy distribution function with ε_0 = 28 MeV/nucleon and σ = 130 MeV/c, as given by fits of the inclusive ^{11}B data of Ref. 1. A neutron energy spectrum, in the frame of the projectile-like fragment emitter, of

$$P_n(E_n) = \sqrt{E_n}\, e^{-E_n/T} \qquad \text{(Eq. 2)}$$

was assumed with T a fixed parameter which was set to values between 3 and 8 MeV for various trials. The computer program itself was constructed as shown schematically in Figure 1. The simulation assumes coplanar geometry.

The simulation results are shown in Figure 2, superimposed on the data of Ref. 1, for ε_0 =

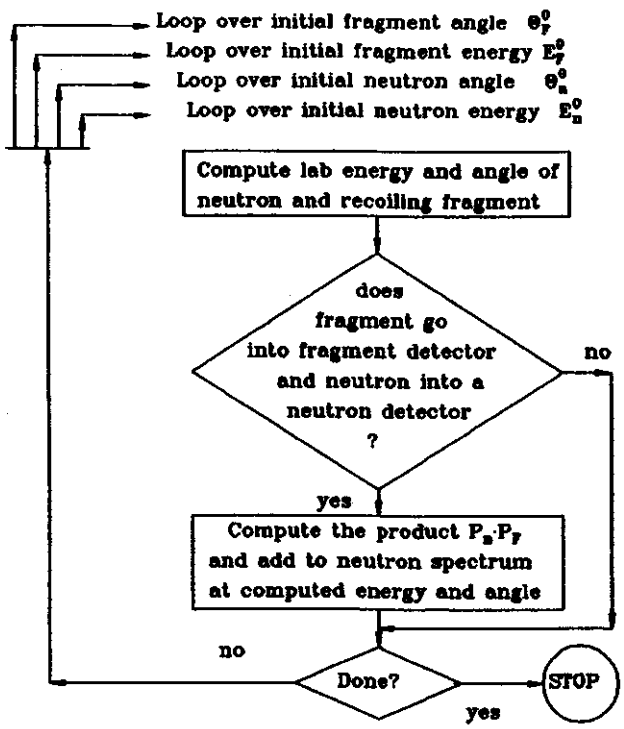

Fig. 1. Flow chart of evaporation recoil computer program. Coplanar geometry is assumed in all cases.

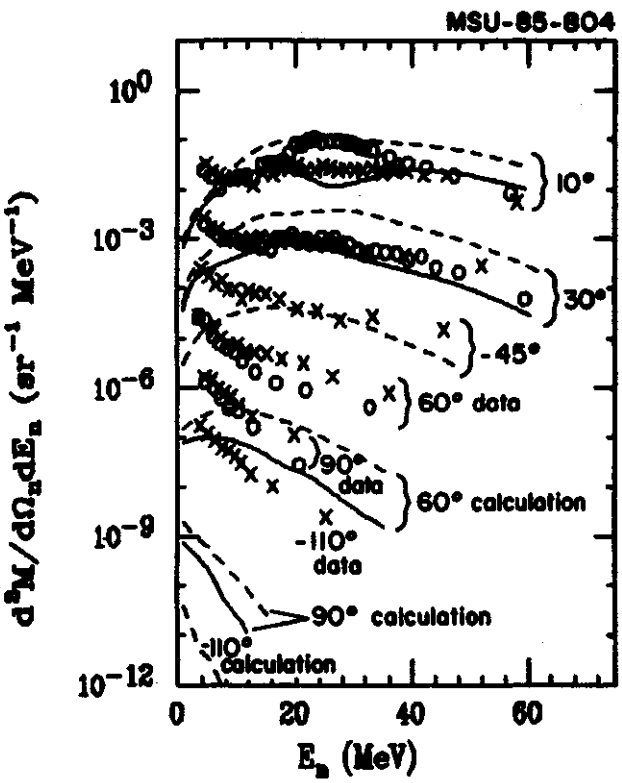

Fig.2 Data from Ref. 1 and calculation for a projectile-like source temperature T=3 MeV, σ = 130 MeV/c, and a centroid kinetic energy of 28 MeV/nucleon. Circles (full lines) are data (calculations) on the same side of the beam as the projectile-like fragment and crosses (dashed lines) are on the opposite side of the beam axis. Structure in the calculations is an artifact of the calculation except for the broad dip in the 10° calculation (solid line) near E_n = 25 MeV. The broad dip here is a manifestation of the low probability of zero energy neutrons initially heading toward the 10° detector. The higher cross section on each side comes from neutrons heading either toward or away from the detector when emitted by the fragment.

28 MeV/nucleon, σ = 130 MeV/c, and T = 3 MeV (Eq. 2). Calculations at -45° were normalized to the data at that angle by eye, and this set the scale for curves at all other angles. Only three angles (+10°, +30°, and -45°) are reasonably described by the calculation. At 10° and 30° the calculation overpredicts the "opposite-side" cross sections, but for $|\theta| \geq 60°$ the calculation underpredicts the data by orders of magnitude. This latter observation is a reflection of the fact that the neutron-fragment angular correlation is strongly influenced by the fragment speed - even if recoil is included.

Another simulation was run with T = 8 MeV, taken from the moving-source fits in Ref. 1. Again, the projectile fragment speed gave an angular distribution which was much stronger than evidenced in the data. Also, allowing the longitudinal and transverse momentum widths to vary did not improve agreement between the simulation and the data. Hence, it is plausible that no reasonable set of parameters can be chosen so as to reproduce the data of Ref. 1, in the purely equilibrium approach of two moving sources.

Since incorporating reasonable fragment energy and angular distributions and accounting for recoil effects in evaporation will not reproduce the data of Ref. 1, the high energy and large angle neutrons must arise from some other mechanism. This is not too suprising since it is known[6] that pre-equilibrium neutron emission begins to be obvious even at energies much lower than 35 MeV/nucleon. The assessment of the origin of the neutrons in Ref. 1 is beyond the scope of this report, but it promises to be of interest in determining the reaction mechanism for these coincidence experiments. Further work has been done to more extensively characterize these coincidence spectra and is given elsewhere in this report[7].

---

1. G. Caskey, A. Galonsky, B. Remington, M.B. Tsang, C.K. Gelbke, A. Kiss, F. Deak, Z. Seres, J.J. Kolata, J. Hinnefeld, and J. Kasagi, Phys. Rev. C (in press).
2. D. Hilscher, J.R. Birkelund, A.D. Hoover, W.U. Schröder, W.W. Wilcke, J.R. Huizenga, A.C. Mignerey, K.L. Wolf, H.F. Breuer, and V.E. Viola, Jr., Phys. Rev. C 20, 576(1979).
3. Y. Eyal, A. Gavron, I. Tserruya, Z. Fraenkel, Y. Eisen, S. Wald, R. Bass, C.R. Gould, G. Kreyling, R. Renfordt, K. Stelzer, R. Zitzmann, A. Gobbi, U. Lynen, H. Stelzer, I. Rode, and R. Bock, Phys. Rev. C 21, 1377(1980).
4. B. Chambon, D. Drain, C. Pastor, A. Dauchy, A. Giorni, and C. Morand, Z. Phys. A 312, 125(1983).
5. This expression derives from the expression
$$d^2\sigma/d\Omega dp \propto p^2 \cdot e^{-(\vec{p}-\vec{p}_0)^2/2\sigma^2}$$
in the case that the longitudinal and transverse momentum widths are equal.
6. A. Gavron, R.L. Ferguson, Felix E. Obenshain, F. Plasil, G.R. Young, G.A. Petit, K. Geoffroy Young, D.G. Sarantites, and C.F. Maguire, Phys. Rev. Lett. 46, 8(1981).
7. B. Remington, et al., elsewhere in this annual report.

NEUTRON SPECTRA AND LEVEL DENSITY PARAMETERS FROM THE $^{16}O + ^{12}C$ FUSION REACTION

J. Kasagi[a], B. Remington, A. Galonsky, F Haas[b], J.J. Kolata[c], L. Satkowiak[c], M. Xapsos[c], R. Racca[d] and F.W. Prosser[d]

The statistical model has often been used to describe the decay of a highly excited nucleus. When that nucleus is formed by the collision of two heavy nuclei the excitation is enriched in high-spin states. We have measured neutron spectra in coincidence with various γ-rays emitted in evaporation residues. Data were obtained at the University of Notre Dame for the $^{16}O + ^{12}C$ reaction at five ^{16}O projectile energies from 43.2 to 56.0 MeV.

Residues following $^{16}O + ^{12}C$ fusion were identified by their characteristic γ-rays. For several transitions in ^{23}Mg, ^{25}Mg, and ^{26}Al coincident neutron spectra were measured at six angles from the time difference between a γ-ray Ge(Li) pulse and a neutron scintillator pulse. The relevant γ-ray transitions are indicated in Fig. 1. In Fig. 2 is shown a neutron energy spectrum (in the laboratory system) in coincidence with γ-rays from the 830-keV transition in ^{26}Al.

For comparison with the statistical model through the program CASCADE[1] we constructed angle-integrated neutron energy spectra in the center-of-mass (CM) system of $^{16}O + ^{12}C$. In the program, excitation energies are divided into four regions and different level density parameters can be used for each region. For the lowest excitation energies (region I), the known levels compiled by Endt and Van der Leun[2] are used with their spins and parities for each nucleus. For the next region (region II), the level density parameters "a" (the usual level density parameter) and Δ (the pairing energy or virtual ground state position) have been reparameterized by Pühlhofer[1], using the compilations of Vonach and Hille[3] and of Dilg et al.[4] These parameterizations are built into the program. The parameter values used for the

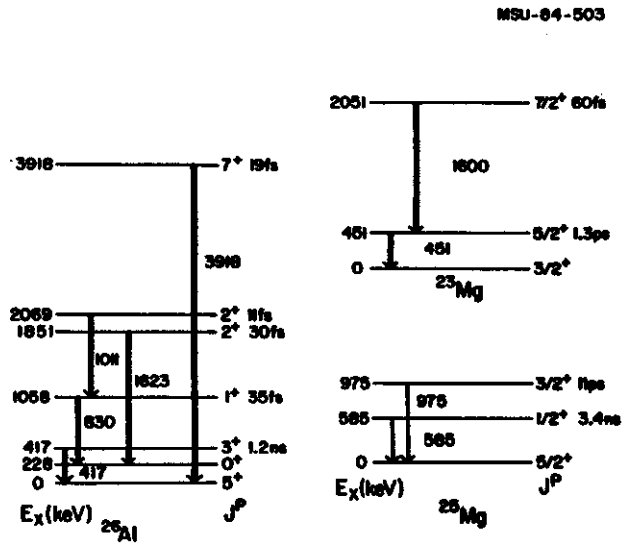

Fig. 1 The observed γ-ray transitions in the three neutron channels studied, i.e., $^{12}C(^{16}O,pn)$ ^{26}Al, ^{12}C $(^{16}O,\alpha n)$ ^{23}Mg, and $^{12}C(^{16}O, 2pn)$ ^{25}Mg. Listed on the left is the energy and on the right the spin, parity, and half-life of each level.

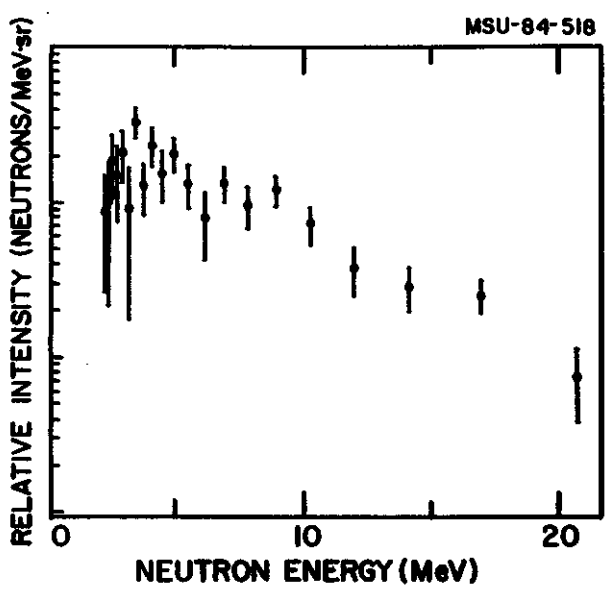

Fig. 2 The laboratory energy spectrum of neutrons at o° in coincidence with 830-keV γ-rays emitted by the residue ^{26}Al.

present calculations are listed in Table 1 for each nucleus. For the highest excitation energies (region IV), where the shell effects on the level density are considered to disappear,[5] the parameter "a" is assumed to have the form A/constant (A is the mass number) and the constant is treated as a free parameter and fitted to the experimental data. The parameter Δ used in this region is calculated from the assumption that the virtual ground state for the level density in this region should coincide with the ground state energy of a spherical liquid drop.[5] The parameter values in region IV are also listed in Table 1. For region III, which corresponds to the region between II and IV, the program interpolates the level density parameters linearly. In summary, region I is the low excitation energy region where the levels are known. Region II extends from region I to 10 MeV, region III is from 10 MeV to 20 MeV, and region IV is from 20 MeV and above. The effective radius parameter r_0, which determines the spin cutoff factor, is also fitted to the data as a free parameter. Thus, there are only two input parameters to be varied in comparing the calculation to the experimental data. One of them is the level density parameter "a" in region IV and the other is the effective radius parameter r_0.

For evaporated particles the program provides energy spectra which have been obtained by integrating over angle and by summing over all the decay steps from the initial compound nucleus to the final evaporation residue. In the present experiment, however, neutron spectra gated by specific γ-rays were measured. In order to compare the calculation with the present experiment, the program was modified to correspond to these conditions.

First we compared theory with experiment for the neutron spectra gated by the 417 keV γ-ray in ^{26}Al. The parameters "a" and r_0 are obtained so as to give the best fits to these spectra; spectra gated by other γ-rays in ^{26}Al have poorer statistical accuracy. Results of the comparison are shown in Fig. 3 for both E_i= 46.0 and 56.0 MeV. The calculated spectra are normalized arbitrarily since the absolute yield has not been measured in the present experiment.

As can be seen in the upper half of the figure, the slope of the high energy side of the calculated spectra is very sensitive to "a", while the lower half shows that the behavior of the low energy part of the spectra is mainly determined by r_0. The calculations for a = A/8, A/9, and A/10 are shown in Fig. 3(a) with dotted, solid and dashed lines, respectively. Although the value of a=A/8 reproduces the data reasonable well, the value of a = A/9 fits the data better between 3 and 7 MeV for all the incident energies. In Fig. 3(b) are shown the calculations with various values of r_0. Dashed, dotted, solid and dot-dashed curves show those with r_0 = 1.8 fm, 1.7 fm, 1.6 fm, and 1.5 fm, respectively. The calculation with r_0=1.6 fm reproduces the data for lower incident energies. To reproduce the data at higher incident energy (E_i=53.8 and 56.0 MeV), larger values of r_0 are

Table 1. Level density parameters "a" (in MeV^{-1}) and pairing energies Δ (in MeV) used in the calculation.

		^{28}Si	^{27}Si	^{27}Al	^{26}Al	^{25}Na	^{24}Mg	^{23}Mg
Region II ($E_x \leq 10$ MeV)	a	2.98	3.05	3.05	2.95	2.86	2.61	2.66
	Δ	1.82	-1.09	-1.09	-2.46	-1.06	2.07	-1.02
Region IV ($E_x \geq 20$ MeV)	a	3.11	3.0	3.0	2.89	2.78	2.67	2.56
	Δ	4.02	-1.16	-0.03	-2.24	-3.04	2.55	-2.17

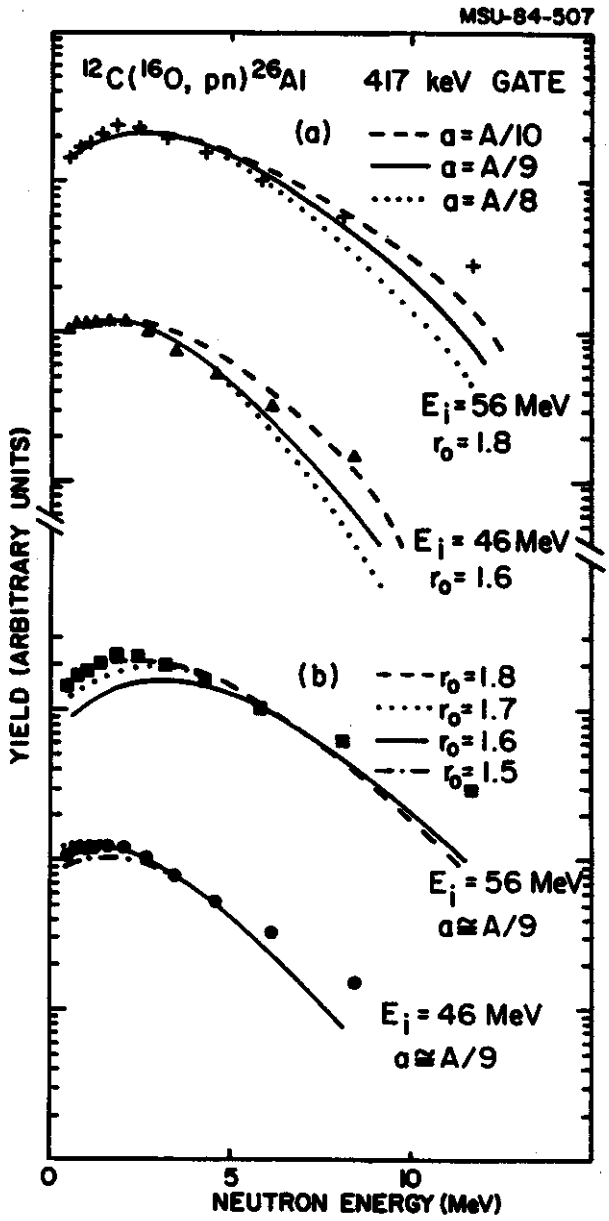

Fig. 3 Calculated neutron spectra compared to the experimental spectra for various values of the radius parameter r_0 and the level density parameter "a" in region IV for the residue ^{26}Al. (a) Top spectrum is for 56 MeV beam energy and r_0=1.8 whereas the lower spectrum is for 46 MeV incident energy and r_0=1.6. In both cases, the dashed line is for a = A/10, solid line for a = A/9, and dotted line for a = A/8.
(b) Top curve is for 56 MeV incident energy and the bottom curve for 46 MeV. The value of "a" in region IV is A/9. The dashed curve is the calculation for r_0=1.8, dotted for r_0=1.7, solid for r_0=1.6, and dot-dashed for r_0=1.5.

required, as seen in the figure. Varying the boundary between regions III and IV does not eliminate this dependence of r_0 on the incident energy. A change of the assumed γ-ray transition strengths makes only slight changes in the neutron spectra. The final values of r_0 obtained in the comparisons with the experimental data are 1.6 fm for E_i=43.2, 46.0, and 48.3 MeV, 1.7 fm for E_i=53.7 MeV and 1.8 fm for the E_i=56.0 MeV.

Spectra gated by other γ-rays can be fitted only by using the above r_0 values for each incident energy.

Although still within the energy uncertainty of the data, the highest energy points in the spectra are systematically higher than the calculations. This larger than expected yield of the high energy neutrons might be caused by processes other than evaporation from the fully equilibrated system that CASCADE assumes to exist at the start.

The value of A/9.0 for "a" in region IV obtained in the present analysis turns out to be almost the same as the values of "a" in region II for each nucleus, as shown in Table 1. Therefore, the present results do not give evidence for the existence of a region of high excitation energy (region IV) where the shell effects on the level density disappear.

On the other hand, the constraint of fitting the neutron spectra for each incident energy clearly requires a dependence on incident energy of the effective radius parameter r_0. Of particular interest is the fact that larger values of r_0 are required for higher incident, and therefore, higher excitation energies. A larger r_0 serves to increase the density of high spin states in the sequentially decaying nuclei, and thereby it enhances the low energy neutron yield. The values of r_0 obtained in the present work are much larger than those determined at lower excitation energies. The value of r_0 = 1.25 fm has been widely used to obtain the level density parameters from experimental data.[3,4,6] It has been pointed out[7], however, that the value of r_0 = 1.4 fm was deduced from a shell model calculation for an average value of the square of the projection of the total

angular momentum for the states around the Fermi level. At high excitaiton energies, little information about the level density has been available so far. Thus, it is highly desirable to systematically obtain level density information for the high excitation energy and high spin region. The present method is very useful for such a purpose, since neutrons are free from the Coulomb barrier and the whole spectrum (including the low energy neutrons) directly reflects the level densities of the sequentially decaying nuclei.

1. F. Pühlhofer, Nucl. Phys. A280, 267(1977)
2. P.M. Endt and C. Van der Leun, Nucl. Phys. A310, 1 (1978).
3. H. Vonach and M. Hille, Nucl. Phys. A127, 289 (1969).
4. W. Dilg, W. Schantl, H. Vonach and M. Uhl, Nucl. Phys. A217, 269 (1973).
5. V.S. Ramamurthy, S.S. Kapoor and S.K. Kataria, Phys. Rev. Lett. 25 (1970) 386; F.C. Williams, Jr., G. Chan and J.R. Huizenga, Nucl. Phys. A187, 225 (1972).
6. A. Gilbert and A.G.W. Cameron, Can. J. of Phys. 43, 1446 (1965).
7. U. Facchini and E. Saetta-Menichella, Energ. Nucl. 15, 54 (1968).

NEUTRON AND GAMMA EMMISION FROM $^{156}Er^*$ and $^{164}Er^*$ AFTER ^{78}Se + ^{78}Se and ^{82}Se + ^{82}Se REACTIONS

W. Kühn,[a] R.V.F. Janssens,[b] T.L. Khoo,[b] K.T. Lesko,[b] W. Henning,[b] D.C. Radford,[b] G.S.F. Stephans,[b] A.M. van den Berg,[b] and R.M. Ronningen

We are studying $^{156}Er^*$ at high spin by measuring neutrons and gamma rays in coincidence with total gamma energy. In the previous two annual reports we described expeiments producing this nucleus using ^{12}C and ^{64}Ni beams with energies near the Coulomb barrier. Some of our results have now been published[1] where we give evidence for a superdeformed shape at high spin.

One purpose of our study is to investigate the ability of the statistical model to predict neutron multiplicity distributions for such reactions leading to neutron deficient nuclei for a wide range of entrance channels, given that the compound nucleus has as nearly as possible the same excitation energy and initial spin. This past year we have used the ^{78}Se + ^{78}Se and ^{82}Se + ^{82}Se reactions to produce $^{156}Er^*$ and $^{164}Er^*$. While ^{156}Er is predicted to have a superdeformed shape at high spin $^{164}Er^*$ is not[2]. Analysis of these experiments is now in progress.

---

a University of Giessen, W. Germany

b Argonne National Laboratory

References

1. W. Kühn, P. Chowdhury, R. V. F. Janssens, T. L. Khoo, F. Haas, J. Kasagi, and R. M. Ronningen, Phys. Rev. Lett. 51, 1858(1983).
2. S. Åberg, Phys. Scripta 25, 23(1982).

COMPLEX PARTICLE EMISSION FROM ^{12}C INDUCED REACTIONS ON ^{197}AU AT E/A=30 MEV.

D.J. Fields, W.G. Lynch, C.B. Chitwood, C.K. Gelbke, M.B. Tsang and J. Aichelin

The emission of complex nuclei (Z_f>2) in processes different from binary fission was first observed in high and intermediate energy hadron-nucleus collision and has been associated with the most violent of these reactions. More recently, similar processes have been observed in nucleus-nucleus collisions over a large range of incident energies. A number of models have been proposed to explain these observations, including the direct cleavage of the target nucleus by the incident projectile,[1,2] sequential[3] and nonsequential[4,7] statistical emission from excited nuclear systems, the coalescence of nuclei from a hot gas of nucleons,[8] and the random shattering of a cold nucleus by the projectile.[9] The approximate power law dependence of the mass yields has been interpreted as a signature of statistical formation of clusters near the critical point in the liquid-gas phase diagram of nuclear matter. This latter theory has spawned considerable theoretical interest.

Until now the existing data and their analysis could not distinguish between different models. For example, recent theoretical investigations indicate that a power law dependence of the mass yields is insufficient to establish the occurrence of critical phenomena, as the experimental dependence is equally well described by other very different models.[3,8,9]

However, the differential cross sections contain information that can considerably constrain reaction models which describe the emission of intermediate mass fragments and perhaps allow choosing from among available models.

We have measured the energy spectra of intermediate mass fragments of ^{12}C induced reactions on ^{197}Au at E/A=30 MeV. A 0.6 mg/cm^2 ^{197}Au target was bombarded with a 360 MeV ^{12}C beam from the K500 cyclotron. Reaction products were detected with a three-element telescope subtending a solid angle of 5 msr and consisting of a 10 cm deep Frisch grid ion chamber[25] followed by two 0.4 mm silicon surface barrier detectors with 450 mm^2 active areas.

The energy spectra measured at laboratory angles of 30°, 50°, 70° and 120° are shown in Fig. 1 for fragments with Z_f=5-10. For lighter elements, the angular distributions are forward peaked, indicating that these elements are emitted prior to the attainment of full statistical equilibrium of the composite nucleus. With increasing element number the angular distributions become less forward peaked, indicating higher degrees of

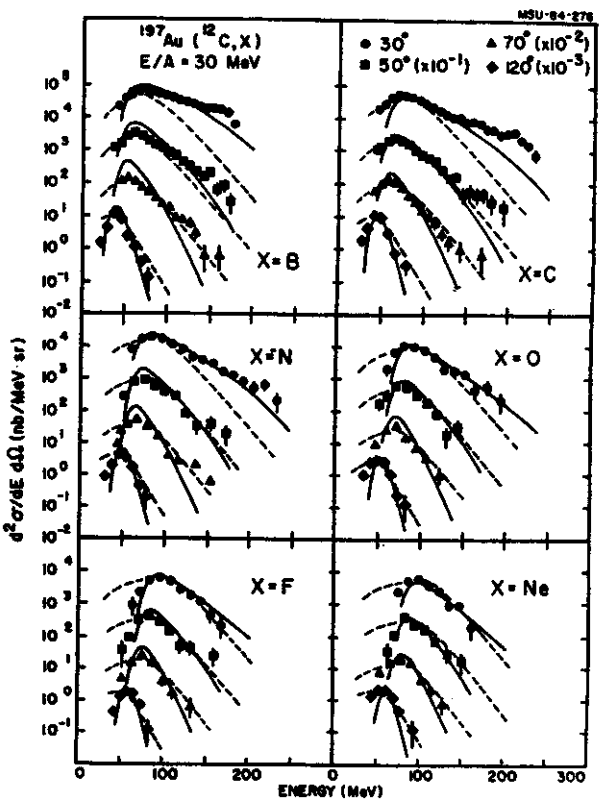

Fig. 1 Differential cross sections for various intermediate mass fragments. The solid lines are a calculation assuming statistical emmission from an excited source. The dashed lines are calculations of nuclear shattering.

ENHANCED EMISSION OF NONEQUILIBRIUM LIGHT PARTICLES IN THE REACTION PLANE

M.B. Tsang, C.B. Chitwood, D.J. Fields, C.K. Gelbke, D.R. Klesch, W.G. Lynch,
K. Kwiatkowski[a] and V.E. Viola, Jr.[a]

Particle emission prior to the attainment of global statistical equilibrium of the composite system is well established for intermediate and high energy nuclear collisions. Present experimental information on nonequilibrium particle emission in fusion-like reactions is consistent with the concept of statistical emission from a localized region of high excitation.[1-10] Emission from localized regions of excitation is expected to be azimuthally anisotropic because of geometrical shadowing or dynamical flow effects.

The experiment reported here was performed at the K500 cyclotron of the National Superconducting Cyclotron Laboratory of Michigan State University. A ^{197}Au target of 0.5 mg/cm^2 areal density was bombarded with ^{14}N ions of 420 MeV incident energy. Triple coincidences between two fission fragments and outgoing light particles, prescaled inclusive light particle and prescaled fission-fission coincidence events were written on magnetic tape and analyzed off-line. Coincident fission fragments were detected with two position-sensitive parallel plate detectors of active area 12cm x 14cm, which were positioned 17cm from the target at angles of θ_{Ao}=70^o and θ_{Bo}=80^o. Light particles emitted far back of the grazing angle (θ_{gr}~11^o) were detected with two ΔE-E telescopes consisting of silicon ΔE and NaI E-detectors. The telescopes had solid angles of 53 msr and 63 msr and were placed at the angles θ_x=55^o, ϕ_x=0^o and θ_x=55^o, ϕ_x=90^o respectively. Here, θ_x denotes the polar angle measured with respect to the beam axis and ϕ_x denotes the azimuthal angle between the light particle telescope and the plane defined by the centers of the two fission detectors and the beam axis. In the triple coincidence data reported here, the azimuthal angle of one of the fission fragments is constrained to lie within 3.5^o of the azimuthal angle corresponding to the center of the fission detector.

For reactions induced on a Au target, fission fragments originate primarily from fusion-like collisions for which the major part of the projectile is absorbed by the target nucleus. The fission fragments are preferentially emitted in the entrance channel scattering plane,[11] as is illustrated in Fig. 1. The curves shown in the figure correspond to the semi-classical probability distributions,[12] $P(\phi)$, for the angle ϕ between the entrance channel scattering plane and the fission plane (defined as the plane containing the beam axis and the fission fragment velocity vectors):

$$P\phi) = \text{const}\cdot\exp[-C \sin^2(\phi)]$$

Since the detailed properties of the

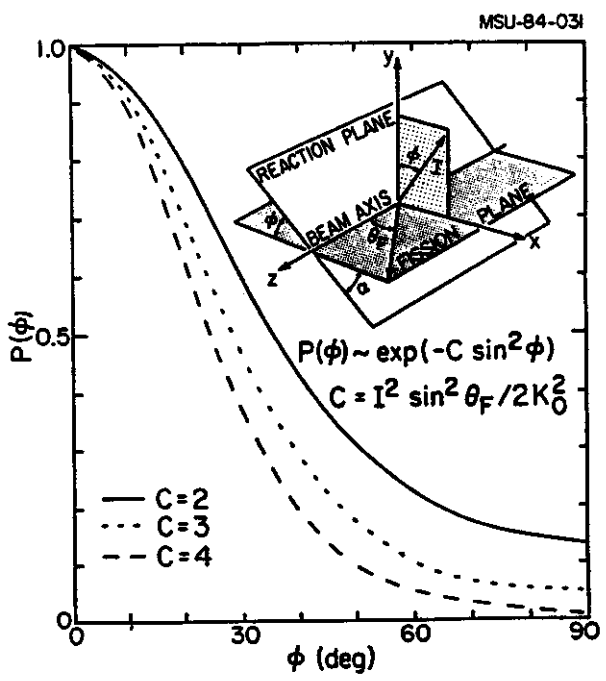

Fig. 1 Characteristic shapes of probability distributions $P(\phi)$ for the fission fragment plane with respect to the reaction plane.

fissioning system are not known, C cannot be specified a priori. The calculated airves correspond to C=2,3 and 4,

The energy spectra of light particles detected in and out-of-plane with two coincident fission fragments are shown by circular and triangular points in Fig. 2. Similar to previous observations for slightly different systems,[1-4] the energy spectra exhibit approximately Maxwellian shapes. However, there is a clear preference for the emission of energetic light particles in the plane of the outgoing fission fragments. To provide a quantitative measure of this enhancement, the ratios of out-of-plane to in-plane energy

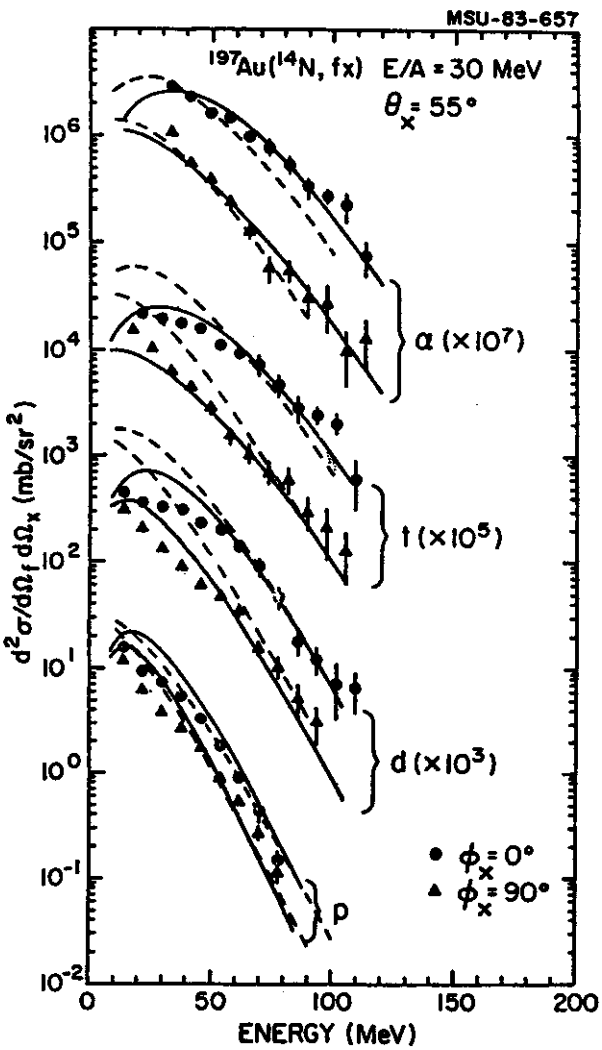

Fig. 2 Energy spectra of p, d, t and α particles measured in coincidence with fission fragments.

integrated coincidence spectra have been plotted in Fig. 3 where the energy integration intervals are indicated by the horizontal bars. The

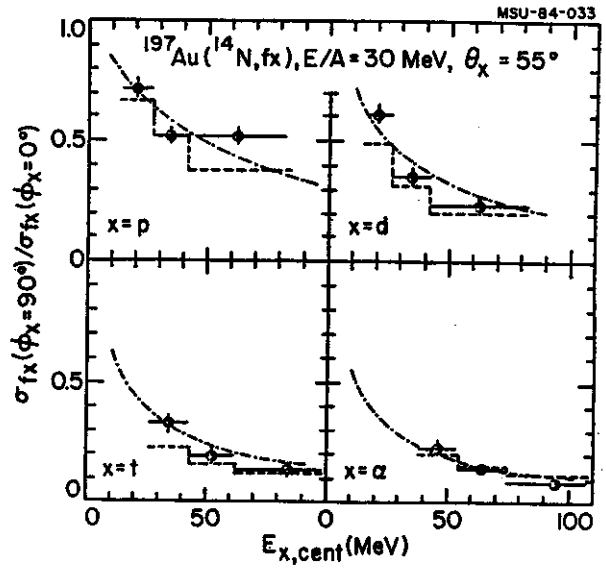

Fig. 3 Ratio of out-of-plane to in-plane coincidences between fission fragments and light particles.

ratios decrease significantly with increasing energy and with increasing mass of the coincident light particles. For the highest energy alpha particles, azimuthal anisotropies of up to one order of magnitude are observed.

Azimuthally asymmetric angular distributions have been predicted in a variety of reaction models. An enhancement of nonequilibrium light particle emission in a direction perpendicular to the entrance channel scattering plane could be caused by nuclear shadowing effects[13] or perhaps by hydrodynamic compression effects[14] both of which lead to a preferential flow of nuclear matter in a plane perpendicular to the line connecting the centers of the two colliding nuclei. Our observation of enhanced emission in the fission plane indicates that these effects are of minor importance. On the other hand, an enhanced emission of nonequilibrium particles in the entrance channel scattering plane might be due to an ordered collective motion of the emitting source in this plane. For illustration, we show the results of

two schematic calculations.

The first calculation corresponds to an emitting source about an axis perpendicular to the entrance channel scattering plane while moving parallel to the beam axis.[15]

The second calculation corresponds to an ordered motion which is purely translational with a significant velocity component perpendicular to the beam in the entrance channel scattering plane.[15]

The results of these calculations are compared to the measurements in Figs. 2 and 3. Calculations with the rotating source appear as solid lines in Fig. 2 and as dashed histograms in Fig. 3. The dashed lines in Fig. 2 and the dot-dashed lines in Fig. 3 were calculated assuming a deflected source.

Since both of these rather simple models qualitatively describe the data, it is likely that similar agreement could be obtained by other models which superimpose random statistical motion of the participating nucleons upon a transverse collective velocity.

---

1. T.C. Awes, et al., Phys. Rev. C24,89(1981)
2. T.C. Awes, et al., Phys. Lett. 103B,417 (1981)
3. W.G. Lynch, et al., Phys. Lett. 108B,274 (1982)
4. T.C. Awes, et al., Phys. Rev. C25,2361 (1982)
5. G.D. Westfall, et al., Phys. Lett. 116B,118 (1982)
6. R.L. Auble, et al., Phys. Rev. Lett. 49,441 (1982)
7. R. Glasow, et al., Phys. Lett. 120B,71 (1983).
8. B.V. Jacak, et al., Phys. Rev. Lett. 51, 1846 (1983)
9. W.G. Lynch, et al., Phys. Rev. Lett 51,1850 (1983)
10. M.B. Tsang, et al., Phys. Lett. 134B,169 (1984)
11. We define the entrance channel scattering plane as the plane containing the beam axis and making the angle ϕ with respect to the fixed quantisation axis which is chosen to be perpendicular to the beam axis. The angle ϕ is defined via the semiclassical relation $\sin\phi=m/l$ where l and m denote the entrance channel orbital angular momentum of relative motion between projectile and target and its projection onto the quantization axis, respectively.
12. L.C. Vaz and J.M. Alexander, Phys. Rep. 97, 1(1983).
13. W.A. Friedman, Phys. Rev. C29,139(1984)
14. M.I. Sobel, et al., Nucl. Phys. A251,502 (1975)
15. For details see M.B. Tsang et al., Phys. Rev. Lett. 52,1967(1984).

AZIMUTHAL CORRELATIONS BETWEEN LIGHT PARTICLES EMITTED IN ^{16}O INDUCED REACTIONS ON ^{12}C AND ^{197}Au AT 400 MeV

M.B. Tsang, W.G. Lynch, C.B. Chitwood, D.J. Fields, D.R. Klesch, C.K. Gelbke, G.R. Young,[a] T.C. Awes,[a] R.L. Ferguson,[a] F.E. Obenshain,[a] F. Plasil,[a] R.L. Robinson[a]

For intermediate energy nuclear collisions, particle emission prior to the attainment of full statistical equilibrium of the emitting nucleus is expected to provide information about the early stages of the reaction. The global trends of single particle inclusive cross sections can be rather well described in terms of the concept of local statistical equilibrium [1-3]. Recent results from two-proton correlation measurements at small relative momenta are consistent with the emission of energetic light particles from a localized region of high excitation [4]. Because of shadowing [5-7] by the surrounding cold spectator matter, emission from such a localized region of high excitation is expected to be left-right asymmetric. In order to search for the possible existence of shadowing effects, we have measured azimuthal angular correlations of light particles emitted in ^{16}O induced reactions on ^{12}C and ^{197}Au at 400 MeV.

The experiment was performed at the Holifield Heavy-Ion Research Facility of Oak Ridge National Laboratory. ^{12}C and ^{197}Au targets of 2.5 and 9.7 mg/cm^2 areal density were bombarded with ^{16}O ions of 400 MeV incident energy. Prescaled singles and coincident light particles (p,d,t) were detected using seven telescopes with solid angles between 13 and 40 msr. Three of these telescopes were mounted at the polar angles measured with respect to the beam axis of θ = 40°, 70°, and 130° and the azimuthal angle of ψ = 0°; the remaining four telescopes were positioned at the polar angles of θ = 40°, 70°, 130°, and 160°; their azimuthal angle ψ was varied between 50° and 180°. In order to reduce systematic errors, the azimuthal correlation is defined by the ratio of the coincidence cross-section divided by the singles cross-sections $\sigma_{xy}/\sigma_x\sigma_y$. In order to reduce contributions from compound nucleus decay, a low energy threshold of 36 MeV was applied in computing the cross-section. Figure 1 shows the azimuthal correlations of two coincident light particles emitted at θ = 40° and 70°. For reactions on ^{197}Au, coincident light particles are preferentially emitted in a plane which contains the beam axis, (Fig.1a). Similar

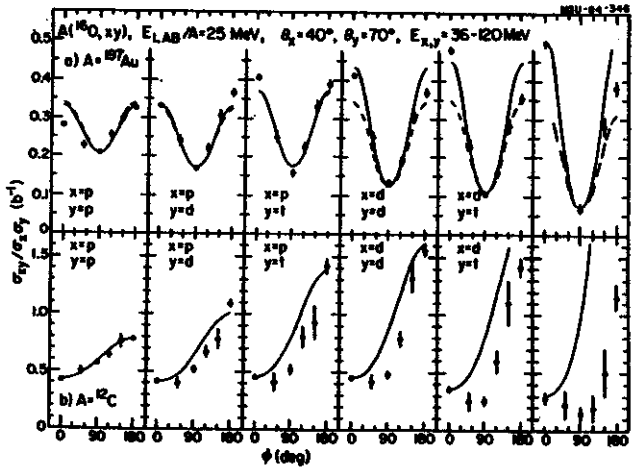

Fig. 1 Azimuthal angular correlations between coincident light particles emitted at θ =40° and 70° with respect to the beam axis for ^{16}O induced reactions on ^{197}Au (a) and ^{12}C (b) at 400 MeV incident energy. A low energy threshold of 36 MeV was applied. See text for detail explanation of solid and dashed curves In part b, the solid curves were calculated with the model of ref. 9, assuming emission from a source of A_s=28 nucleons and temperature T=7 1 MeV moving with the velocity of the compound nucleus, v_o=0 13c.

observations were made [8] for ^{14}N induced reactions on ^{197}Au at 420 MeV. It was shown [8] that non-compound light particles are preferentially emitted in the entrance channel reaction plane (defined as the plane which contains the beam axis and which is

perpendicular to the semiclassical orbital angular momentum vector for the relative motion between the projectile and target nuclei). These observations could be described by assuming the superposition of a collective motion in the reaction plane on the random motion of the individual nucleons. To corroborate this point, we have performed schematic calculations corresponding to emission from a rotating moving source [8] and, alternatively, by assuming emission from two sidewards deflected sources.[9)]

The calculations with the rotating source parameterization are shown by the solid curves in Fig. 1a. The calculations for two sidewards deflected sources are shown by the dashed curves in Fig. 1a. Both of these schematic calculations can reproduce the overall trends of the azimuthal correlations rather well. Momentum conservation and nuclear shadowing effects are expected to affect the relative magnitude of the coincidence cross sections corresponding to coincident particle emission to the same (ϕ=0°) and to opposite (ϕ=180°) sides of the beam axis where ϕ denotes the relative azimuthal angle of the two particles. Since these effects are not incorporated in the simple parameterizations of eqs. 1 and 2, the relative magnitudes of these cross-sections are not reproduced.

In contrast to reactions on ^{197}Au, there is a clear enhancement for the emission of two coincident light particles to opposite sides of the beam axis for reactions on ^{12}C, see Fig. 1b. These correlations may be understood in terms of the phase space constraints imposed by momentum conservation [10]. Because of the small size of the colliding nuclei shadowing effects are expected to be negligible. In order to illustrate the effect of momentum conservation, we performed schematic calculations [10] for a source of A_s=28 nucleons and temperature T=7.1 MeV moving with the velocity of the compound nucleus, v_o=0.13c. In these calculations it is assumed that the momentum P_x of the emitted particle with mass number A_x changes the mean velocity of the second particle by $\Delta v_o = A_x P_x / m_x (A_s - A_x)$, i.e. the entire residual source is assumed to recoil to conserve total linear momentum. As is shown by the solid lines in Fig 1b, these schematic calculations reproduce the overall trends of the data rather well indicating that the preferential emission of coincident light particles to opposite sides of the beam axis may be explained in terms of the phase space constraints imposed by momentum conservation on finite nucleon systems. The influence of these constraints becomes more pronounced with increasing mass of the detected light particles.

The ratios $\sigma_{xy}(\phi=180°)/\sigma_{xy}(\phi=0°)$ of the coincidence cross sections for emission to opposite sides divided by the cross-sections for emission to the same side of the beam axis are given in Fig. 2. For reactions on ^{197}Au, this ratio decreases with increasing mass of the two coincident light particles, in striking contrast to the strong increase measured for reactions on ^{12}C. The dot-dashed and dashed lines in the figure illustrate the effects due to momentum conservation for momentum conserving subsets consisting of A_s=28 and A_s=40,60,90,213 nucleons, respectively. For these calculations, particles were assumed to be emitted with Maxwellian distributions corresponding to a temperature of T=7.1 MeV and initial mean velocity parallel to the beam axis of v_o=0.13c (dot-dashed line) and v_o=0.11c (dashed lines).

Qualitatively, our observations might be explained in terms of the competing effects caused by shadowing and momentum conservation. If preequilibrium emission originates from a localized region of high excitation, absorption or rescattering by the adjacent spectator nuclear matter will enhance emission to the same side of the beam axis. Momentum conservation, on the other hand, will favor emission to opposite sides of the beam axis. Whether coincident light particles are preferentially emitted to the same or to opposite sides of the beam axis will depend on the relative magnitude of these two opposing effects. Absorptive effects are expected to be more pronounced for the emission of composite light particles than

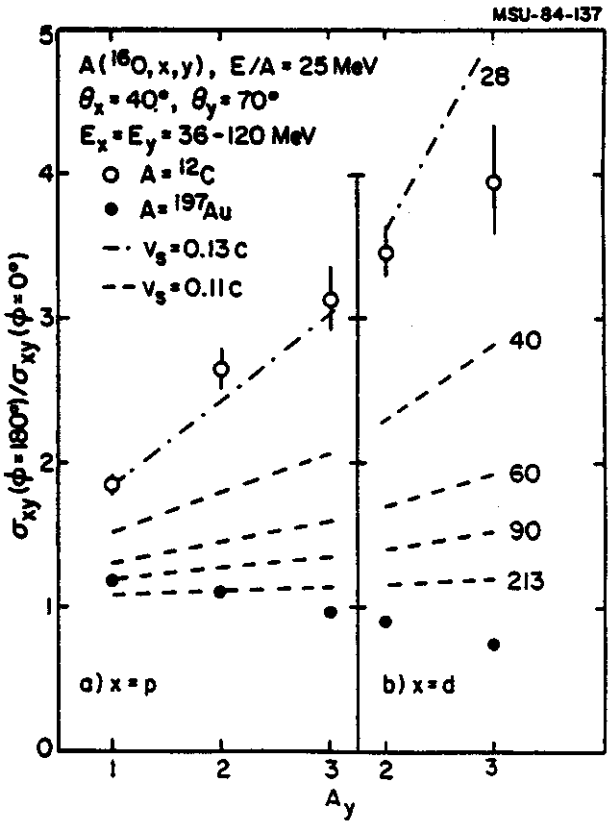

Fig. 2 Ratio of cross sections corresponding to emission of coincident light particles to opposite sides divided by the emission to the same side of the beam axis for ^{16}O induced reactions on ^{12}C (open points) and ^{197}Au (full points) at 400 MeV incident energy. The dashed and dot-dashed curves illustrate the effects of momentum conservation for systems with finite number of nucleons. The dot-dashed curve corresponds to emission from a source of A_s=28 nucleons and temperature T=7.1 MeV moving with the velocity of the compound nucleus, v_o=0.13c. The dashed curves were calculated for sources consisting of A_s=40, 60, 90, and 213 nucleons of temperature T=7 1 MeV and initial velocity v_o=0 11c.

for the emission of nucleons. This is in qualitative agreement with the trends measured for reactions on ^{197}Au where it is observed that coincident protons have a slight preference to emerge at opposite sides of the beam axis, whereas coincident composite light particles have a slight preference to emerge at the same side of the beam axis.

1. T.C. Awes, et al., Phys. Lett. 103B,417 (1981).
2. T.C. Awes, et al., Phys. Rev. C25,2361 (1982).
3. G.D. Westfall, et.al., Phys. Lett. 116B,118(1982).
4. W.G. Lynch, et.al., Phys. Rev. Lett. 51,1850(1983).
5. P.A. Gottschalk and M. Weström, Nucl. Phys. A314,232(1979).
6. G.-Y. Fan, et.al., Z. Phys. A310,269(1983).
7. W.A. Friedman, Phys. Rev. C29,139(1984).
8. M.B. Tsang, et.al., Phys. Rev. Lett 52, 1967(1984).
9. For details see M.B. Tsang, et al., Phys. Lett. 148B,265(1984).
10. W.G. Lynch, et.al., Phys. Lett. 108B,274(1982).

FINAL STATE INTERACTIONS BETWEEN NONCOMPOUND LIGHT PARTICLES FOR ^{16}O INDUCED REACTIONS ON ^{197}Au AT E/A = 25 MeV

C.B. Chitwood, J. Aichelin, D.H. Boal, G. Bertsch, D.J. Fields, C.K. Gelbke, W.G. Lynch, M.B. Tsang, J.C. Shillcock,[a] T.C. Awes,[b] R.L. Ferguson,[b] F.E. Obenshain,[b] F. Plasil,[b] R.L. Robinson,[b] and G.R. Young

Two-particle correlations at small relative momenta may contain information about the space-time characteristics of the emitting source because of their sensitivity to final-state interactions[1] and quantum statistical effects[2,3]. Previous investigations of the space-time characteristics of highly excited nuclear systems were based on analyses of two-pion[4-7] and two-proton[8-10] correlations. Because of their larger reaction cross sections, composite light particles may be expected to stay in thermal equilibrium for a longer period of time, corresponding to a lower freeze-out density, as compared to nucleons or pions.[11] Furthermore, the interpretation of light particle correlations may be complicated by additional sensitivities to ensemble averaging[12], reaction dynamics[12], momentum conservation[9], and the sequential decay of particle unbound resonances.[13-15] Correlations between different light particles are expected to exhibit different sensitivities to these effects. As a consequence, the simultaneous measurement of correlations between several light particle pairs, including composite light particles, may provide a unique tool to investigate the dynamical expansion of the interaction region and to reduce the uncertainties of interpretation.

We have measured sizable correlations between composite light particles emitted in ^{16}O induced reactions on ^{197}Au at E/A = 25 MeV. The experiment was performed at the Holifield Heavy-Ion Research Facility. Small angle correlations between coincident light particles were measured with six ΔE-E telescopes consisting of silicon ΔE and NaI(Tl) E detectors, mounted in a closely packed hexagonal array centered at θ_{lab}=15°.

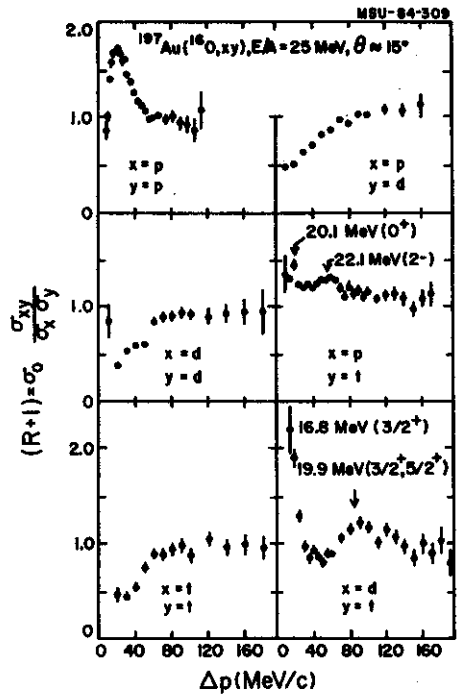

Fig. 1 Experimental correlation functions, 1+R(Δp), plotted as a function of the momentum of relative motion. The locations of several known particle unstable resonances are indicated by arrows. The errors are purely statistical.

We define the correlation function, $R(\vec{p}_1,\vec{p}_2)$, in terms of the singles cross sections, $\sigma(\vec{p}_1)$, $\sigma(\vec{p}_2)$, and the coincidence cross section, $\sigma(\vec{p}_1,\vec{p}_2)$,

$$\sigma(\vec{p}_1,\vec{p}_2) = N\ \sigma(\vec{p}_1)\ \sigma(\vec{p}_2)\ [1 + R(\vec{p}_1,\vec{p}_2)] \quad (1)$$

where $\vec{p}_1$ and $\vec{p}_2$ denote the momenta of particles 1 and 2. The normalization constant, N (used for all correlations shown in Figure 1), was determined previously[9] by requiring the two-proton correlation function to vanish for sufficiently large relative momenta at which final state interactions are negligible. The

experimental correlation functions shown in Fig. 1 were obtained by inserting the measured cross sections into Eq. 1 and by summing both sides of the equation over all energies and angles corresponding to a given momentum of relative motion, $\Delta p = \mu|\vec{p}_1/m_1 - \vec{p}_2/m_2|$, where m_1 and m_2 denote the masses of particles 1 and 2 and μ is the reduced mass. This procedure corresponds to a significant averaging process and tends to reduce the measured correlation function[9]. Due to limited statistical accuracy we did not make energy cuts for the composite particle correlation functions.

The two-proton correlations have been discussed previously[9]. Because of the dominance of the attractive s-wave interaction, correlations arising from the emission and decay of unbound ^{2}He nuclei can be very similar to those caused by final state interactions between protons randomly emitted from a source of small space-time extent[13-15]. More generally, light particle correlations resulting from final state interactions should be more pronounced for systems with sharp resonances. The locations of several known particle unbound states of ^{5}He and ^{5}He, decaying into p+t and d+t, respectively, are indicated by arrows in Fig. 1. The enhanced correlations at these locations may be interpreted in terms of final state interactions or, alternatively, in terms of emission of particle unstable nuclei. However, the strong suppression of the p+d, d+d, and t+t coincidences at small relative momenta cannot be interpreted in terms of the emission and decay of particle unstable nuclei.

In order to illustrate that non-resonant final state interactions between composite light particles contain useful information about the space-time characteristics of the emitting system, we have extended the treatment of hadron interferometry previously applied to two-proton[1] and two-pion[2,3] correlations to two-deuteron and two-triton correlations.

For each partial wave, the nuclear potential was parameterized in terms of a Woods-Saxon potential. The potential parameters V_o, R, and a were determined by fitting the energy dependent phase shifts extracted from d-d scattering. The most complete set of phase shifts in the energy range required for our calculations was extracted by a coupled channel R-matrix approach[16] and led to predominantly repulsive potentials (labelled RM in Fig. 2). We have also performed calculations with potential parameters obtained from an older analysis of d-d scattering data at higher energy by the resonating group approach[17] (RG). These phase shifts lead not only to predominantly attractive potentials, but even show resonant behavior in the ℓ=1 partial wave at energies below 2 MeV.

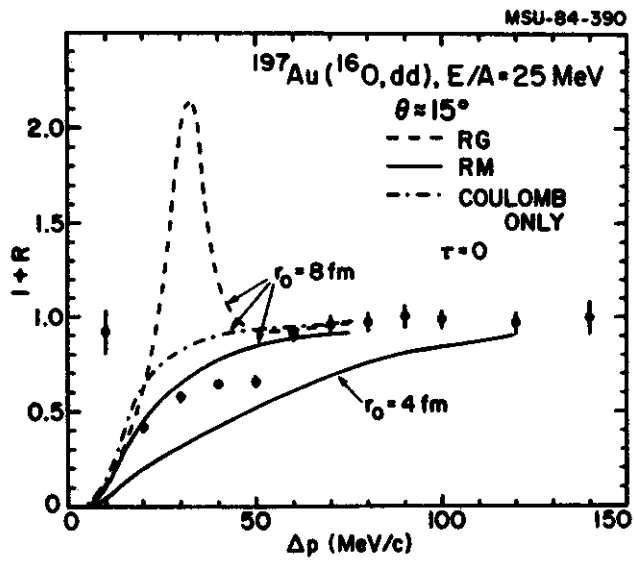

Fig. 2 Comparison of d-d correlation function data with calculations based on phase shifts of Ref. 16 (RM) and 17 (RG). The dot-dashed curve neglects the nuclear part of the potential.

Correlations calculated for r_o=8 fm are shown in Fig. 2. The attractive potential set (RG) predicts enhanced correlations at Δp=30 MeV/c. This enhancement becomes more pronounced as r_o is decreased. In contrast, the repulsive potential set (RM) predicts a suppression of the correlation function at these values of Δp. The data clearly favor the phase shifts extracted by the coupled channels R-matrix method. (For comparison we also show the correlations

predicted for the case of pure Coulomb interaction between the two deuterons, see dot-dashed curve.) In order to illustrate the sensitivity of the calculations to the source radius, we show two calculations for the repulsive potential set (RM) corresponding to r_o=8 and 4 fm, respectively. Although the two-deuteron correlations appear to be less sensitive to the source dimensions than two-proton correlations, they indicate a larger source radius of r_o=6-8 fm compared to the values $r_o \lesssim 4$ fm extracted from two-proton correlations.[9]

In terms of the thermal model, final state interactions were suggested[11] to keep composite light particles close to equilibrium for a longer period of time than nucleons. The freeze-out densities for nucleons and composite light nuclei may be estimated by using a cascade model[18] for the fireball expansion phase of the reaction. According to such calculations, the freeze-out density for deuterons and tritons is lower by about a factor of three than the one for protons. While the corresponding change in scale of $3^{1/3} = 1.4$ should not be directly equated with the approximate factor of 1.5-2 obtained from the analysis of the correlation measurements ($r_o \leq 4$ fm for p-p, $r_o \approx$ 6-8 fm for d-d and t-t), the scale change is suggestive.

References

1. S.E. Koonin, Phys. Lett. 70B,43(1977).
2. G.I. Kopylov and M.I. Podgoretskii, Sov. J. Nucl. Phys. 18,336(1974), G.I. Kopylov, Phys. Lett. 50B,472(1974).
3. F.B. Yano and S.E. Koonin, Phys. Lett. 78B, 556(1978).
4. S.Y. Fung, et al., Phys. Rev. Lett. 41,1592 (1978).
5. D. Beavis, et al., Phys. Rev. C27,910(1983).
6. D. Beavis, et al., Phys. Rev. C28,2561(1983).
7. W.A. Zajc, et al., Phys. Rev. C29,2173(1984).
8. F. Zarbaksh, et al., Phys. Rev. Lett. 46,1268(1981).
9. W G. Lynch, et al., Phys. Rev. Lett. 51,1850 (1983).
10. H.A. Gustafsson, et al., Phys. Rev. Lett. 53,544(1984).
11. D.H. Boal, Phys. Rev. C30,749(1984).
12. M. Gyulassy, Phys. Rev. Lett. 48,454(1983).
13. M.A. Bernstein, et al., Phys. Rev. C29,132 (1984), and to be published.
14. P.D. Bond and R.J. de Meijer, Phys. Rev. Lett. 52,2301(1984).
15. W.G. Lynch, et al., Phys. Rev. Lett. 52, 2302(1984).
16. G.M. Hale, and B.C. Dodder, "Few-Body Problems in Physics", ed. B. Zeitnitz, Elsevier, Amsterdam 1984, Vol. II, p. 433.
17. F.S. Chwieroth, et al., Nucl. Phys. A189,1 (1972).
18. D.H. Boal and J.C. Shillcock, to be published.

STATISTICAL EMISSION OF ^{2}He FROM HIGHLY EXCITED NUCLEAR SYSTEMS

M.A. Bernstein,[a] W.A. Friedman,[a] W.G. Lynch, C.B. Chitwood, D.J. Fields, C.K. Gelbke, M.B. Tsang
T.C. Awes[b], R.L. Ferguson[b], F.E. Obenshain[b], F. Plasil[b], R.L. Robinson,[b] and G.R. Young[b]

As the excitation energy per nucleon is increased, new statistical mechanisms such as target fragmentation, or the statistical emission and subsequent decay of light particle-unstable nuclei (^{2}n, ^{2}He, ^{2}H*, α*, ^{5}He, ^{5}Li, etc.) become important. While the emission of light particle- unstable nuclei has been safely neglected at low excitation energies, this process is expected to be important for the decay of highly excited nuclear systems (T >> 1 MeV).[1-3] The positive identification of these decay channels requires the measurement of correlated fragments which are produced by the subsequent decay of the emitted particle-unstable nucleus[1]. We have tested these concepts by comparing two proton correlation data to calculations based on the statistical emission of ^{2}He from the compound nucleus and the subsequent decay of the two-proton virtual state.

In an experiment performed at the Holifield Heavy Ion Research Facility ^{12}C and ^{27}Al targets were bombarded with ^{16}O ions of 400 MeV incident energy. Light particle correlations were measured with six ΔE-E telescopes which subtended individual solid angles of 0.76 msr and consisted of silicon ΔE and NaI E detectors. These telescopes were mounted in a close-packed hexagonal array which was centered at a scattering angle of 15^{0}. The angular resolution and the angular separation between adjacent telescopes were 1.6^{0} and 5.1^{0}, respectively. Absolute cross sections, accurate to 10% were obtained from the integrated beam current, the target thickness, and the solid angles of the telescopes. Energy calibrations, accurate to 3% were obtained by measuring the energies of recoil protons backscattered from a Mylar target by a 200 MeV ^{16}O beam.

A contour diagram for coincident protons produced in reactions on the ^{12}C target at θ_{Lab} $=15^{0}$ and relative proton angles of 5.1^{0} is plotted in Fig. 1 as a function of the energies of the two protons. Due to limited statistics there is considerable uncertainty associated with the location of the contours. (Insufficient statistics precluded construction of a similar plot for the ^{27}Al target.) At nearly equal energies of the coincident protons, a situation which corresponds to small relative momenta $\Delta p = |p_1 - p_2|/2 < 10$ MeV/c, there is a suppression of the cross section, while at slightly larger relative momenta, Δp = 20 MeV/c, broad maxima are observed for protons of 20-30 MeV. This dependence on relative momentum is demonstrated more quantitatively by the correlation function

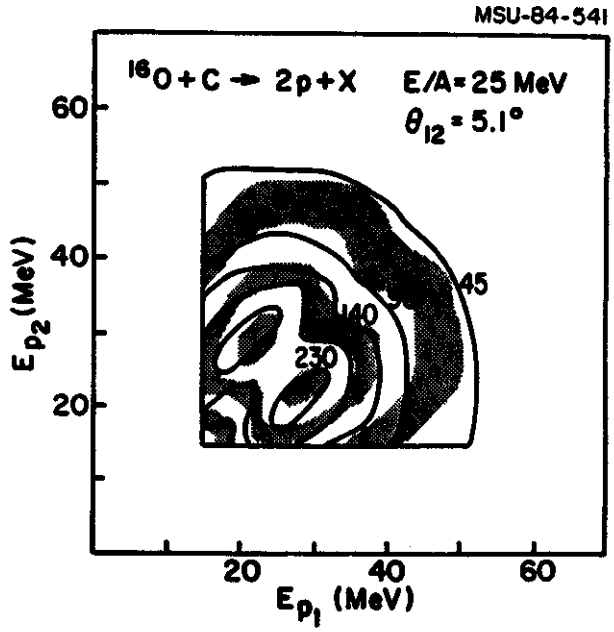

Fig. 1 Coincident cross sections. The solid lines indicate contours for the experimental cross section (μb/(MeV-sr)²), produced in reactions on ^{12}C at θ_{Lab}=15°and relative proton angles of 5.1°, as a function of the energies of the two protons. The alternating clear and shaded zones indicate the comparable contour regions calculated by the model described in the text.

(1+R(Δp)) defined by

$$\sigma(p_1,p_2) = C\sigma(p_1)\sigma(p_2)(1 + R(\Delta p)) \quad (1.)$$

where $\sigma(p_1,p_2)$ and $\sigma(p_i)$ denote the coincidence and the singles cross sections, respectively. The experimental correlation functions for the ^{12}C and ^{27}Al targets, shown in fig. 2, were obtained by inserting the experimental cross sections in Eq. 1 and by summing both sides of the equation over all energies and angles corresponding to a given relative momentum. The normalization constant C has been determined by requiring R(Δp) = 0 at Δp = 70 MeV/c.

The light particle inclusive spectra for ^{12}C and ^{27}Al, and the maxima in the coincidence cross section of Fig. 1, are compatible with considerable contributions from statistically emitting compound-like residues[4] (equilibrated residues from fusion-like reactions). For light targets these emitted particles are kinematically focussed to forward angles in the laboratory. This stands in contrast to the negligible contributions at forward angles from compound-like residues observed for ^{197}Au.[4]

We have calculated the correlations resulting from the statistical emission and subsequent decay of particle- unstable ^{2}He nuclei. For simplicity, emission from the fully equilibrated compound nucleus is assumed. The spectra and multiplicities of ^{2}He, protons (as well as other nuclei in their particle-stable and unstable states) are calculated with the formalism of Ref.5. This formalism approximates the distribution of individual decay chains by particle emission from one ensemble averaged excited nucleus. The relative kinetic energy, E_r) of the two protons generated by ^{2}He decay is assumed to have the spectral distribution:

$$dN(E_r)/dE_r \propto \exp(-E_r/T)] \cdot$$
$$[(\exp(2\pi\eta)-1)\sin^2\delta]/[\eta E_r^{\frac{1}{2}}] \quad (2.)$$

The Boltzmann factor incorporates the phase space constraints imposed by the compound nucleus which is at temperature T. The second factor arises from the Watson-Migdal approximation.[6,7] It contains information pertaining to the Coulomb repulsion through the Sommerfeld parameter, η, and the singlet s virtual state through the phase shift, δ.

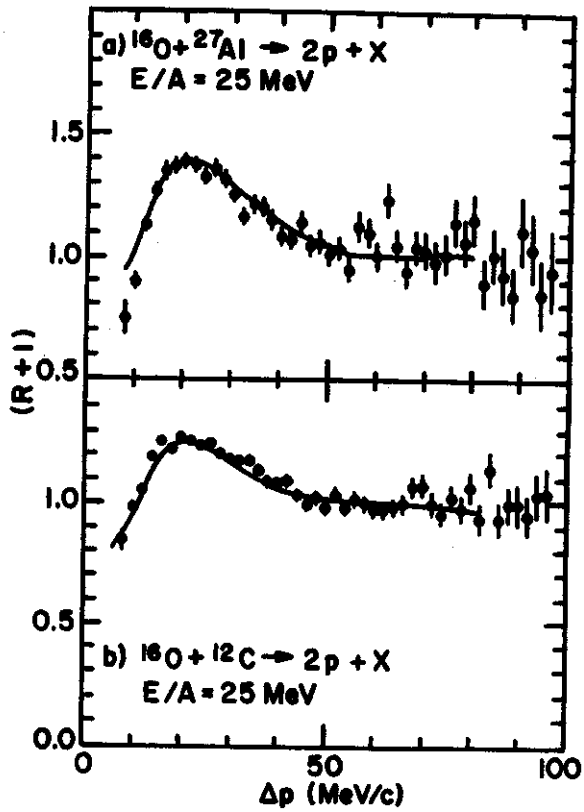

Fig. 2 a) The experimental correlation function 1+R(Δp) plotted as a function of the relative momentum for protons produced in reactions on the ^{27}Al target. The theoretical correlation function is drawn as the solid line. b) Corresponding experimental and theoretical correlation functions for reactions on the ^{12}C target.

The Boltzmann factor also serves to cut off the high relative energy contributions for which the Watson-Migdal expression is invalid. The ^{2}He spectrum is combined with Eq. 2 to obtain the proton spectra in the laboratory frame of reference.

In addition to protons from the decay of the ^{2}He, we include coincident protons which are emitted sequentially from the compound nucleus. For light targets, the coincidence cross section for sequentially evaporated

protons is sensitive to constraints imposed by momentum conservation.[8] To take these effects into account, we require that the residual nucleus recoils coherently from the emission of the first proton and that the second proton is emitted from this recoiling system. For simplicity, it is assumed that the more energetic proton is emitted first, and that the recoiling system is the ensemble averaged compound nucleus at the average temperature for proton emission. For low energy protons, the recoil corrections have a small effect, however, the importance of momentum conservation increases with the energy of the detected proton. The mean separation between sequentially evaporated protons, corresponding to the parameter $v'\tau$ in Koonin's model[9], is rather large (25-30 fm). For this reason we neglect final state interactions between independently emitted protons. We estimate that the greatest corrections to the correlation caused by final state interactions between these sequentially evaporated protons should occur at small relative momenta ($\Delta p < 15$ MeV/c) where the long ranged Coulomb interaction is dominant. In calculating the correlation cross section we have also neglected contributions from non-compound emission of protons. This is consistent with the magnitudes of the fusion cross sections which are assumed. The magnitude of non-compound contributions cannot easily be determined experimentally, since, for light targets, the compound and non-compound emission are not kinematically separated.

The spectra and multiplicities for ^{2}He and protons were calculated with the formalism of Ref. 5. This formalism predicts the multiplicities to be respectively .16 and 2.4 for the ^{12}C target, and .22 and 2.9 for the ^{27}Al target. Initial temperatures, 9.4 MeV for mass 28 (^{12}C target) and 9.9 MeV for mass 43 (^{27}Al target), follow from the assumption of a completely fused system treated as a Fermi gas with Fermi energies of 25 MeV and 33 MeV for the mass 28 and 43 systems. These energies are consistent with information from electron scattering.[10]

The calculated coincidence cross section for the ^{12}C target is shown in Fig. 1. This calculation was performed using the exact experimental detector configuration as input. It was determined to be insensitive to angular averaging effects arising from the finite detector solid angles. The calculated correlation is in excellent agreement with the data. A fusion cross section of 475mb is required to match the peak of the experimental coincidence cross section of 250μb/(MeV-sr)^2 which occurs at E_1, E_2 equal to 21, 28 MeV respectively. This corresponds to about 45 percent of the geometric cross section. The theoretical correlation functions $1+R(\Delta p)$ for the ^{12}C and ^{27}Al targets, normalized to 1 at 70 MeV/c (as was the data), are drawn as solid lines in Fig. 2. It should be noted that the correlation function in Fig. 2 is insensitive to the fusion cross section, therefore the excellent agreement is obtained here without any adjustable parameters.

Further information may be gained by investigating the correlation function $1+R(\Delta p)$ as a function of the total energy of the two coincident protons. This energy dependence for reactions on the ^{12}C and ^{27}Al targets is shown in Fig. 3 for the relative momentum intervals of $\Delta_1 p$ = 15-25 MeV/c (where the singlet s state strongly contributes) and $\Delta_2 p$ = 50-70 MeV/c (where the calculated correlation function primarily reflects contributions from noninteracting sequentially emitted protons). The decrease of the correlation functions with total proton energy for the large relative momentum bin $\Delta_2 p$ arises from the influence of momentum conservation on the correlation between sequentially emitted protons.[11] The structure in the calculated correlation functions for the small relative momentum bin $\Delta_1 p$ depends in a detailed way on the differences between the spectra for ^{2}He and for protons, and also on the Jacobians arising from kinematic coordinate frame transformations.

The correlation functions reported

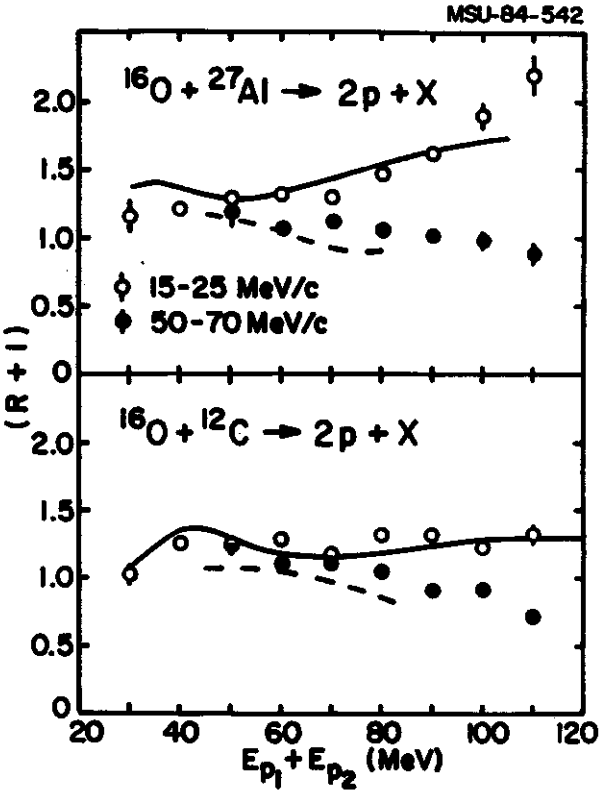

Fig. 3 a) The correlation function 1+R(Δp), gated on relative momentum intervals of 15-25 and 50-70 MeV/c, plotted as a function of the sum energy of the two protons for reactions on the ^{27}Al target. The theoretical correlation functions at the two momentum intervals are drawn as solid and dashed lines. b) Corresponding experimental and theoretical correlation functions for reactions on the ^{12}C target.

earlier[11] in ^{16}O reactions on ^{197}Au are considerably larger at Δp = 20 MeV/c than those shown here. The emission of ^{2}He from equilibrated compound nuclei cannot account for the correlations observed with the ^{197}Au target. In particular, for correlations measured at forward angles with heavy targets, e.g. Ref.11, the contributions from compound nuclear emission are negligible[4] compared to those from other processes such as direct or preequilibrium emission. In addition, the calculated multiplicity of ^{2}He statistically emitted from compound nuclei formed in reactions with the ^{197}Au target is smaller by a factor of 10 than multiplicities calculated for ^{12}C and ^{27}Al targets, while the proton inclusive cross sections are comparable.

---

a University of Wisconsin, Madison, WI

b ORNL, Oak Ridge, TN

1. M.A. Bernstein, et al., Phys. Rev. C29,132 (1984);30,412(E)(1984).
2. J. Gosset, et al., Phys. Rev. C18,844 (1978).
3. H. Stocker, J. Phys. G. Nucl. Phys. 10,L111 (1984).
4. M.B. Tsang, et al., Phys. Lett. 148B,265(1984).
5. W.A. Friedman and W.G. Lynch, Phys. Rev. C28,16(1983).
6. K.M. Watson, Phys. Rev. 88,1163(1952).
7. A.B. Migdal, Sov. Phys.-JETP 1,2(1955).
8. W.G. Lynch, et al., Phys. Lett. 108B,274 (1982).
9. S.E. Koonin, Phys. Lett. 70B,43(1977).
10. E.J. Moniz, et al., Phys. Rev. Lett. 26,445 (1971). .p-4,1
11. W.G. Lynch, et.al., Phys. Rev. Lett. 51,1850(1983).

CHARGE BINARY REACTIONS INDUCED BY 20 MeV/NUCLEON ^{14}N

H. Utsunomiya, D.J. Morrissey, R.A. Blue, E.C. Deci, L.H. Harwood, R.M. Ronningen,
K. Siwek-Wilczynska[a] and J. Wilczynski[b]

We report on cross sections of charge binary reactions that emit nitrogen, carbon and boron isotopes induced by 20 MeV/nucleon ^{14}N on ^{165}Ho and ^{164}Dy . The experiment was performed using 20 MeV/nucleon ^{14}N beam extracted from the K500 cyclotron at the National Superconducting Cyclotron Laboratory of Michigan State University. Two targets, 2.3 mg/cm^2 ^{165}Ho and 2.0 mg/cm^2 ^{164}Dy, were used in order to produce even Z nuclei (Dy and Er isotopes) as heavy residues. The binary nature of the reaction was determined by observing particle-γ-ray coincidences.

The isotopes of projectile-like fragments (PLF) were detected and clearly identified in a telescope consisting of 100μm silicon ΔE of high planarity and 1mm E detector. The telescope was located at 14° (near the classical grazing angle) with respect to the beam. The telescope had an opening angle of ±3.5° and a solid angle of 12.6 msr. Isotope separation was maintained by cooling the silicon detectors to -30°C during the measurements. Complete energy spectra of PLF with $5 \leq Z \leq 8$ were obtained, while fragments with $Z \leq 4$ punched through the E detector. Absolute cross sections were obtained from the known target thickness, the solid angle, and the integrated beam current collected by the Faraday cup. Because of the large opening angle of the particle counter and very steep angular distribution, the cross sections represent average quantities over an angular range of 10.5° - 17.5° with appropriate weights.

Two high purity germanium detectors with volumes of 89 cm^3 and 77 cm^3 were placed approximately 16 cm and 13 cm from the target, respectively, as indicated in Fig.1. Energy resolution of the HPGe detectors was about 1.9 keV at low count-rates and about 2.1 keV at a count-rate of 14 Kcps. The count-rate was

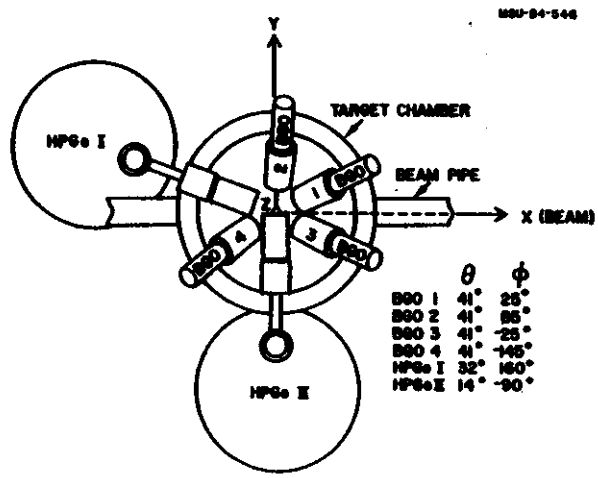

Fig.1 Sketch of arrangement of two high purity germanium detectors and four bismuth germanate detectors.

maintained at approximately 20 Kcps during the measurements. Gamma-ray signals with energies between 80 keV and 2 MeV were accepted. Photopeak efficiencies were measured using standard γ-ray sources. Coincidence cross sections for the charge binary reactions were obtained as in Ref.1. The photopeak yields were corrected for the electron conversion coefficients, branching ratios, angular anisotropies, and the pileup in the spectroscopy amplifier. The $4^+ - 2^+$ transition was used to dertermine the cross section for most even-even target-like fragments (TLF), unless the transition suffers from an neighboring unresolved peak in which case the $6^+ - 4^+$ transition was used. In both cases, the branching ratio was assumed to be 1. For the odd mass TLF, we used the transitions of $17/2^+ - 13/2^+$ or $21/2^+ - 17/2^+$ etc., avoiding the doublet problem. We determined the branching ratio for each transition with the help of the data of in-beam γ-ray spectroscopy.[2] The angular anisotropies were estimated by comparison of

spectra taken with the two HPGe detectors. The pileup probability, for which a correction was not made in a preliminary report,[3] was fairly large in our experimental arrangement. We used ORTEC 572 spectroscopy amplifiers each with a shaping time of 3 μsec. The amount by which the photopeak yield is reduced due to pileup was found to be 43±4% at a
γ-ray count-rate of 20 Kcps.

Inclusive energy spectra of the projectile-like fragments have a familiar shape with large cross sections centered at an energy approximately corresponding to the beam velocity and by long tails extended toward large negative Q-values. Fig.2 shows typical discrete γ-ray spectra taken in coincidence with ^{12}C and ^{11}B. We observed a dominant reaction channel of (^{14}N, bxn) (b=nitrogen, carbon, or boron isotopes), where missing particles are just neutrons. In addition, we also observed very weak γ transitions from another reaction subchannel of (^{14}N,bαxn), where missing particles include an α particle as well as neutrons.

In Table I, we summarize the ratios of the exclusive cross sections, summed over "xn" and "αxn" subchannels, to the inclusive cross sections. It should be pointed out that small fractions, in the range of 4%-13%, of the inclusive cross sections for nitrogen, carbon, and boron isotopes are associated with "charge binary" reactions. We compare the cross sections of binary reactions determined by the present measurements with the data[4] at 10 MeV/nucleon by the same method and the data[5] of the plastic box experiment. Fig.3 summarizes the cross sections for transfer reactions of 1 or 2 units of charge relative to the inclusive cross sections. For the present data and the data at 10 MeV/nucleon (indicated with "KVI"),[4] the cross sections of ^{12}C and ^{11}B are plotted, where the binary cross sections do not have strong isotope dependence. For the data of the plastic box experiment (indicated with "LBL"),[5] we chose those data with ejectiles of Z=8 and 9 for which the plastic box registered no additional charged

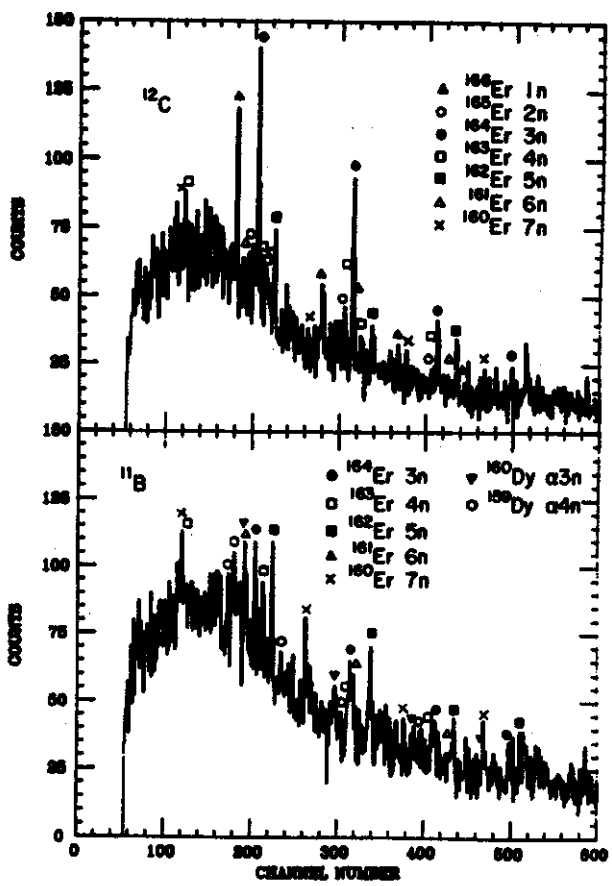

Fig.2 Discrete γ-ray spectra taken with the HPGe detector in coincidence with ^{12}C from collisions of ^{14}N on ^{165}Ho and with ^{11}B from collisions of ^{14}N on ^{164}Dy at 20 MeV/nucleon.

TABLE I. Cross sections summed over all xn and αxn subchannels and their fractions of the inclusive cross sections.

Reaction	$(d\sigma/d\Omega)_{14^\circ}$ (mb/sr)	Fractions (%)
$^{164}Dy(^{14}N, ^{15}Nxn)$	6.5±1.3	4.1±0.8
$^{164}Dy(^{14}N, ^{13}Nxn)$	3.6±0.5	11. ±2.
$^{165}Ho(^{14}N, ^{13}Cxn; ^{13}Caxn)$	7.7±3.5	4.9±2.2
$^{165}Ho(^{14}N, ^{12}Cxn; ^{12}Caxn)$	24.9±9.	7.6±2.9
$^{165}Ho(^{14}N, ^{11}Cxn; ^{11}Caxn)$	3.8±2.7	11. ±8.
$^{164}Dy(^{14}N, ^{12}Bxn; ^{12}Baxn)$	2.0±1.3	13. ±8.
$^{164}Dy(^{14}N, ^{11}Bxn; ^{11}Baxn)$	11. ±4.	9.5±3.8
$^{164}Dy(^{14}N, ^{10}Bxn; ^{10}Baxn)$	6.8±2.8	13. ±5.

particles. One can see considerable discrepancy between the particle-γ coincidence measurements done with the use of a ^{14}N beam and the plastic box measurements with a ^{20}Ne beam over incident energies from 10 to 20 MeV/nucleon. At present,

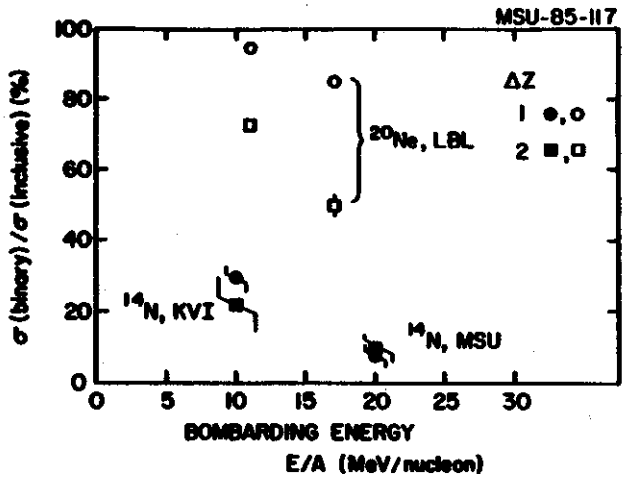

Fig.3 Binary cross sections vs incident energies. The binary cross sections are given in units of inclusive cross sections of the corresponding ejectiles. The data marked with KVI were taken from Ref.4. The data marked with LBL were taken from Ref.5.

the discrepancy remains unresolved.

---

a. On leave from Institute of Experimental Physics, University of Warsaw, 00-681, Poland; present address: Lawrence Berkeley Laboratory, Nuclear Physics Division, Berkeley, CA 94720

b. On leave from Institute for Nuclear Studies, 05-400 Swierk (Warsaw), Poland; present address: Lawrence Berkeley Laboratory, Nuclear Physics Division, Berkeley, CA 94720

1. L. Westerberg, D.G. Sarantites, R. Lovett, J.T. Hood, J.H. Barker, C.M. Currie, and N. Mullani, Nucl. Inst. and Method, 145,295(1977).
2. Table of Isotopes and references therein, edited by C.M. Lederer and V.S. Shirley, seventh edition,(a Wiley-Interscience Publication, John Wiley & Sons, Inc., New york, Chichester, Brisbane, Tronto, 1978).
3. H. Utsunomiya, D.J. Morrissey, R.A. Blue, L.H. Harwood, R.M. Ronningen, K. Siwek-wilczynska, and J. Wilczynski, Proc. the INS-RIKEN Internatinal Symposium on Heavy-Ion Physics, Mt. Fuji, Japan, 1984.
4. J. Wilczynski, K. Siwek-Wilczynska, J. van Driel, S. Gonggrijp, D.C.J.M. Hageman, R.V.F. Janssens, J. Lukasiak, R.H. Siemssen, and S.Y. van der Werf, Nucl. Phys. A373, 109(1982).
5. R.G. Stokstad, C.R. Albiston, M. Bantel, Y. Chan, P.J. Countryman, S.B. Gazes, B.G. Harvey, H. Homeyer, M.J. Murphy, I. Tserruya, K. van Bibber, and S. Wald, Proc. the INS-RIKEN Internatinal Symposium on Heavy-Ion Physics, Mt. Fuji, Japan, 1984.

ENERGY SPECTRA OF BEAM LIKE FRAGMENTS NEAR THE GRAZING ANGLE

E.C. Deci, D.J. Morrissey and H. Utsunomiya

I. Energy Spectra of Fragments lighter than the Beam.

Fragmentation is an important process in heavy ion reactions at energies above the Coulomb barrier. The fragmentation process is characterized by broad peaks in the energy spectra of fragments lighter than the beam. These peaks are centered near the energy corresponding to beam velocity. Models,[1-4] of the fragmentation process have been suggested that described the momentum of each fragment in terms of two components; the fragments's fraction of the beam momentum and the momentum due to internal motion. The intrinsic momentum is described by a probability distribution in momentum space which gives rise to the broad peaks in the observed energy spectra. We have extended these models to predict target fragment excitation and have tested the model against recent data.

The K500 cyclotron of the National Superconducting Cyclotron Laboratory at Michigan State University provided a beam of ^{14}N at 20 MeV/A. The target was ^{165}Ho with a thickness of 2.0 mg/cm^2. The inclusive energy spectra of projectile fragments were measured in a Si telescope. Discrete γ-rays from target fragments were also obtained in coincidence with the projectile fragments in a pair of intrinsic Ge detectors. Spectra for ten isotopes were determined and examples are shown in figures 1 and 2.

The peripheral model of Friedman was used to calculate the probability of fragmentation as a function of the internal momentum of the fragments assuming the following sequence of events. At the point of fragmentation Coulomb repulsion has slowed the beam nucleus while the target nucleus, at rest initially, has acquired velocity. The energy and momentum conservation laws governing the break up include the target

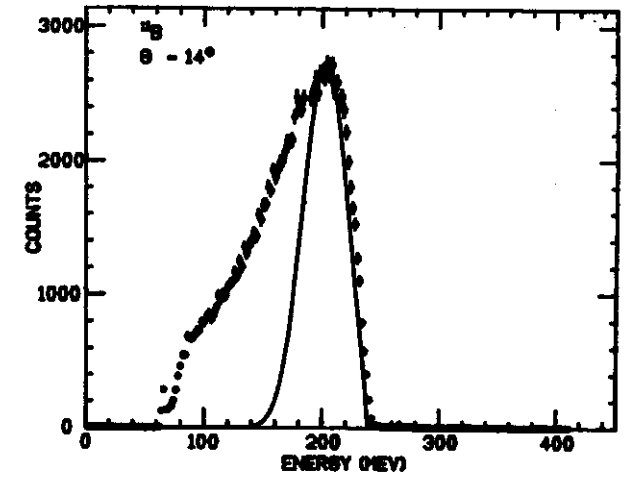

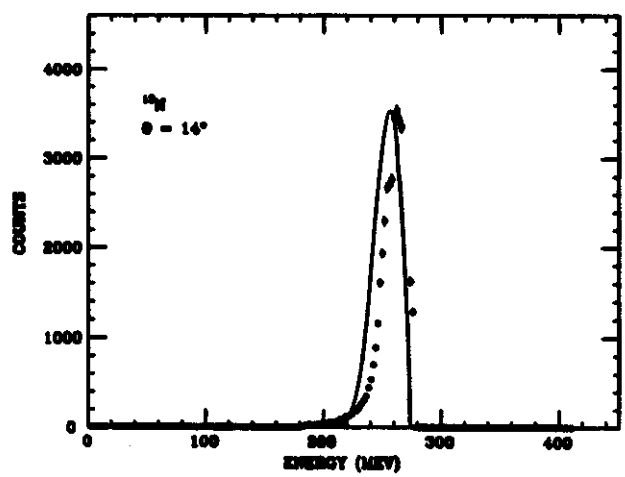

Figs. 1 and 2 Inclusive spectra for ^{11}B and ^{13}N fragments, the theoretical fits are discussed int the text.

and were written assuming the momentum of the fragments are the sum of intrinsic and beam like momenta. The available kinetic energy is diminished by their separation energy. After fragmentation the new Coulomb repulsion accelerates the fragments away from the target. Our experimental results indicate that the unobserved fragment is absorbed by the target less than 20% of the time (discussed below) but the small effect of the charge of the unobserved fragment was estimated by adding it to the

target charge. A Rutherford probability distribution was folded into the calculations and angular dependences were integrated over the acceptance of the detector.

The calculated spectra reproduce the experimental peak positions and shapes rather well. (see examples Fig. 1 and 2) The worst fit is for ^{13}N. The calculated peak is about 4 MeV too low in energy.

II. Absorbtive Fragmentation and Neutron Evaporation from the Target.

An important aspect of the present study is the correlation of projectile like fragments (PLF) with target like products. We are able to make a more stringent test of the fragmentation mechanics described above by comparing the observed target like fragment (TLF) mass distributions with model predictions. We analyze the cases where the unobserved partner in the fragmentation process is transfered to the target. The momentum distribution of this transfered fragment produces a distribution of excitation energies and angular momenta in the compound nucleus. The expected decay of the excited compound nucleus was calculated with the ALICE[5] computer code. A comparison of the numbers of evaporated neutrons predicted by this calculation with the experimental results are presented in fig 3. In most cases the fits are good. For ^{12}B and ^{13}C the calculation is clearly inadaquate. For these exit channels sequential decay feeding and other intermediate reactions make the assumptions underlying the calculations invalid.

III. Particla Pickup Spectra.

The experimental data also include reaction products heavier than the beam. Inclusive energy spectra for ^{15}N, ^{15}O, and ^{16}O were measured. These spectra can be predicted through an extention of the Friedman fragmentation model[6]. In this extension particle pickup is assumed to be a two step process where the target undergoes a virtual breakup into two parts followed by a transfer of one of the parts to the beam nucleus. The first

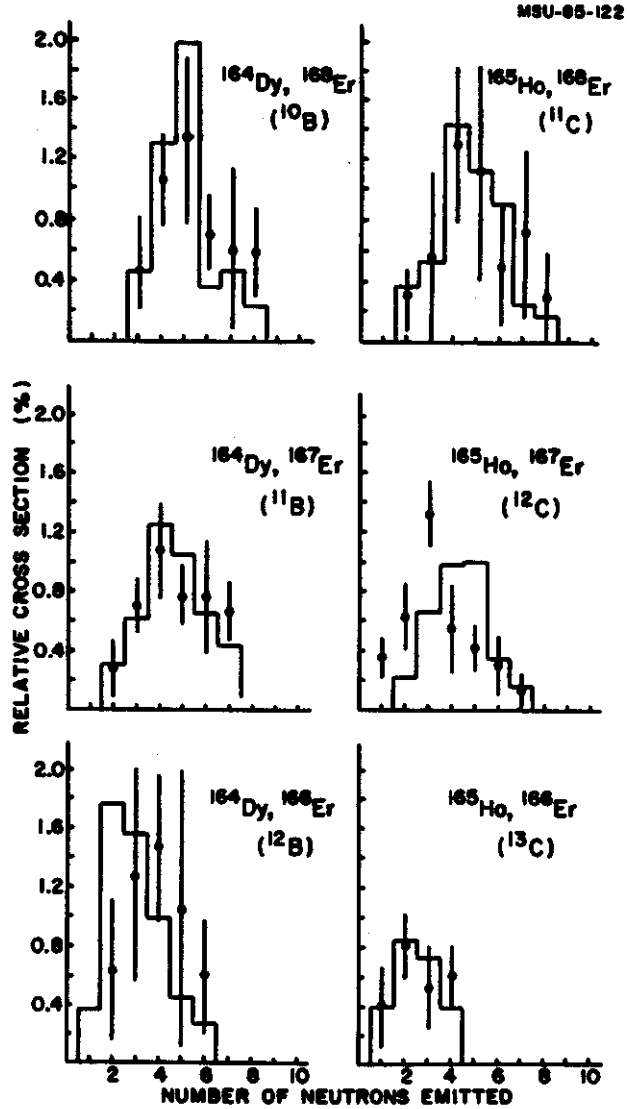

Fig. 3 Comparison of the observed isotopic distributions of TLF (points) with a simple calculation (histograms).

step is analogous to the fragmentation of the beam described above. The second set up where the beam nucleus absorbs the transfered target fragment is the reverse of the fragmentation process. The sequence of events is represented below.

The probability for pick up will then be given by

$$P \alpha |V_1|^2 |V_2|^2$$

where $|V_1|$, and $|V_2|$ are the vertex functions for fragmentation and absorbtion respectively. The

vertex functions reduce to

$$|V_1|^2 = e^{-(\vec{P}_E - \vec{P}_B)^2/2\sigma_1^2}$$

$$|V_2|^2 = e^{-(\vec{P}_E - \vec{P}_B(1+b))^2/2\sigma_2^2}$$

when momentum delta functions are invoked. B is the ratio of the mass of the transferred fragment to the mass of the beam nucleus. If we define a reduced width σ_r and a ratio u by

$$\sigma_r^2 = \frac{\sigma_1^2 \sigma_2^2}{\sigma_1^2+\sigma_2^2} = \frac{\sigma_1^2}{1+u} \qquad u=\frac{\sigma_1^2}{\sigma_u}$$

then

$$P \alpha e^{-\frac{1}{2\sigma_r^2}(\vec{P}_E - \frac{(1+u(1+b))}{(1+u)}\vec{P}_B)^2}$$

The exponential in this last equation produces a peak that is narrow and centered near the energy conservation cut off. (see Fig. 4) This model produces calculated spectra that well fit the experimental spectra in both position and shape.

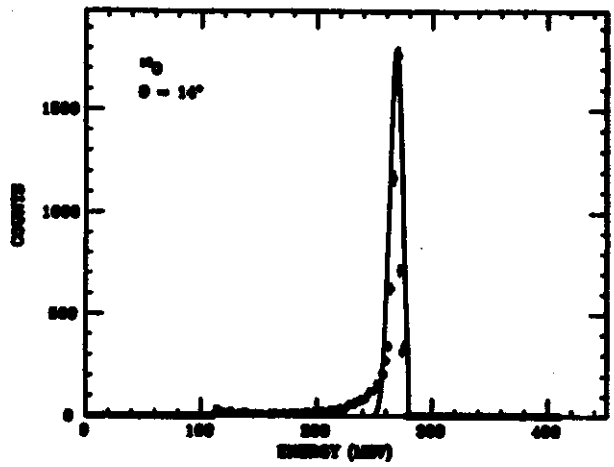

Fig. 4 Inclusive spectra for ^{15}O, an example of spectra of fragments heavier than the beam. The curve is calculated by the extended Friedman model.

1. R. Serber, Physical Review 72,1008(1947)
2. N. Matsuoka, A. Shimizu, H. Hosono, T. Saito, M. Kondo, H. Sakaguchi, Y. Toba, A. Goto, F. Chtani and N. Nakanishi, Nuclear Physics A311,173(1978)
3. S.L. Tabor, L.C. Dennis and K. Hbdo, Physical Review C 24,2552(1981)
4. W.A. Friedman, Physical Review C 27,569(1983)
5. M. Blann and F. Plasil. report ORNL-TM-6054
6. W.A. Friedman, private communication

DETECTION OF HEAVY-ION REACTION PRODUCTS IN BOUND EXCITED STATES

K. Siwek-Wilczynska[a], R.A. Blue, L.H. Harwood, R.M. Ronningen, H. Utsunomiya, J. Wilczynski,[b] and D.J. Morrissey

The population of bound (γ-decaying) states of the projectile-like fragments from the ^{14}N + ^{164}Dy reaction at 20 MeV/nucleon was studied by measuring coincidences between these fragments and γ-rays detected with large volume bismuth germanate detectors. The results indicate that products of pickup and exchange reactions are more likely to be excited than products of stripping reactions, particularly in fast, peripheral collisions.

In this communication we report an application of the gamma-particle coincidence method to select events in which light products of heavy-ion induced reactions(i.e., the projectile-like fragments, PLF) are produced in specific excited states that decay via gamma emission. In this method, projectile-like fragments (fully indentified by Z and A) are detected in coincidence with discrete γ-rays emitted from them. Typical γ-transitions in these light reaction products (A = 10-20) are rather energetic, up tp about 8 MeV.

Information on the population of various ejectiles in specific bound excited states can give important information on the question of the partition of the excitation energy between the reaction partners in asymmetric systems. Partition of the excitation energy in such systems that is not consistent with statistical equilibrium has already been reported by Awes et al. [1] and Vandenbosch et al. [2]. These indications were based on an analysis of the results on charge distributions and neutron multiplicity in supposedly binary reactions of rather heavy systems, as well as on mass asymmetry of fission fragments.

The average excitation energy of light fragments in very asymmetric systems can be studied more directly by observing either the particle decay or the γ-decay of the known excited states of the primary light products. Whereas the α-PLF coincidences yield similar information in the lower region of excitations, i.e., below the particle decay threshold. Thus, both methods complement one another, making possible a study of light fragment excitations over a broad range.

The present work was done in conjunction with an experiment that provided complementary information on target-like fragments in charge binary reactions [5]. A beam of 20 MeV/nucleon ^{14}N from the K500 cyclotron at the National Superconducting Laboratory of Michigan State University was used to bombard a metallic ^{164}Dy target of 1.95 mg/cm^2 thickness. Projectile-like fragments were detected at an angle of 14^0 (i.e., near the classical grazing angle) with a solid-state telescope consisting of a high planarity 100 μm ΔE detector and a 1 mm E detector. Isotopes of the elements up to oxygen were clearly resolved. Energetic γ-rays corresponding to transitions of up to 6 to 8 MeV (depending on the sign and magnitude of the Doppler shift correction) were detected with four large volume (7.6 cm x 7.6 cm) bismuth germanate (BGO) detectors. These detectors have a considerably larger photofraction for energetic photons than NaI(Tl) detectors of comparable volume[6]. The BGO detectors were placed at a distance of 17.5 cm from the target, above the reaction plane, with their axes pointing at the target and inclined at an angle of about 49^0 with respect to the horizontal plane (the corresponding azimuthal angles were 25^0, 85^0, -25^0, and -145^0).

Fig. 1 shows the six γ-ray spectra obtained with one of the BGO detectors, gated by ^{11}B, ^{12}C, ^{14}C, ^{15}N, ^{15}O and ^{16}O ejectiles,

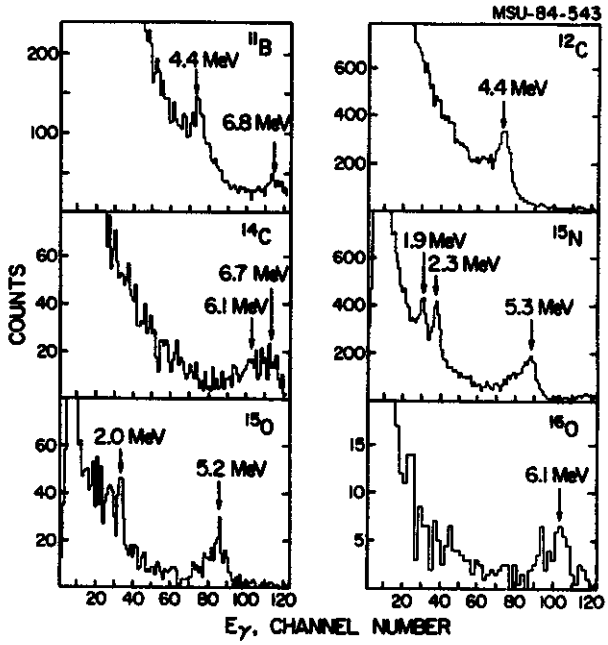

Fig. 1 Gamma-ray spectra taken in coincidence with selected ejectiles (^{11}B, ^{12}C, ^{14}C, ^{15}N, ^{15}O and ^{16}O) from the ^{14}N + ^{156}Dy at reaction at 20 MeV/nucleon.

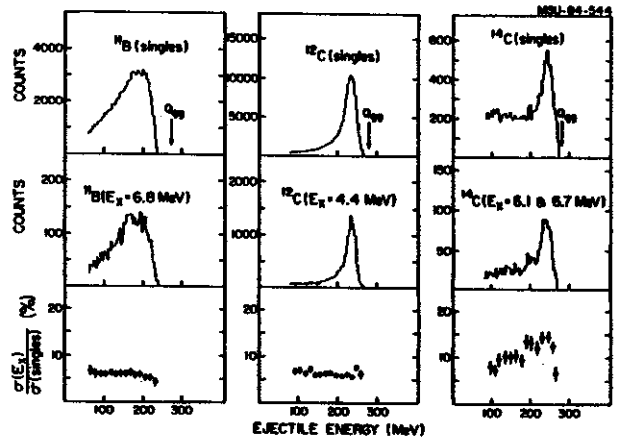

Fig. 2 Comparison of the singles energy spectra of ^{11}B, ^{12}C, and ^{14}C with those gated by photopeaks corresponding to specific γ-transitions in these nuclei. The diagrams at the bottom show the cross section for the population of the excited state in question relative to the inclusive cross section, as a function of the kinetic energy of the ejectile. The kinetic energies corresponding to the binary reactions leading to both fragments in the ground states are indicated by the arrows (Q_{gg}).

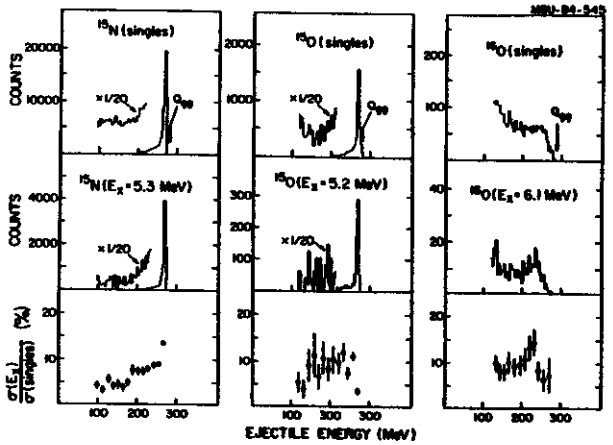

Fig. 3 Same as Fig. 2, except that the ejectiles are ^{15}N, ^{15}O and ^{16}O.

respectively. (These particular ejectiles show distinct γ-transitions of $E_\gamma > 4$ MeV, i.e., in the region where the background of the continuum γ-rays from the target-residue nuclei is small.) The γ-ray spectra were calibrated with a Be-Pu source (the 4.44 MeV transition in ^{12}C) and other standard calibration sources. The energies corresponding to the positions of the peaks (indicated by the arrows in Fig. 1) were calculated from the calibration curves, and corrected for the Doppler shift corresponding to the average ejectile velocity given by the centroid of the ejectile energy spectrum. These calculated energies exactly agree with the known γ-transitions in the respective nuclei.

Figs. 2 and 3 (middle rows) show the kinetic energy spectra of the chosen ejectiles observed in coincidence with the known γ-ray transitions. The inclusive energy spectra of the same ejectiles are shown above (upper rows) for comparison. The gated and ungated spectra for each ejectile look very similar. However, their ratio σ(Ex)/σ(singles) were calculated by summing up the data for all four BGO detectors and by using the known energy dependence of the photopeak efficiency of these detectors [7]. The γ-rays angular distributions were assumed to be isotropic in the rest frame of the ejectile.

The ratio σ(Ex)/σ(singles) ranges from 5% to 15%, depending on the ejectile, its observed excited state, and the energy of the ejectile. There is a clear difference in the energy dependence of this ratio between stripping-like reaction products (^{11}B and ^{12}C) and pick-up or

exchange reaction products (^{14}C, ^{15}N, ^{15}O and ^{16}O). In stripping reactions the ratio $\sigma(Ex)/\sigma(singles)$ is almost constant (5% to 7%) over the whole range of ejectile energies. In contrast, the ratio for pick-up and exchange reactions is approximately 5% at low energies, but increases up to about 15% in the quasielastic region. This indicates that the total excitation energy produced in the collision is not shared statistically (i.e., according to the available phase space of the equilibrated system), but rather depends on the direction of the mass transfer. One can speculate that the excitation energy associated with the transfer. One can speculate that the excitation energy associated with the transfer of mass is primarily shared as in the Oppenheimer-Phillips mechanism [8,9]. (A generalization of this mechanism for multinucleon transfer or exchange reactions has been proposed by Siemens et al [10]. In this mechanism the transferred nucleons leave the parent nucleus near the ground state of the daughter nucleus and bring their average individual momenta into the receiving fragment. Consequently the receiving fragment gets all the excitation energy in the earliest stages of the collision, i.e., immediately after the transfer. Any redistribution of the excitation energy presumable depends on the length of time of the nuclear interaction: the longer collision time, the more "relaxed" the expected partition of the excitation energy. As a result, the fastest reactions (peripheral collisions which shown up as the quasi-elastic peak in the energy spectra) would be expected to retain the pattern of the primary partition of the excitation energy. Thus this model predicts that the population of excited pick-up or exchange reaction products should be enhanced in the region of quasi-elastic peak. The data shown in Figs. 2 and 3 agree with this prediction.

Summarizing, we have shown that the γ-deexcitation of light projectile-like fragments can be relatively easily studied by measuring coincidences between these light fragments and γ-rays detected with large volume bismuth germanate detectors. The first measurements with this technique, a study of $^{14}N + ^{164}Dy$ reaction at 20 MeV/nucleon, showed a distinct difference, in the population of excited states, between stripping and pick-up (or exchange) reactions. In the latter type of reaction one observes an enhanced population of the excited states in the region of final kinetic energies corresponding to peripheral collisions.

---

a. On leave from Institute of Experimental Physics, University of Warsaw, 00-681, Poland; present address: Lawrence Berkeley Laboratory, Nuclear Science Division, Berkeley, CA 94720

b. On leave from Institute for Nuclear Studies, 05-400 (Warsaw), Poland; present address: Lawrence Berkeley Laboratory, Nuclear Science Division, berkeley, CA 94720

1. T.C. Awes, R.L. Ferguson, R. Novotny, F.E. Obenshain, F. Plasil, S. Pontoppidan, V. Rauch and G.R. Young, Physical Review Letter 52,252(1984)
2. R. Vandenbosch, A. Lazzarini, D. Leach, D.K. Lock, A. Ray and A. Seamster, Physical Review Letter 52,1964(1984)
3. J. van Driel, S. Gonggrijp, R.V. Janssens, R.H. Siemssen, K. Siwek-Wilczynska and J. Wilczynski, Physical Letters 98B,351(1981)
4. W.D.M. Rae, A.J. Cole, B.G. Harvey and R.G. Stockstad, Physical Review C 30,158(1984)
5. H. Utsunomiya, D.J. Morrissey, R.A. Blue, L.H. Harwood, R.M. Ronningen, K. Siwek-Wilczynska and J. Wilczynski, Proc. the INS-RIKEN International Symposium on Heavy-Ion Physics, Mt. Fuji, Japan, 1984
6. D.J. Morrissey, S.H. Wering and R.A. Blue, Nuclear Instruments and Methods 221,641(1984)
7. C.E. Moss and E.W. Tissinger, Nuclear Instruments and Methods 221,378(1984)
8. J.R. Oppenheimer and M. Phillips, Physica Review 48,500(1935)
9. R. Serber, Physical Review 72,1008(1947)
10. P.J. Siemens, J.P. Bondorf, D.H.E. Gross and F. Dickmann, Physical Letters 36B,24(1971)

LIGHT PARTICLE-COMPLEX FRAGMENT COINCIDENCE CROSS SECTIONS FROM INTERMEDIATE ENERGY NUCLEUS-NUCLEUS COLLISIONS

B.E. Hasselquist, G.M. Crawley, B.V. Jacak, Z.M. Koenig, G.D. Westfall, J.E. Yurkon, R.S. Tickle, J.P. Dufour and T.J.M. Symons

In the past decade experimental efforts in the field of heavy ion nuclear physics have concentrated on projectile energy regions below 20 MeV/nucleon and above 200 MeV/nucleon. The energy range in between is a particularly interesting regime because it covers projectile velocities ranging from below the fermi velocty in nuclei up to velocities several times the speed of sound in nuclei. New accelerators operating in this energy range have led to a number of investigations of inclusive light particle production from carbon-, oxygen-, neon-, and argon-induced reactions.[1-11] The double differential cross sections for particles with $1 \leq A \leq 4$ indicate the existence of a thermalized emission source moving at a velocity intermediate between the target and projectile velocities.[3,5,7] Fragment production cross sections for 42, 92, and 137 MeV/nucleon ^{40}Ar-induced reactions suggest that all intermediate rapidity particles ($1 \leq A \leq 14$) originate from a common source.[5] It is clear however that light particles and complex fragments may originate from different impact parameter collisions.[12] Results from 4π detectors such as the Plastic Ball[13] demonstrate that inclusive measurements are not sufficient to delineate clearly between various models for the reaction mechanisms.

To clarify the source of high energy fragments from these collisions we have measured the production of light particles in coincidence with projectile-like fragments (PLFs) which originate in gentle, grazing collisions and with intermediate rapidity fragments (IRFs) which come from highly inelastic collisions. By studying the properties of the light particle spectra triggered by these different classes of events and by comparing to the untriggered, inclusive data one may examine the differences between peripheral and more central collisions yielding complex fragments.

The present work investigates the dependence of the light particle spectra ($Z \leq 2$) on fragment production for the reactions ^{12}C + Al and Au at 30 MeV/nucleon and ^{40}Ar + Au at 92 MeV/nucleon. Light particle spectra for complex fragment triggers with $3 \leq Z \leq 6$ were obtained for the ^{12}C-induced reactions and spectra for trigger fragments with $3 \leq Z \leq 18$ were obtained for the ^{40}Ar-induced reaction. The complex fragments were either PLFs or IRFs depending on the angle of the trigger counter (forward angles are projectile-like and wider angles come from more violent reactions) and the energy ranges of the particle detectors.

In order to quantify the changes in the triggered light particle spectra, we have parametrized the spectra with a moving source model where the temperature, cross section and source velocity are extracted. These parameters are compared for inclusive and triggered data. A hydrodynamics calculation[14] has also been performed for the ^{40}Ar-induced coincidence spectra. To illustrate possible contributions from simple kinematics and conservation laws in the coincidence spectra, we also present a momentum conservation model calculation.

The 30 MeV/nucleon measurements were carried out using the K500 superconducting cyclotron at NSCL. The 92 MeV/nucleon work was done with the Bevalac at the Lawrence Berkeley Laboratory. The experimental apparatus consisted of an array of light particle detectors on one side of the beam axis along with two sets of complex fragment detectors placed on the opposite side of the beam. One set of fragment detectors was placed at forward angles and the dynamic range of the counters was

set to detect PLFs ranging from the beam down to Li. These fragments generally had energies corresponding to the projectile energy/nucleon. The second set of triggers was designed to detect IRFs and was placed at angles outside the region of PLFs with the dynamic range of the counters set to detect Li-O fragments.

The light particle array consisted of seven plastic scintillator-CaF_2 "phoswich" telescopes each of which used a single photomultiplier tube to collect both the plastic scintillator and the CaF_2 signal. The plastic scintillator was 17 cm thick and the CaF_2 was 2mm thick. The telescope array was moved during the experiments and covered in-plane angles from approximately 38 to 97°. The energy calibration of the telescopes was done using ^{4}He beams of 25 MeV/nucleon at NSCL and 150 MeV/nucleon p and ^{4}He at LBL. The light particle inclusive and coincidence spectra have been corrected for reaction losses in the scintillators and for particles scattering out of the detectors. The fragment detectors were composed of stacks of silicon detectors. Two different IRF stacks were used in the 92 MeV/nucleon work to provide sufficient dynamic range. The PLF detectors were placed outside the grazing angle to suppress elastic scattering. The grazing angles for 30 MeV/nucleon ^{12}C+Al, ^{12}C+Au, and 92 MeV/nucleon ^{40}Ar+Au were 3°, 12°, and 3° respectively.

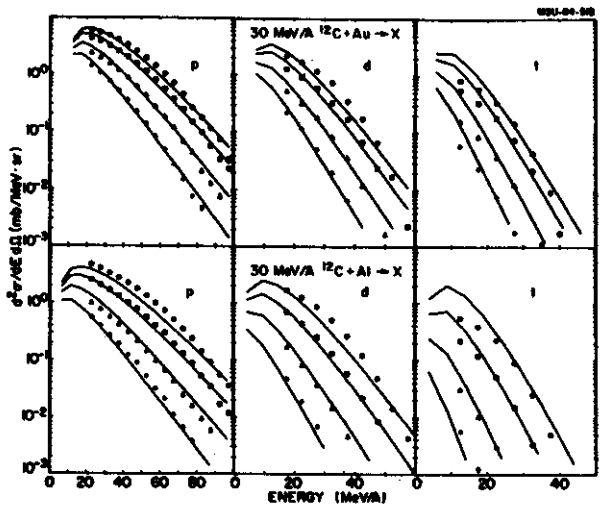

Fig. 1. Inclusive spectra for p,d and t from 30 MeV/nucleon ^{12}C + Au and Al. The angles were 47° (•),56° (□),71° (Δ) and 90° (diamonds) for Au and 45° (•),56° (□),71° (Δ) and 90° (diamonds) for Al. The solid lines are moving source fits.

Light particle inclusive spectra have been measured for the reaction 30 MeV/nucleon ^{12}C+Al at the angles 45, 56, 71, and 90° and at 47, 56, 71 and 90° for 30 MeV/nucleon ^{12}C+Au. Energy spectra for the hydrogen isotopes are shown in Fig. 1. The solid curves in the figure are moving source fits to the data.Light particle inclusive spectra have been measured for the reaction 92 MeV/nucleon ^{40}Ar+Au at angles of 45, 67.5, and 90° in the laboratory. Energy spectra for p, d, t, ^{3}He and ^{4}He are shown in Fig. 2.

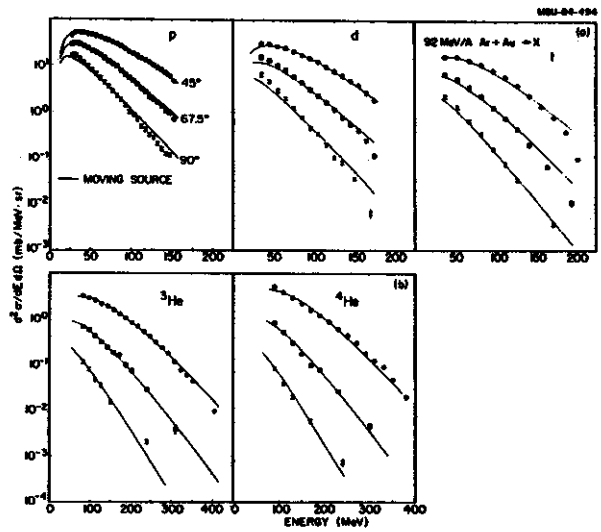

Fig. 2. Inclusive spectra for p,d,t,^{3}He and ^{4}He from 92 MeV/nucleon ^{40}Ar + Au. The solid lines correspond to moving source fits and the dot-dashed lines represent firestreak model calculations.

Again the solid lines correspond to moving source calculations. The 92 MeV/nucleon inclusive data are qualitatively similar to the 30 MeV/nucleon data. There is no drastic change in the inclusive light particle spectra in spite of the differences in the incident energies. At 30 MeV/nucleon the extracted source temperatures for the two targets are quite similar. The source velocities for the Al

target spectra are ≈30 percent higher than for the Au target. The temperatures and velocities agree with systematics of O- and Ne- induced reactions on heavy targets[3] as shown in Fig. 3.

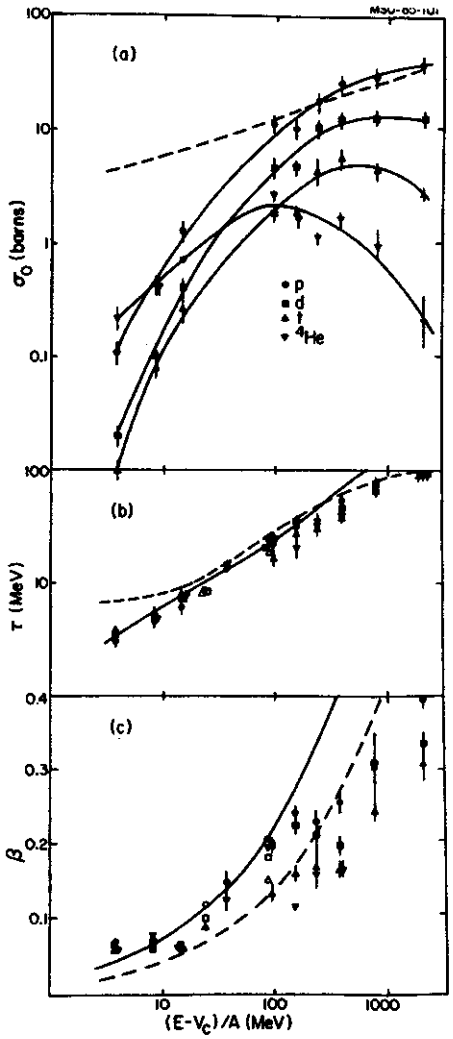

Fig. 3. Systematics of moving source parameters extracted from O- and Ne-induced reactions on heavy nuclei. The solid lines are to guide the eye and the dashed lines are fireball model calculations. Present results for ^{12}C- and ^{40}Ar-induced reactions are given in open symbols.

To focus on more central collisions, we have measured light particles in coincidence with high energy complex fragments emitted at wide angles. These trigger fragments are not associated with either the projectile or target nuclei but instead appear to be emitted from a source moving with velocity or rapidity intermediate between the projectile and target velocities. All of the coincidence spectra presented below have been divided by the solid angle of the trigger detector. Proton spectra triggered on IRFs with 3≤Z≤6 for 30 MeV/nucleon ^{12}C+Al are shown in Fig. 4. Spectra for protons

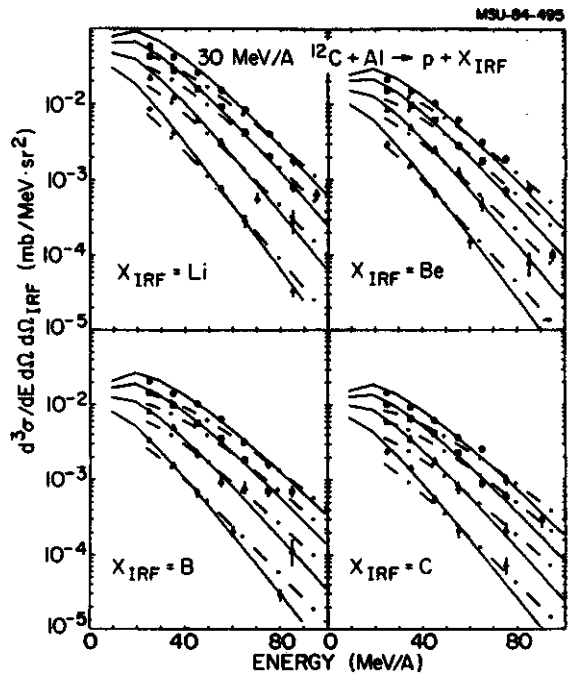

Fig. 4. Proton spectra from 30 MeV/nucleon ^{12}C + Al triggered by intermediate rapidity fragments (IRFs). The spectra were measured at 45° (•),56° (□),71° (Δ) and 90° (diamonds). The solid lines represent moving source fits and the dot-dashed lines show momentum conservation model calculations as described in the text.

coincident with IRFs from 92 MeV/nucleon ^{40}Ar+Au are shown in Fig. 5. The inclusive light particle spectra have been included in the figures for comparison with the coincidence spectra. The coincidence spectra have the same general features as the inclusive spectra for all measured light particle - IRF combinations suggesting that these fragments have a common source. The solid curves in the Figs. 4 and 5 are moving source fits to the IRF-triggered data and the extracted parameters are given in Fig. 6. There seems to be no significant dependence of the temperature and velocity parameters on the particular type of light particle measured.

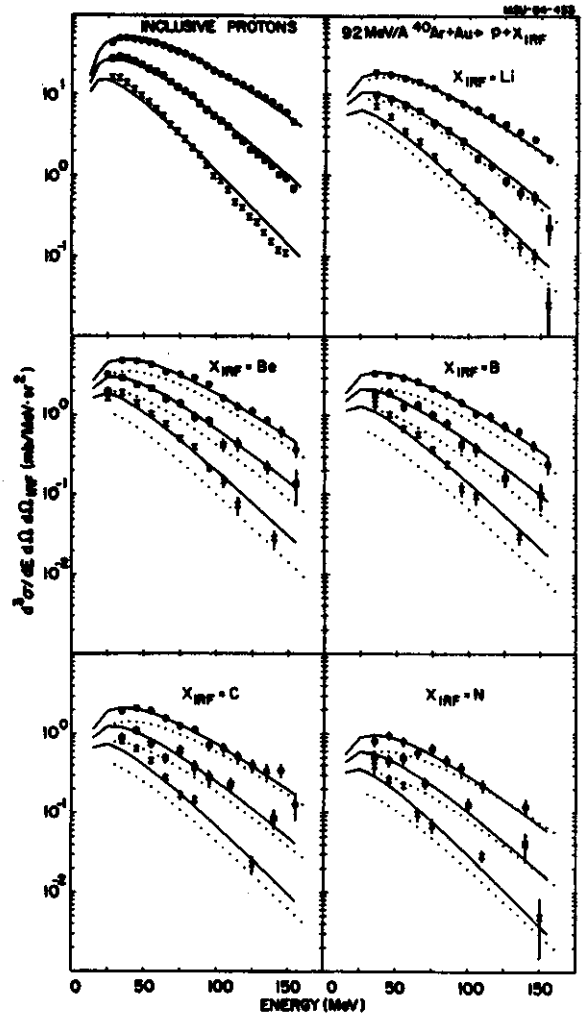

Fig. 5. Inclusive and intermediate rapidity fragment (IRF) triggered spectra for protons from 92 MeV/nucleon ^{40}Ar + Au at 45° (·), 67.5° (□) and 90° (▮). The solid lines represent moving source fits and the dotted lines show the momentum conservation model as described in the text.

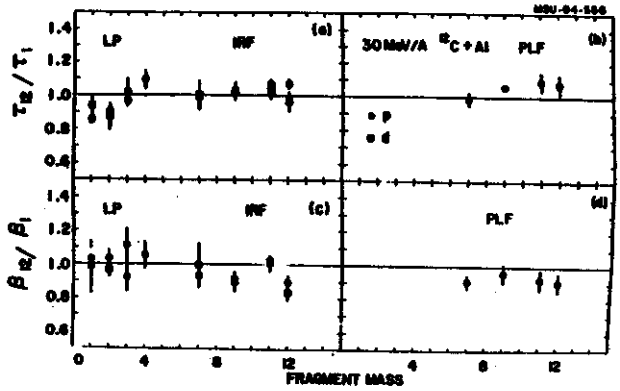

Fig. 6. Ratios of moving source parameters extracted from triggered and inclusive proton and deuteron spectra from 30 MeV/nucleon ^{12}C + Al. The trigger in (a) and (c) is intermediate rapidity fragments (IRFs) and in (b) and (d) it is projectile like fragments (PLFs).

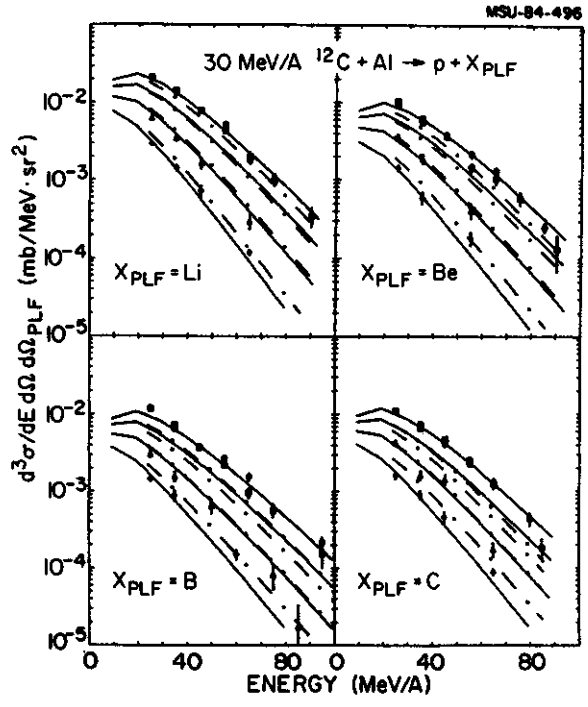

Fig. 7. Proton spectra from 30 MeV/nucleon ^{12}C + Al triggered by projectile like fragments (PLFs). The spectra were measured at 45° (·),56° (□),71° (Δ) and 90° (diamonds). The solid lines represent moving source fits and the dot-dashed lines show momentum conservation model calculations as described in the text.

Coincidence spectra between protons and projectile velocity fragments from 30 MeV/nucleon ^{12}C + Al are shown in Fig. 7. Spectra for coincidences between protons and projectile-like fragments from 92 MeV/nucleon ^{40}Ar+Au are shown in Fig. 8. The spectra for coincident fragments with 9≤Z≤15 have been summed together to obtain reasonable statistics. The inclusive light particle spectra have been included in these figures for comparison with the coincidence spectra. The coincidence spectra for the Li through N PLF triggers appear to be very similar to the inclusive spectra. However, it can be seen from Fig. 8 that the

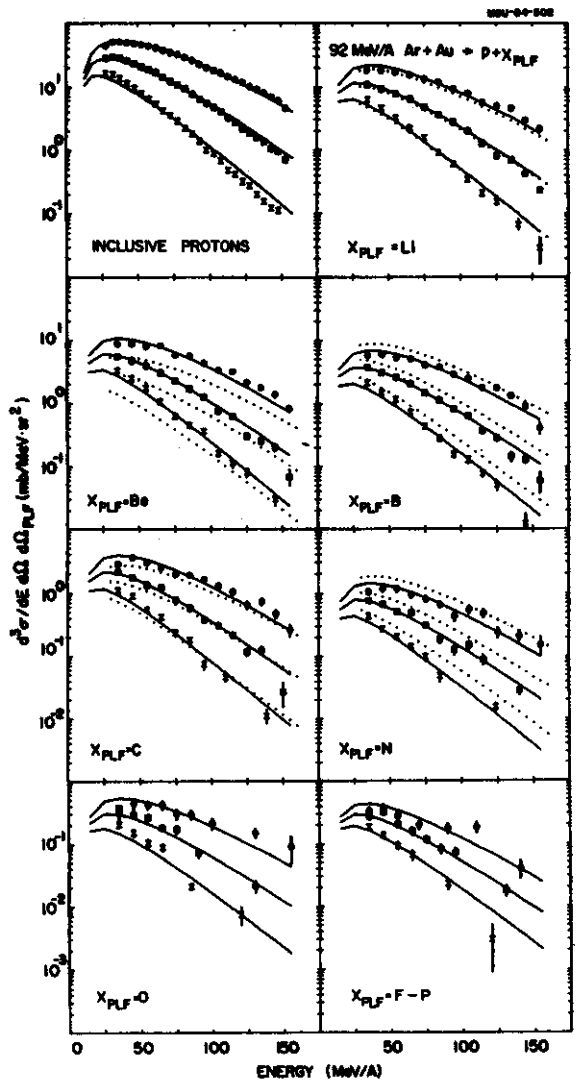

Fig. 8. Inclusive and projectile like fragment (PLF) triggered spectra for protons from 92 MeV/nucleon ^{40}Ar + Au at 45° (•), 67.5° (□) and 90° (▣). The solid lines represent moving source fits and the dotted lines show the momentum conservation model as described in the text.

proton coincidence cross sections for the O and the F through P PLF triggers have a slightly flatter angular distribution than the inclusive cross sections characteristic of a lower source velocity. The extracted moving source fit parameters are given in Fig. 9. As was true for the light particle - IRF spectra, the temperature parameter shows no variation with the PLF trigger fragment mass. This constancy could reflect the fact that the PLF spectra at 13° may contain a large contribution from

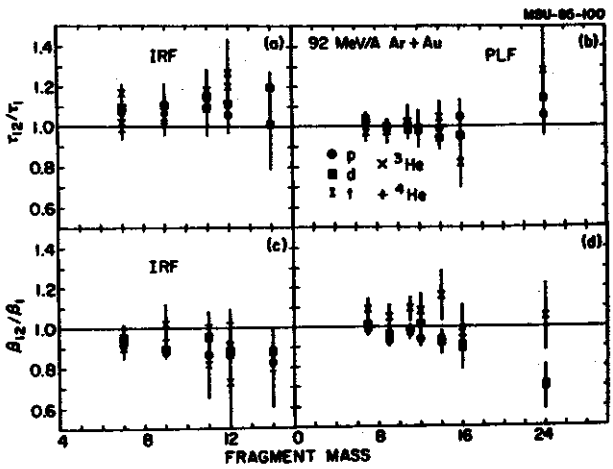

Fig. 9. Ratios of moving source parameters extracted from triggered and inclusive p, d, t, ^{3}He and ^{4}He spectra from 92 MeV/nucleon ^{40}Ar + Au. The trigger in (a) and (c) is intermediate rapidity fragments (IRFs) and in (b) and (d) it is projectile like fragments (PLFs).

thermal sources. In contrast, the velocities show a clear trend toward decreasing velocities with increasing trigger fragment mass. An apparent velocity 30 percent below the inclusive result is obtained for the average projectile mass of A=24 which is consistent with the concept of emission from an excited residual target nucleus.

The interpretation of coincidence spectra has as an inherent hazard the possibility of assigning special significance to phenomena which had their origins in simple conservation laws. The calculation presented here assumes that two coincident particles are emitted sequentially from a single moving source. The results of the momentum conservation model for 30 MeV/nucleon induced coincidence spectra triggered by IRFs are shown as dot-dashed or dotted lines in Figs. 4,5,7, and 8. Based on the assumption that IRFs originate from a fireball-like system, this model should demonstrate the effect of simple momentum conservation on the coincidence spectra. For the case of ^{12}C + Al the model calculation with the FB geometry prediction of A=18 exhibited extreme effects due to the source recoil that were not observed in the data. To obtain better

agreement with the data, the source size was increased to A=27 and the results of these calculations are shown in Fig. 4 as dot-dashed lines. This comparison suggests that the emitting source is larger than A=27 and perhaps could be as large as the projectile/target system. In contrast to the 30 MeV/nucleon data, the IRF triggered spectra at 92 MeV/nucleon are well described by this model using the FB geometry as shown in Fig. 5 in the form of dotted lines. This system apparently has sufficient kinetic energy and number of particles to make momentum conservation effects negligible. For PLF-triggered spectra the model should only describe light particle spectra in coincidence with PLFs that exhibit a thermal rather than a projectile-like velocity distribution. Indeed the results of this calculation shown in Fig. 7 for 30 MeV/nucleon ^{12}C + Al as dot-dashed lines agree for Li PLFs and disagree for C PLFs. This result indicates that the C PLFs are fragmentation products and are not emitted from the same source as the light particles.

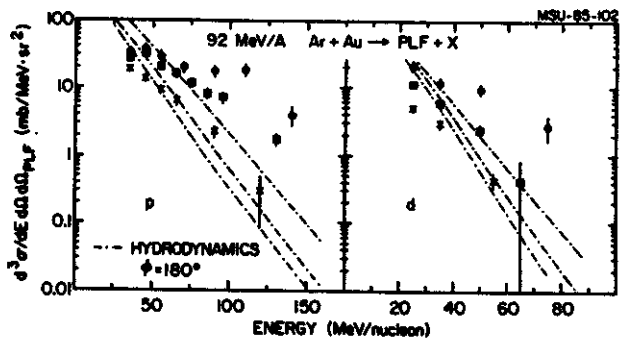

Fig. 10. Proton and deuteron spectra triggered by projectile like fragments from F to P from 92 MeV/nucleon ^{40}Ar + Au. The dot-dashed lines correspond to non-azimuthally averaged hydrodynamics calculations for ϕ = 180° corresponding to angles in the reaction plane opposite the direction of the projectile.

Fig. 10 shows the results of the hydrodynamics (HD) calculations of Buchwald[14] for the reaction 92 MeV/nucleon ^{40}Ar+Au compared to p and d spectra triggered by PLFs from F to P at -13°. The observation of the PLF determines the reaction plane. The dot-dashed lines are the predicted p and d spectra for θ=45, 70 and 90° and an azimuthal angle of ϕ=180°. An azimuthal angle of ϕ=180° corresponds to the opposite side of the reaction plane in which the projectile nucleus is scattered in the HD calculation. The calculation is averaged for impact parameters from 0 to 7 fermi. The calculation is not azimuthally averaged as was the HD calculation used in comparison to the inclusive light particle spectra. The normalizations are arbitrary to allow comparisons of the shapes. The hydrodynamics prediction for ϕ=0° can be characterized by the enhancement of the forward angle spectra while the ϕ=180° prediction is almost isotropic. The lack of agreement between the theory and the data could be due to the inability of the experimental arrangement to completely determine the reaction plane. Another explanation could be that the incompressibility constant, K, used in the HD calculation was 200 MeV whereas recent results[15] have shown that a much stiffer equation of state is required with K=380 MeV which would subtantially alter the calculations shown in Fig. 10 in the direction of producing more apparent forward motion.

---

1. B. Jakobsson, L. Carlen, P. Kristiansson, J. Krumlinde, A. Oskarsson, I. Otterlund, B. Schrøder, H.-A. Gustafsson, T. Johansson, H. Ryde, G. Tibell, J. P. Bondorf, G. Fài, A.O.T. Karvinen, O.B. Nielsen, M. Buenerd, J. Cole, D. Lebrun, J.M. Loiseaux, P. Martin, R. Ost, P. de Saintignon, C. Guet, E. Monnand, J. Mougey, H. Nifenecker, P. Perrin, J. Pinston, C. Ristori, and F. Schussler, Phys. Lett. 102B,121(1981).
2. J.B. Natowitz, M.N. Namboodiri, L. Adler, R.P. Schmitt, R.L. Watson, S. Simon, M. Berlanger, and R. Choudhury, Phys. Rev. Lett. 47,1114(1981).
3. G.D. Westfall, B.V. Jacak, N. Anantaraman, M.W. Curtin, G.M. Crawley, C.K. Gelbke, B. Hasselquist, W.G. Lynch, D.K. Scott, M.B. Tsang, M.J. Murphy, T.J.M. Symons, R. Legrain, T.J. Majors, Phys. Lett. 116B,118(1982) and references therein.
4. R.L. Auble, J.B. Ball, F.E. Bertrand, C.B. Fulmer, D.C. Hensley, I.L. Robinson, P.H. Stelson, C.Y. Wong, D.L. Hendrie, H.D. Holmgren, and J.D. Silk, Phys. Rev. C28,1552(1983).
5. B.V. Jacak, G.D. Westfall, C.K. Gelbke, L.H.

Harwood, W.G. Lynch, D.K. Scott, H. Stöcker, M.B. Tsang, and T.J.M. Symons, Phys. Rev. Lett. 51,1846(1983).
6. R. Glasow, G.Gaul, B. Ludewigt, R. Santo, H. Ho, W. Kühn, U. Lynen and W.F.J. Müller, Phys. Lett. 120B,71(1983).
7. G.D. Westfall, Z.M. Koenig, B.V. Jacak. L.H. Harwood, G.M. Crawley, M.W. Curtin, C.K. Gelbke, B. Hasselquist, W.G. Lynch, A.D. Panagiotou, D.K. Scott, H. Stöcker, and M.B. Tsang, Phys. Rev. C29,861(1984).
8. D.J. Fields, W.G. Lynch, C.B. Chitwood, C.K. Gelbke, M.B. Tsang, H. Utsunomiya, and J. Aichelin, MSU Cyclotron Laboratory Preprint MSUCL 471,(1984).
9. V. Borrel, D. Guerreau, J. Galin, B. Gatty, D. Jacquet, and X. Tarrago, Z. Phys. A314,191 (1983).
10. J. Mougey, R. Ost, M. Buenerd, J. Cole, C. Guet, D. Lebrun, J. M. Loiseaux, P. Martin, M. Maurel, E. Monnand, H. Nifenecker, P. Perrin, J. Pinston, C. Ristori, P. de Saintignon, F. Schussler, L. Carlen, B. Jakobsson, A. Oskarsson, I. Otterlund, B. Schrøder, H.-A. Gustafsson, T. Johansson, H. Ryde, J.P. Bondorf, O.B. Nielsen, and G. Tybell, Phys. Lett. 105B, 25(1981).
11. F. Rami, J.P. Coffin, G. Guillaume, B. Heusch, P. Wagner, A. Fahli, and P. Fintz, report CRN/PN.8407(1984).
12. B.V. Jacak, H. Stöcker, and G.D. Westfall, Phys. Rev. C29,1744(1984).
13. H.A. Gustafsson, H.H. Gutbrod, B. Kolb, H. Löhner, B. Ludewigt, A.M. Poskanzer, T. Renner, H. Riedesel, H.G. Ritter, A. Warwick, F. Weik, and H. Wieman, LBL Preprint LBL-17678,(1984) and Phys. Rev. Lett. 18,1590(1984).
14. G. Buchwald, private communication and H. Stöcker, L.P. Csernai. G. Graebner, G. Buchwald, H. Kruse, R.Y. Cusson, J.A. Maruhn, and W. Greiner, Phys. Rev. C25,1873(1982).
15. D. Hahn and H. Stöcker, MSUCL-505,(1985).

MULTIPARTICLE CORRELATIONS IN HIGH ENERGY NUCLEUS-NUCLEUS COLLISIONS

Z.M. Koenig, G.D. Westfall, R.S. Tickle, G.M. Crawley, D. Fox, R. Fox, B.E. Hasselquist, D. Horn, B.V. Jacak, J. Wilcynski and K. Siwek-Wilczynska

There has recently been a lot of interest in the study of collective, dynamic effects in nucleus-nucleus collisions at intermediate energies (above 20 MeV/nucleon and below 200 MeV/nucleon) in order to provide a new test of the applicability of hydrodynamic models of nuclear matter in this energy range. At these energies, one is far below the free nucleon-nucleon threshold for pion production and yet above energies where mean field phenomena dominate. Thus, one can speculate that this energy regime will be appropriate to observe hydrodynamic phenomena such as mass flow and compression without large amounts of background being created from particle production and high thermal energies.

A great deal of information concerning high energy nucleus-nucleus collisions has been obtained using single particle inclusive measurements[1,2,3]. A comparison between these data and theoretical predictions shows that models incorporating widely differing assumptions are equally successful in reproducing the data. Consequently, several large scale experiments (HISS, The Plastic Ball/Wall, TASS, The Particle Correlation Spectrometer, etc.) have been mounted to study multiparticle final states. All of these experiments have concentrated on incident energies above 200 MeV/nucleon. The streamer chamber and emulsions have also been used to study multiparticle events at all energies. All of these previous studies have suffered from various limitations. The emulsion and streamer chamber results suffer from lack of statistics. The Plastic Ball/Wall is ideally suited for measuring light particles in the intermediate rapidity region in reactions above 200 MeV/nucleon but can only observe particles with ranges greater than protons above 40 MeV/nucleon. However, at beam energies below 100 MeV/nucleon, the lower energy cutoff precludes the Plastic Ball from making a complete measurement. In addition, the relative proportion of heavy fragments ($3 \leq Z \leq 7$) at intermediate rapidities increases as the beam energy is lowered[4]. We have measured the yield of these fragments as a function of incident energy using 50,100, and 150 MeV/nucleon ^{40}Ar beams incident in Ca and Au targets[4] and have shown that the production of heavier mass fragments at the lower beam energy is apparent. Thus, in order to study multiparticle final states and intermediate energies, one must detect not only light particles, but intermediate mass fragments as well.

An important observable that results from multi-particle measurements is triple differential cross sections. In Fig. 1, the triple differential cross section predictions of the fluid dynamics model[5] are shown for the case of 137 MeV/nucleon Ar+Au. A clear peak is seen for the case of $\phi = 0$ and 180^0. In contrast, a cascade calculation would not produce these bumps but would instead produce a relatively azimuthally isotropic distribution[5]. These differences presumably would become more marked in the vicinity of 100 MeV/nucleon incident energies.

An example of a multi-particle measurement that has succeeded in discriminating between various models is one in which protons observed at angles from 20 to 130^0 are tagged with the multiplicity of charged particles emerging from the reaction of 393 MeV/nucleon Ne+U[6]. For high multiplicity the forward emission of low energy protons is suppressed. Calculations such as firestreak, nuclear cascade, and rows-on-rows fail to reproduce this suppression while a hydrodynamical calculation successfully predicts

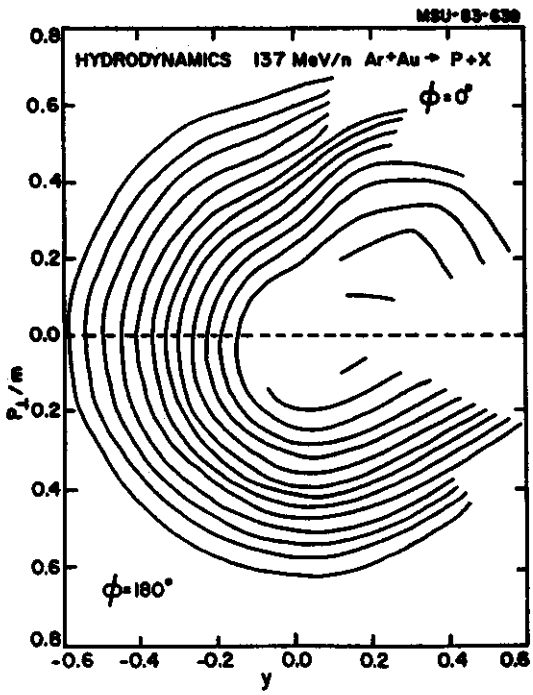

Fig. 1 Triple differential cross sections predicted using the fluid dynamics model.

the sidewards peaking. Evidently at the relatively high bombarding energy of 393 MeV/nucleon, hydrodynamical effects can be observed. A measurement of the triple differential cross sections therefore provide a further important test of the validity of hydrodynamic models for nuclear matter in intermediate energy collisions.

The present work consists of multiparticle measurements for the systems ^{12}C + Au and ^{12}C + C at 15 and 30 MeV/nucleon at the NSCL K500 cyclotron and ^{40}Ar + Au at 100 MeV/nucleon at the Low Energy Beam Line of the LBL Bevalac. The key to these experiments was a new detection system. At intermediate energies, it is important to study not only light particles and projectile-like fragments, but also intermediate rapidity medium mass fragments and fission fragments thus necessitating the new counters. Our study of multiparticle final states at intermediate energies used to different light particle array devices, the first consists of a three plane, multiwire proportional chamber (MWPC) backed by seven light particle telescopes, which was used in a previous experiment[7]. The second device consists of a Parallel Plate Avalanche Counter (PPAC), a Bragg Curve Counter (BCC), and six CaF_2-plastic scintillator telescopes. The light particle coincidence spectra were taken with four trigger conditions; heavy fragments from the target in the PPAC, projectile-like fragments at 15^0 (MSU) or 7^0 (LBL), intermediate rapidity medium mass fragments in the BCC, and self-triggered by several light particles in the CaF_2-plastic telescopes.

An important feature of the LBL experiment was three light particle telescopes above the plane to give a partial picture of the dependence of the triple-differential cross sections on azimuth. These detectors were placed at θ = 45, 60, and 135^0 at $\phi = 90^0$. The triple differential cross sections in Fig. 1 are presented for ϕ = 0 and 180^0 only, but the intermediate azimuthal angles also exhibit striking peaks and must be measured, at least for a specific θ.

1. G.D. Westfall, B.V. Jacak, N. Anantaraman, M.V. Curtin, G.M. Crawley, C.K. Gelbke, B. Hasselquist, W.G. Lynch, D.K.Scott, M.B. Tsang, M.J. Murphy, T.J.M. Symons, R. Legrain and T.J. Majors, Phys. Lett.116B,118(1982).
2. A. Sandoval, H.H. Gutbrod, W.G. Meyer, R. Stock, Ch. Lukner, A.M. Poskanzer, J. Gosset, J.-C. Jourdain, C.H. King, G. King, Nguyen Van Sen, G.D. Westfall and K.L. Wolf, Phys. Rev.C21,1321(1980).
3. S. Nagamiya, M.-C. Lemaire, E. Moeller, S. Schnetzer, G. Shapiro, H. Steiner, and I. Tanihata, Phys. Rev. C.24,971(1981).
4. B.V. Jacak, G.D. Westfall, C.K. Gelbke, L.H. Harwood, W.G. Lynch, D.K. Scott, H. Stöcker, M.B. Tsang and T.J.M. Symons, Phys. Rev. Lett.51,1846(1983).
5. H. Stöcker, L. Csernai, G. Graebner, G. Buchwald, H. Kruse, R.Y. Cusson, J.A. Maruhn and W. Greiner, Phys. Rev. C.25,1873(1982), H. Stöcker, private communication.
6. H. Stöcker, G. Buchwald, G. Graebner, J.A. Maruhn, W. Greiner, K. Frankel, M. Gyulassy, B. Shurmann, G.D. Westfall, J.D. Stevenson, J.R. Nix and D. Strottman, Phys. Rev. Lett.47,1807(1981).
7. B.E. Hasselquist, G.M. Crawley, B.V. Jacak, Z.M. Koenig, G.D. Westfall, J.E. Yurkon, R.S. Tickle, J.P. DuFour and T.J.M. Symons, submitted to Phys. Rev. C.

IMPORTANCE OF DIRECT VS. THERMAL EMISSION IN 40 MeV/NUCLEON $^{12}C+C$

D. Fox, D.A. Cebra, Z.M. Koenig, J.J. Molitoris, P. Ugorowski, H. Stöcker and G.D. Westfall

The relative importance of direct nucleon-nucleon reactions versus phenomena involving many nucleons simultaneously is important to the understanding of the reaction mechanisms between two high energy nuclei. At incident energies near the coulomb barrier one expects nuclei to interact through their mean fields. As one raises the relative velocity between the two nuclei, one expects direct nucleon-nucleon scattering to become the dominate reaction mechanism at energies that are high compared to the fermi energy and the binding energy of the constituent nucleons. If enough nucleon-nucleon reactions occur, the system may approach thermal kinetic equilibrium. If such a system has a lifetime comparable to the formation and decay time of nuclear and baryonic resonances the system may also approach chemical equilibrium. There is evidence for thermal behavior in nucleus-nucleus collisions where an apparent thermal source of nucleons and complex fragments has been observed with a velocity intermediate between those of the projectile and target for a wide range of incident energies.[1-3]

The relative contributions of direct versus multiparticle interactions has been studied in $^{12}C+C$, $^{40}Ar+KCl$ and $^{12}C+Pb$ at 800 MeV/nucleon.[4] When the ratio of in-plane to out-of-plane correlations was measured for the C+C case a significant enhancement was observed at energies and angles corresponding to quasielastic nucleon-nucleon scattering. For the heavier system Ar+Cl the similar measurements showed less enhancement. Using the reaction C+Pb the ratio was nearly constant as a function of the observed proton energy and angle indicating that a thermalized system had been created.

At 40 MeV/nucleon one might expect that the low multiplicity of protons ($\approx$ 2/collision)[5] might lead to a strong apparent direct component. On the other hand the fermi spheres of the two nuclei almost overlap in momentum space possibly washing out any quasi-elastic correlation in proton-proton scattering at these energies. Our measurements for the ratio of in-plane to out-of-plane correlations show no peak at quasi-elastic angles and energies. A comparison with the calculation of these collisions using a model incorporating mean field effects and Pauli blocking reproduces the ratio of in-plane to out-of-plane correlations at 45°.

The measurements were carried out with the K500 superconducting cyclotron at the National Superconducting Cyclotron Laboratory using a beam of 40 MeV/nucleon ^{12}C with an average intensity of 2 particle namps. The target consisted of a 15 mg/cm^2 graphite target. Three particle telescopes were used each consisting of a 100 μm Si ΔE detector and a 10 cm NaI E detector. Two of these counters were fixed in place at $(\theta,\phi) = (45°,90°)$ and $(45°,180°)$ comprising an out-of-plane and an in-plane coincidence detector, respectively. A third telescope was moved, covering angles from 25° to 120° in plane (ϕ=0°). The low energy cut-off of the detectors was approximately 10 MeV for protons which allowed the observation of the quasielastic peak when the counters were placed at 45°.

In Fig. 1 the ratio of the in-plane to out-of-plane coincidence spectra at 45° is given. This ratio is constant as a function of energy up to 60 MeV and then apparently increases. The average value for the ratio at this angle is 1.12. There is clearly no peak at 20 MeV in the in-plane coincidence spectra or in the ratio of in-plane to out-of-plane coincidence spectra as one would expect from free proton-proton scattering. This result argues for the production of a thermalized system. The results of the VUU calculation reproduce the observed

ratios.

In Fig. 2 the ratio of in-plane to out-of-plane correlations is plotted as a function of angle assuming that the ratio was constant as a

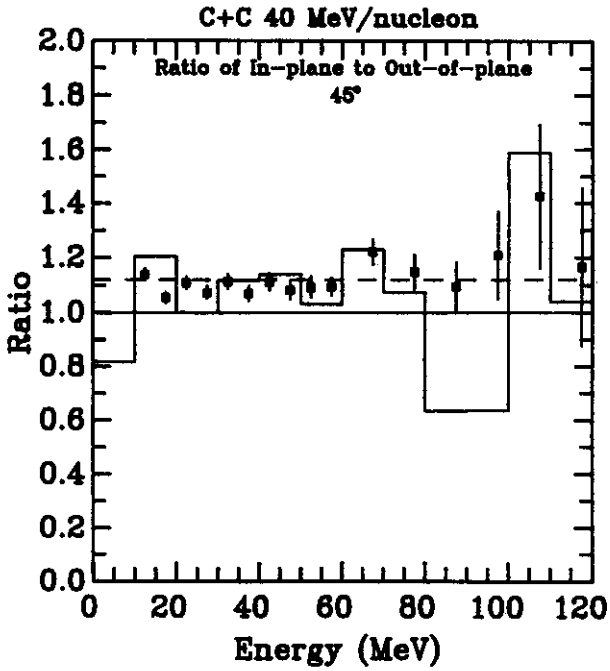

Fig. 1. The ratio of the in-plane to the out-of-plane coincidence spectra for protons at 45° from 40 MeV/nucleon $^{12}C+^{12}C$. The dashed line represents the average value of 1.12. The solid histogram depicts the results of the VUU calculation.

function of energy at each angle. There is a peak in the angular distribution of the ratios at ≈40° which roughly corresponds to the quasielastic angles from free proton-proton scattering. The VUU calculation roughly agrees with the observed angular distribution but there seems to be a peak in the data that may be the result of direct knock-out contributions.

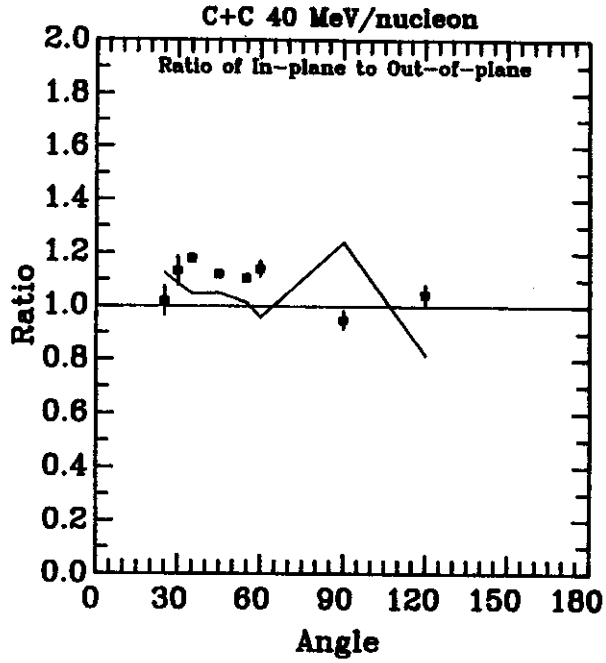

Fig. 2. Angular distribution of the ratio of in-plane to out-of-plane correlations. The solid lines show the results of the VUU calculation.

1. T.C. Awes, S. Saini, G. Poggi, C.K. Gelbke, D. Cha, R. Legrain, and G.D. Westfall, Phys. Rev. C25, 2361 (1982).
2. G.D. Westfall, B.V. Jacak, N. Anantaraman, M.V. Curtin, G.M. Crawley, C.K. Gelbke, B. Hasselquist, W.G. Lynch, D.K. Scott, M.B. Tsang, M.J. Murphy, T.J.M. Symons, R. Legrain, and T.J. Majors, Phys. Lett. 116B, 118 (1982).
3. B.V. Jacak, G.D. Westfall, C.K. Gelbke, L.H. Harwood, W.G. Lynch, D.K. Scott, H. Stöcker, M.B. Tsang, and T.J.M. Symons, Phys. Rev. Lett. 51, 1846,(1983).
4. I. Tanihata, M.-C. Lemaire, S. Nagamiya, and S. Schnetzer, Phys. Lett. 97B, 363 (1980).
5. G.D. Westfall, Z.M. Koenig, B.V. Jacak. L.H. Harwood, G.M. Crawley, M.W. Curtin, C.K. Gelbke, B. Hasselquist, W.G. Lynch, A.D. Panagiotou, D.K. Scott, H. Stöcker, and M.B. Tsang, Phys. Rev. C29, 861 (1984).

CLUSTER KNOCKOUT STUDIES IN ^{6}Li

R.E. Warner[a], J-Q. Yang[b], D.L. Friesel[b], P. Schwardt[b], G. Caskey, A. Galonsky, B. Remington, A. Nadasen[c], N.S. Chant[d], F.Khazaie[d], and C. Wang[d]

Knockout reactions at intermediate energies measure, in principle, the probability that a cluster of nucleons exists in atomic nuclei and the momentum distribution of that cluster. We recently reported[1] noncoplanar ^{6}Li(p,pd) measurements, at 120 MeV bombarding energy, which measured the distorted momentum distribution for p_α to about 160 MeV/c. They yielded an α+d spectroscopic factor of 0.75 and a momentum distribution FWHM of 73 MeV/c, which agree with the results of coplanar measurements[2]. We have since made new ^{6}Li(p,pd) noncoplanar measurements at 200 MeV bombarding energy. These measurements were made to determine whether the DWIA yields energy-independent spectroscopic factors. The experimental technique, in which proton and deuteron are detected in coincidence with germanium telescopes, is described in more detail in Ref. 1. The data were taken at the I.U.C.F.

Measured cross-sections vs. detected deuteron energy (i.e., "energy-sharing spectra") are shown in Fig. 1 for eight values of the azimuthal noncoplanarity angle ϕ. For all spectra the projectile energy at target center was 200.2 MeV and the polar angles (θ_p,θ_d) of the detectors were (54°,-48.9°). The cross sections are plotted vs. the deuteron lab energy E_d.

The energy-sharing spectrum for each noncoplanarity angle shows a broad peak centered near the minimum recoil momentum, as is characteristic of s-state cluster knockout. The peak cross section varies significantly with ϕ. This feature is more clearly illustrated in Fig. 2a, where the integrated cross section is plotted vs. ϕ; to provide good statistical accuracy, this cross section was integrated over the 20 MeV deuteron energy interval in which the coplanar quasi-elastic peak is centered.

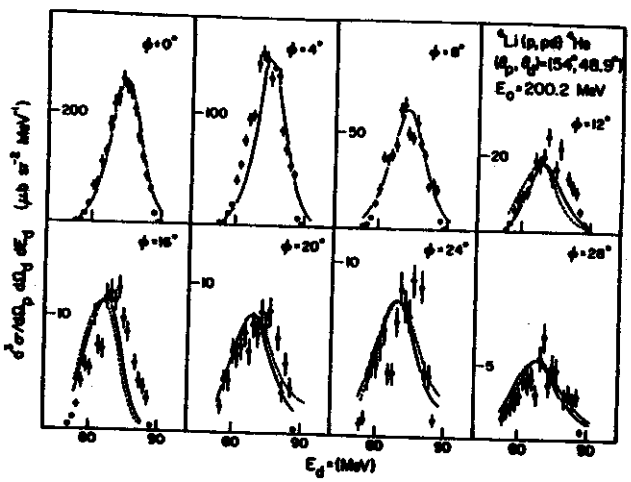

Fig. 1. Cross sections vs. deuteron lab energy for the ^{6}Li(p,pd)^{4}He reaction at E_0=200.2 MeV and the quasi-free angle pair $(\theta_p\ \theta_d)^0$ = (54°π - 48.9°), for eight values of the noncoplanarity angles ϕ. The solid curves are DWIA predictions, generated by optical potential parameters,[3-5] when α+d move in a Woods-Saxon potential of radius 1.85 fm in the ^{6}Li ground state. The dashed curves show predictions for the optical model parameters used in our earlier[1] 120MeV study, where such predictions differ perceptibly from the solid curves.

Theoretical spectra were calculated by the DWIA, using a ^{6}Li ground-state wavefunction for a Woods-Saxon d+α interaction, and standard nuclear optical potentials [3-5] to generate the incoming and outgoing distorted waves are shown by solid lines in Fig. 1. These predictions reproduce fairly well the energy-dependence of the yields.

Our initial calculations used the same optical potentials employed in earlier studies of this reaction at 120 MeV[1]. Predictions from these potentials, where they differ from those of the standard potentials, are shown as dashed curves in Fig. 1. The peak shifts between the two sets of DWIA predictions are much smaller than those between either prediction and the

experimental data. Moreover, the predicted peak locations changed negligibly when the Woods-Saxon ground-state wavefunction was replaced by a soft-core wavefunction.[6] The cause of the shifts is not understood.

The purpose of noncoplanar breakup measurements is to sample the distorted momentum distribution for progressively larger spectator momenta by maintaining constant projectile-ejectile scattering conditions as θ increases. Fig. 2a shows the dependence of the integrated cross section upon the noncoplanarity angle, which determines the range of momenta sampled. Similar data from the earlier 120 MeV experiment are shown, for comparison with these data and with some new theoretical predictions, in Fig. 2b.

Figure 2 shows that, at 200 MeV as well as at the lower energy, the measured large-θ cross sections exceed those predicted; this explains

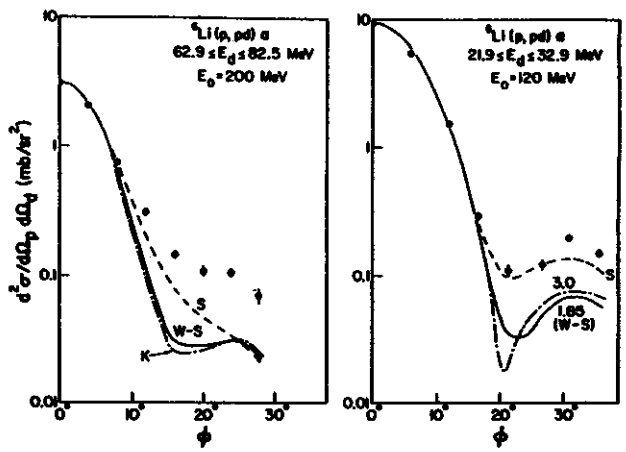

Fig. 2. Cross sections vs. noncoplanarity angle at 120 and 200 MeV bombarding energy. Both predicted and measured cross sections are integrated over the specified detected deuteron energy ranges. S and K are predictions for soft-core [6]) and Kikulin three-body [7]) ground-state wavefunctions. Predictions are also shown for a Woods-Saxon ground-state potential of 1.85 fm radius at 200 MeV and for two indicated radii at 120 MeV.

the need for separate normalization factors for the spectra in Fig. 1. The soft-core potential[6] comes somewhat closer to reproducing the data. The minimum generated by the Woods-Saxon potential with R=1.85 fm is much more shallow than that at 120 MeV. This effect follows the trend of the data since the observed minimum at 200 MeV is either absent or much less pronounced than at 120 MeV.

The DWIA with a woods-Saxon potential (R=1.85 fm) gives d-α spectroscopic factors of 0.76 and 0.84 at 120 MeV and 200 MeV, respectively, when normalized to the data as shown in Fig. 2. Kukulin et al.[7] recently solved the ^{6}Li three-body (αNN) problem by the Faddeev formalism, including exact treatment of Coulomb effects. We obtain a spectroscopic factor of 0.76 using the Kuklin ground state wavefunction at 200 MeV. At 100 MeV Roos et al.[8] obtained factors between 0.45 and 0.72. Thus we find that this quantity is only weakly energy-dependent.

---

a Oberlin College
b Indiana University
c University of Michigan, Dearborn
d University of Maryland

1) R.E. Warner et al., Nucl. Phys. A422,205(1984).
2) D.R. Lehman and M. Rajan, Phys. Rev. C25,2743(1982).
3) G.R. Satchler and R.M. Haybron, Phys. Lett. 11B,313(1964).
4) B. Tatischeff and I. Brissaud, Nucl. Phys. A155,89(1970).
5) V. Comparat et al., Phys. Rev. C12,251(1975).
6) J. Jänecke et al., Nucl. Phys. A343,161(1980) (Set S, Table 3).
7) V.I. Kuklin et al., Nucl. Phys. A417,128(1984).
8) P.G. Roos et al., Nucl. Phys. A257,317(1976).